DEVELOPMENT, OPTIMIZATION AND CHARACTERIZATION OF NiCrBSi-TiB₂ VACUUM FUSED FLAME-SPRAYED COATINGS

Teză destinată obţinerii
titlului ştiinţific de doctor inginer
la
Universitatea Politehnica Timişoara
în domeniul INGINERIA MATERIALELOR
de către

Ing. Norbert Kazamer

Conducător ştiinţific: Prof.univ.dr.ing Viorel-Aurel Șerban

Referenţi ştiinţifici: Dr.ing. Gabriela Mărginean
                          Prof.univ.dr.ing. Corneliu Munteanu
                          Prof.univ.dr.ing. Ion Mitelea

Ziua susţinerii tezei: 9 iulie 2019

Foreword

Rezumat,

Prezenta cercetare se concentrează pe investigarea caracteristicilor unor straturi pulverizate termic și tratate în cuptorul cu vid utilizând pulbere de NiCrBSi ranforsată cu particule de TiB$_2$. Prin analiza datelor prelucrate statistic s-a reușit optimizarea timpului și temperaturii de menținere a straturilor în cuptorul cu vid precum și selectarea concentrației volumetrice optime între matrice și ranforsant.

Probele de NiCrBSi-TiB$_2$ au prezentat o porozitate redusă, duritate satisfăcătoare, o compoziție de faze complexă precum și o legătură metalurgică puternică între strat și substrat, fapt dovedit printr-o excelentă rezistență la propagarea fisurilor. Experimentele tribologice și măsurătorile potențiodinamice au arătat pentru materialele dezvoltate rezistențe superioare la uzare și coroziune în comparație cu un strat convențional de NiCrBSi ales ca referință.

Keywords: NiCrBSi, TiB$_2$, NiCrBSi-TiB$_2$, thermal spraying, vacuum furnace post-processing, optimisation, wear, corrosion

Abstract,

The current research focused on the optimization and characterization of combustion thermally sprayed and fused depositions using as feedstock NiCrBSi powder reinforced with TiB$_2$ particles. A statistical approach was used to optimize the holding time and temperature during the vacuum furnace heat treatment and to select the best proportions among the samples with different matrix-reinforcement volumetric concentration.

The optimized NiCrBSi-TiB$_2$ sample presented low porosity, satisfactory hardness, a complex phase composition and a strong coating-substrate metallurgical bonding that led to an excellent indentation fracture toughness. A thermally-sprayed and vacuum remelted NiCrBSi coating was chosen as a reference sample for further destructive tests. Tribological and potentiodinamic measurements showed superior tribological and corrosion resistance for the developed material in comparison with a conventional NiCrBSi chosen as a reference.

Contents

Abstract

Taking into account the current state of the art in the area of wear and corrosion resistant coatings and considering the demand of the market with regard to optimization and post-treatment, the present research focuses on investigating the characteristics of thermally sprayed and post-treated coatings using as feedstock NiCrBSi, one of the most established Ni-based powders, reinforced with TiB_2 particles. The deposition method used for materials was the combustion flame spraying technology. It is one of the most widespread methods of metallic parts protection because of factors such as the ease of handle, the low costs and the high-end quality results it gives.

The chosen matrix and reinforcement have been mechanically mixed in four different volumetric mixes using a screw conveyer. The technology ensured that through rotating the powders in the conveyor, the risk of powder segregation was partially eliminated. By using the mixing technology on powders with such a big size difference, it was possible to make the TiB_2 particles attach to the matrix, which allowed the deposition of a partially homogeneous reinforcement distribution in the thermally sprayed coating. The different volumetric concentrations of NiCrBSi-TiB_2 were successfully deposited using gravitational feeding combustion flame-spraying equipment. For Ni-based self-fluxing alloys, the post-processing is extremely important and it decisively influences the quality of the entire deposition. The selected treatment in vacuum furnace turned out to be of great benefit for the quality of the coating. The advantages of the technology, such as keeping the surface clean, removing contaminations and creating a metallurgic bonding between the coating and substrate, supported a good behaviour of the material when tested against diverse destructive methods.

Acknowledging the importance of the process, one of the main focuses, in the present work was to optimize the parameters of the vacuum furnace post-processing. The design of experiments is an established method to gather the maximum amount of information from a minimum number of probes and invested energy. The response surface methodology is the design of experiments (DOE) procedure that was used to optimize the post-processing parameters as it is a step-by-step approach with a relatively low number of runs and a high statistical efficiency. The suggested process factors from the DOE highlighted the best volumetric concentration between the matrix and the reinforcement delivering the optimal type of coating to be further characterised and tested.

A comprehensive characterisation using different methods was used to investigate the porosity, chemical composition, phase distribution and interface region of the optimized NiCrBSi-TiB_2 coating. A vacuum-remelted NiCrBSi coating deposited with the same matrix material has been selected as a comparison sample. The result analogy is extremely important as it can give an idea of how the developed coating is behaving in the same conditions as one that is already used in the industry. The tribological and corrosion behaviour of the reinforced coating was analysed in comparison with the established and industry applied NiCrBSi sample.

The developed NiCrBSi-TiB_2 coating is an ideal solution for machine components that need a long lifespan in particularly challenging environments. The TiB_2 reinforced coatings, because of their proven excellent tribological behaviour can be a real alternative for the more common NiCrBSi in applications like valve seats, pump sleeves or shafts.

Abbreviations

1SLD	One-step laser deposition technique
AC	Alternating current
ASM	American society for metals
AS	Arc spraying
APS	Atmospheric plasma spray
BSE	Backscattered electrons
CCD	Central composite design
CE	Counter electrode
COF	Coefficient of kinetic friction
CSLM	Confocal laser scanning microscopy
CTE	Coefficient of thermal expansion
CVD	Chemical vapour deposition
DC	Direct current
DF	Degrees of freedom
DOE	Design of experiments
DTA	Differential thermal analysis
EBSD	Electron backscatter diffraction
EDX	Energy dispersive x-ray spectroscopy
EU	European Union
FEM	Finite element method
ff	Flow factor
FS	Flame spraying
FSP	Friction stir processing
GDP	Gross domestic product
HIP	Hot isostatic pressing
HF	High frequency
HVOF	High velocity oxy-fuel
LPPS	Low-pressure plasma spraying
NTBX	NiCBSi-TiB$_2$ powder mix where X=(5,10,15,20)
PVD	Physical vapour deposition
RE	Reference electrode
RF	Radio frequency
RSM	Response surface methodology
RT	Room temperature
SCC	Stress corrosion cracking
SCE	Saturated calomel electrode
SE	Secondary electrons
SEM	Scanning electron microscopy
SHS	Self-propagation synthesis
SPS	Suspension plasma spraying
SPSS	Solution precursor plasma spraying
TEM	Transmission electron microscopy
TGA	Thermogravimetric analysis
TS	Thermal spraying
VPS	Vacuum plasma spraying
WE	Working electrode
XRD	X-ray diffraction

1. Research objectives

"We have to remember that what we observe is not nature itself, but nature exposed to our method of questioning."

Werner Karl Heisenberg[1]

1.1.   Background

The development of performant coatings is a continuous challenge with an entangled history. A quick overview of key works in the area shows how early the research started and how much interest the topic is still getting. The first known document dates from the Antiquity with the *Dioscorides and Pliny* report. It is stated there that natural resins were used as coatings [1]. In the 11th Century, *Rogerus von Helmershausen* published the *Schedula Diversarium Artium* book describing the first known recipes of coating materials [2]. Another important development has been realized by the *von Eyk* brothers in the early 15th Century in the area of dilution and drying of painting materials [3]. Probably the most influential book in technology in the middle age was the *De re metallica* compendium published by *Georgius Agricola* in 1556 where the state of the art in metallurgy and mining technology was gathered and presented [4]. Just a few decades after the industrial revolution, *Henry Ford* and *Max Ulrich Schoop* made significant developments in the domain, the first employing quick drying paints on a large industrial scale [1] while the later was inventing the thermal spraying technology [5].

Among the many functions of coating, protection and decoration are probably the ones on which the industry focuses the most. The skilled workers have to keep up with the rapid changes and adapt to new techniques. An important area in the coating industry, thermal spraying, realized significant progress over the last century and there is still room for growth. The first technological breakthroughs at the beginning of the 20th Century started with steel, stainless steel and zinc deposition by wire-arc metallizing [6]. Meaningful developments were done around the Second World War with a powder deposition technique consisting in feeding the material into a flame using the Venturi effect [7,8]. The most recent significant technological progress period from the deposition point of view was in the early 1960s with the development of the combustion, plasma, electric arc and detonation gun [6]. Nevertheless, since then, although the processes share the same basic working principle and they encountered important advanced, they are still challenged on aspects like post-treatment, optimization or environmental impact.

The coating deposition technology developed to a point where it can be used almost on any material, benefiting a large variety of economical branches [9]. Metals, oxides, cermets gradient depositions, reinforcements and *in situ* synthesis are all used to create different coatings for industries like automotive, chemical processing, mills, aerospace, food processing, oil and gas exploration, medical, nuclear, textile or transportation [10]. Materials have enormously progressed for outstanding functional performances; however, a high demand still exists for better protection in different

---

[1] *German physicist. Awarded with Nobel Prize "for the creation of quantum mechanics".*

harmful environments. The objectives of this research are directed towards protection against wear and corrosion.

Finding the appropriate combination of materials, technology and design for each application can be a difficult task for engineers and scientists. Another challenge in the field is to preserve the advantage of depositing materials on almost any type of substrates.

In terms of market, the global demand for paint and coatings is predicted to increase 3.7% per year to reach 54.7 mil. metric tons reaching 2020. It's current total worth of about 160 mil. euro will exceed 180 mil. euro by 2022 [11,12]. Suppliers in the developing countries are especially likely to profit from the infrastructure investments, which would boost the production and maintenance need in the industrial sector. The statistics showed in *Figure 1.1* highlight that the European market in 2017 is a key player worldwide, representing together with Middle East and Africa 30% of the total industry [13]. Taking into account the predicted 2.5% GDP growth rate of the EU in 2018 [14] there are strong reasons to believe in a positive impact on the coating industry as well.
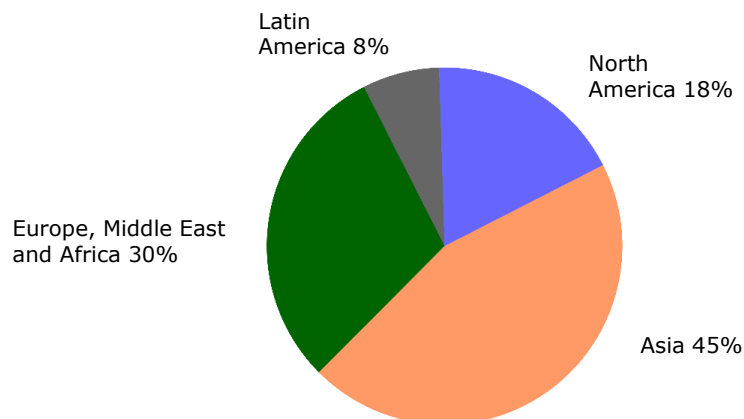
Figure 1.1 Distribution of the coatings market value worldwide in 2017 by region

Considering the consumption by technology, the powder based one almost doubled between 2009 to 2016 from 1.2 mil. tons to 2 mil. tons. The sector is predicted to increase 24% to 2.7 mil. tons by 2021 [15] and continue to dominate the sector along water-based and solvent-based technologies. The cost-effectiveness of the deposition also has to be taken into account, as during coating deposition, a considerable amount of material can be lost. The deposition efficiency is typically defined as the amount of material that is sprayed on a substrate in comparison with the amount of sprayed materials [16,17]. If a big quantity of material is lost during the process, the deposition efficiency can be affected to the point that the process is done at economical loss. Design of experiments helps obtaining a high deposition efficiency.

The need for a high life-cycle of the coatings leads to other motivations as well. The life of the component can be extended through several means. An important part of them are directed towards reducing the adhesive, abrasive, erosive wear or lower the corrosion realized through exposure to different environments. Functional performances like high temperature exposure or reconditioning of coatings can open the way to improvements in the field.

After the production of the coating, the coated article in its life cycle is greatly challenged by degradation very likely caused by wear and corrosion. Even though the expertise of the researchers and industry greatly increased during the last decades, they are constantly confronted to damage turning to unwanted expenditures. The cost of both wear and corrosion is believed to be a significant fraction of the national GDP's of about 3-5% and reaching in the developing countries even up to 10% [16,18]. These, however, do not include the environmental effects, resource waste nor production loss. Thermal sprayed coatings among other important techniques like inhibitors or cathodic protection contribute in protecting from damages.

The ongoing demand for quality optimization and rationalization taking into account the impact on the surrounding environment is fuelling a wide interdisciplinary field of research and experimentation within the coating industry. Several current tendencies could shape the future of the industry like: continuing the advances in the process control equipment (robotics, sensors, feedstock filling, motion control, *etc.*), developing methods for non-destructive testing of the coatings, post-processing with several technologies (furnace, flame or electromagnetic) or understanding and optimizing of the spray processes or post-treatment [19,20]. The latest research on both materials and processes are opening new opportunities to employ thermal spraying in novel applications and enter new markets.

1.2.   Motivation

Spraying with the right material, being efficient during deposition and obtaining the right properties for a certain application are constant challenges in the industry. A possible solution for improvement can be represented by reinforced Ni-based powders. These type of powders are well-known in the industry being used for a large number of applications. An important progress in the branch where Ni-based powders are used against wear and corrosion protection can be obtained by adding reinforcements to this extensively used material. Effectiveness can be boosted in the thermal spraying of Ni-based materials by finding optimal chemical composition and post-processing parameters. Taking into account the current state of the art in the field of wear and corrosion resistant coatings and considering the demand of the market with regard to optimization and post-treatment, the present research focuses on investigating the characteristics of thermally sprayed and post-treated coatings using as feedstock NiCrBSi, one of the most established Ni-based powders, reinforced with TiB_2 particles. Although technologies like Atmospheric Plasma Spraying (APS), High Velocity Oxy-Fuel (HVOF) or cold spraying are frequently used and well established processes, powder flame spraying is still the most widespread method because of the low costs, the ease of handle and the good coating characteristics. The chosen reinforcement powder used for this work is TiB_2, a ceramic material known for its high melting point, low density and good hardness. NiCrBSi and TiB_2 have common elements in their chemical composition, and through mechanical mixing, deposition and through an optimized and well-chosen post-treatment performant coatings can be obtained. A post-treatment increases the probability to create a metallurgical bonding and in consequence a strong adhesion to the substrate. These materials, sprayed and then fused, can represent viable solutions for applications that require thick ductile coatings resistant to wear and corrosion.

Therefore, the main objective of the research is to obtain optimized flame sprayed and vacuum furnace post-processed $NiCrBSi-TiB_2$ coatings. After the deposition process of the material on a low-alloyed steel, to maximize the results, an optimization through design of experiments was performed to the

matrix-reinforcement fraction on one hand and to three response variables (porosity, hardness and standard deviation of the hardness) through the variation of two of the most important heat-treatment parameters, time and temperature, on the other hand. Thermal behaviour of the selected powder was analysed with the aid of the Differential Thermal Analysis (DTA). Light and confocal scanning laser microscopy (CSLM) were employed for image processing and microstructure and wear track analysis. The morphology, chemical composition as well as the quality of the coating-substrate interface region have been examined using Scanning Electron Microscopy (SEM) combined with Energy Dispersive Spectroscopy (EDX). For the determination of the phase changes during the heat treatment, the powder, the as-sprayed and the heat-treated coating were analysed using X-Ray Diffraction (XRD). The size and distribution of pores have been processed using image analysis. Surface and cross-section hardness was evaluated by Vickers indentation. Tribological investigation using a pin-on-disc arrangement helped compare the friction coefficient and calculate the wear rates of the substrate, as-sprayed and post-processed samples. Electrochemical corrosion tests were employed to evaluate the corrosion behaviour of both the substrate and coatings using potentiodynamic polarization with a three-electrode cell.

Possible applications of the gathered results are ones where ductile, corrosion and wear resistant parts are needed like heat exchangers, turbine, extruders, laminators or the agriculture industry.

The limitations of the technology are the relative small velocity of the particles (<100 m·s^{-1}), a lower adhesion of the coating to the substrate in comparison to other techniques and a porosity which can reach 6-8%. Another drawback would be considered the certain degree of dependency on the worker, who needs to constantly supervise the production.

Therefore, the goal of the present thesis is to find solutions to a part of the challenges of the thermal spraying industry regarding the post-treatment and optimization and to obtain and characterize densified corrosion and wear resistant coatings.

The thesis has been structured as following:
- Chapter 1 describes the background and the motivation behind the research work.
- Chapter 2 covers the state of the art in the thermal spraying technology. Fundaments of the coating build-up and pre-spray processing are first presented. A more in depth view with regard to the fundaments of post-spray treatment is presented with a focus on the vacuum furnace treatment. Aspects of the design of experiments and materials are considered in the section that follows. The last part is dedicated to applications and methods of testing and characterization of thermal sprayed coatings.
- Chapter 3 focuses on the methodology and experimental procedures employed for the experimental part. Details regarding the morphological, chemical and physical characterization along with mechanical and corrosion testing are considered.
- Chapter 4 highlights the experiments and results of the thesis with regard to the materials, deposition, vacuum furnace optimization and characteristics and coating behaviour.
- Chapter 5 includes the conclusions and personal contributions. It also provides an outlook for future developments.

2. State of the art

2.1. Introduction to thermal spraying

In order to qualify as an established stakeholder in the coating industry, a company has to ensure both quality and profitability. Necessary requirements for a successful business are among others repeatability, a certain coating thickness with a precise tolerance, defined microstructure, a phase composition ensuring the wanted properties, acceptable defects and cost-effectiveness.

Several types of coating processes emerged in the industry; the main ones are considered in *Figure 2.1*. When choosing which method to use, aspects like substrate nature and temperature achieved during the coating, the used materials and obtained properties have to be considered. Each technique has a well-known niche of application, pros and cons. Ion implantation can provide important advantages in different applications. The structural modifications can determine *e.g.* in steel surface a higher impact resistance or in prosthesis production a better corrosion resistance. Nevertheless defects like vacancies or interstitials [21] can occur. Chemical vapour deposition (CVD) and physical vapour deposition (PVD) can produce coating uniformity even on hard-to-reach surfaces. Even though applications exhibit exceptional properties, the use of such processes is restricted to relatively small parts [22]. Although electroplating is one of the first developed methods in the coating area and it is still largely used for both corrosion and decorative purposes, it cannot be easily fitted into a product line and generates a lot of waste [21]. Welding occupies a special category as it has a functional role of joining two materials and permits a large freedom in design. Although welding permits mechanization, the problem of inducing residual stresses, harmful radiations and, often, the need for skilled workers, make the processes sometimes hard to put in practice [23].
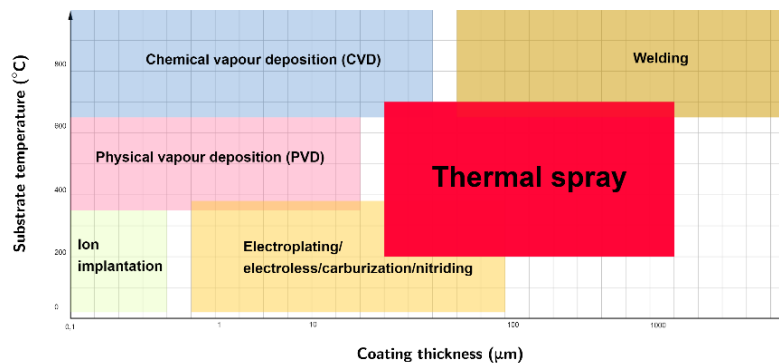
Figure 2.1 Comparison of the different coating processes in the market

Considering the temperatures and the thicknesses of the coatings deposited by different techniques, one can see in *Figure 2.1* that the thermal spraying (TS) process distinguishes itself covering a wide spectrum of the graph. As defined by ASTM, thermal spraying is "a group of processes wherein finely divided metallic or

non-metallic materials are deposited in a molten or semimolten condition to form a coating. The surfacing material can be in the form of powder, rod, cord, or wire." [24].

There are two broadly accepted classifications of thermal spraying. One of them is according to EN 657 (ISO 14917) standard [25], splitting the techniques into four main classes by the energy source needed, each dividing afterwards into subclasses. The main classes and subclasses are: thermal spray by beam (laser spraying), thermal spray by liquid (molten bath spraying), thermal spraying by gas (flame spraying, detonation spraying, HVOF, cold gas spraying) and thermal spray by electric gas discharge (arc spraying, plasma spraying). The other classification is realized by following the definition. Coatings in thermal spraying can be deposited only if the particles are sufficiently rapidly plastically deformed. Their heating and acceleration is primarily occurring through a gas stream [26]. Consequently, the coarse classification used in academia, seen *Table 2.1*, is based on the way of gas stream generation [26].

Table 2.1 Jets and flames methods of generation employed in thermal spraying [26]

Energy input to gas	Variation	Spray technique
	DC arc	arc spraying (AS), APS, vacuum plasma spraying (VPS)
Electric discharge	Pulsing arc	torches described by *Witherspoon et al.* [27]
	High frequency (HF) / radio frequency (RF) glow discharge[a]	RF plasma spraying described by *Bouyer et al.* [28]
Combustion	Continuous	HVOF, flame spraying (FS)
	Explosive	D-gun
Decompression of air	-	cold-gas spraying method

[a]*RF discharge is employed as well to initiate discharges in a DC arc*
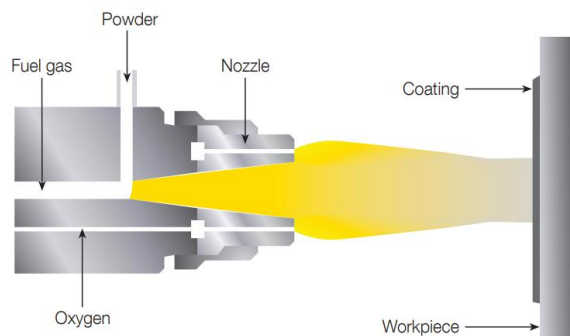
Figure 2.2 Principle of the continuous combustion powder flame spraying process [29]

In the flame powder spraying, with the schematics in *Figure 2.2* , feedstock is fed through a built pipe system or through a special funnel into the oxy-fuel flame, partially or totally melted, and carried by the flame and air jets towards the substrate [6]. The gas flow can reach about 11 $m^3 \cdot h^{-1}$, the particle speed around 100 $m \cdot s^{-1}$, while the flame temperature gets as high as 2500°C. The bond strength of the formed coatings is influenced by the spraying distance, the powder fraction or the spraying angle but there have been reported values between 40 MPa [30] and 250 MPa [31].

The porosity can also vary mainly depending on which material is used. Although a value below 5% is typically desired [6], higher values can also be obtained. Different post-processing techniques may be used to reduce porosity.

Spray rates increase when the melting point of the material is low and can vary between 0.5 kg·h^{-1} and 9 kg·h^{-1}. Other equipment parameters are the power ranging between 25 kW and 75 kW and the energy required to melt which varies between 11 kW·kg^{-1} and 22 kW·kg^{-1}. The moderate costs associated to powder flame spraying are also playing a big part in its popularity in the industry, as this coating process is considered as one of the most inexpensive ones [6].

Considering the current status in the equipment development, one should know that the company Monitor Coatings Ltd. received a patent for a new type of gun which the HVOF method where the combination of the gases is performed in the chamber, exhausting a single stream [32]. Because the powder is injected through a particular area of the gun, the feedstock contacts only the generated gas stream and the in-flight risk of oxidation is reduced and a uniform heating of the material is assured. Future trends in developing numerical investigation of flow dynamics of HVOF spray guns have been done by *Wang et al.* [33]. The studies showed clear separation between ignition, burning and acceleration regions in the chamber, the flow pattern showing a recirculation in the axial direction near the ignition therefore powder injection could avoid the recirculation region. The research also concluded that the fuel atomization has a great effect on the flow characteristics for fine powders with a size under 20 μm. Another recommendation in the equipment development area was to introduce hybrid processes to create dense coatings [34]. Fully dense NiCr-Mo coatings were produced by increasing the deposition temperature over the critical bonding. *Olakanmi et al.* carried out a thorough review of the laser-assisted cold-sprayed equipment and presented several example of dense and almost porosity free coatings that can be deposited [35].

The end result of a deposition process in thermal spraying is the coating being built up by separate particles. As the definition states [24], the droplets can be semimolten or completely molten at the moment of coating formation. Particles which are not in a molten state are not desired because they do not adhere to the substrate, can be trapped inside the deposition and weaken the adhesion of the coating. As shown in *Figure 2.3* and supported by peer reviewed literature [22,26,36], the temperature of the molten droplets during the transfer from the gun towards the substrate is increasing, reaching ideally close to the melting point of the material. Approximately 30 different typical impacting particle shapes (the so-called splats) have been identified [22], but they can be widely categorized in three depending on their melting degree. The three groups are exemplified in *Figure 2.4* [37].

The impacting of a particles is done in two stages. In the first period having a duration of approximately 10^{-9}-10^{-7} s, a series of shock waves are initiated at the particle-substrate contact surface [22]. At this stage, the unmolten particles could bounce off and create problems that would later affect the coating adhesion and quality. The surviving particles would enter in the second stage of irreversible deformation, a hydrodynamic phase of impact taking place. The yield stress and the solid-state viscosity, values that can be mathematically determined [22], are crucial properties for the particle flattening degree and the ability of the material to resist mechanical stress. If possible, a substrate preheated in a furnace with well-defined data is preferred as it promotes a high contact angle between the two materials and can produce oxide layers. When heated using a torch, even with programmed parameters, the local temperature varies with the relative movement of the torch [38]. Afterwards, during the deposition process, the first layer is usually forming

5-15 lamellae through the movement of the torch over the sample depending on parameters such as spraying distance, velocity of the gun or of the particles [26].
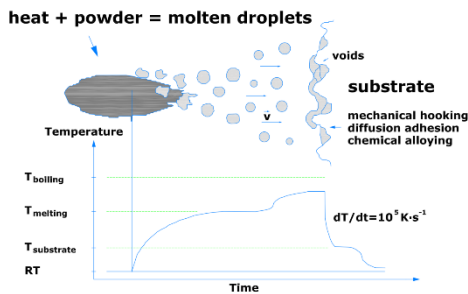
Figure 2.3 Fundamentals of the process showing the formation of the particle transition from the gun to the substrate forming the coating (top) and a corresponding time versus temperature plot (bottom) [22]
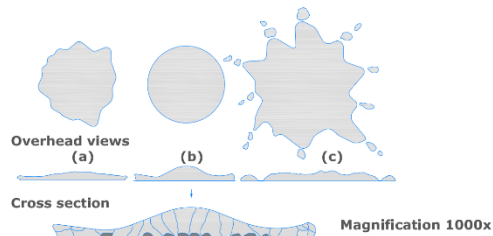
Figure 2.4 Particle melting effect on the lamellae formation at the impact with the substrate: (a) semimolted , (b) properly molted and (c) overheated particles [37]

After the impact of the splat, a fast cooling of the particles takes place (*e.g.* for a tungsten particle deposited on a steel rates of 3-7·10^7 K·s^{-1} are reported [26]). Solidification starts through the release of the heat approximately 1.5 µs after the particle hits the substrate through the bottom side of the formed lamellae [36]. The nucleation of the formed crystals can be either heterogeneous or homogeneous depending on the undercooling effect (referring to the nucleation temperature lower than the melting point) and the thermal contact resistance (referring to the heat evacuation). During a heterogeneous nucleation, the cooling rate is higher and a columnar structure formation is likely to be generated [39]. A homogeneous nucleation is favoured by a low heat rate removal, starting inside the lamellae, favouring a fine equiaxial microstructure [26]. Current developments using simulation software are performed in the area of particle impact during different spraying processes (*e.g.* thermo-mechanical analysis of particles [40] or plastic deformation phenomena using cold spraying on metallic materials [41]).

Although much attention is given to quality and investigation, one should always have in mind that a coating will never protect a substrate if it does not succeed to adhere to it. Generally, three adhesion mechanisms are considered: diffusion, chemical and mechanical.

The diffusion adhesion of metals and alloys takes place in thermal spraying when the temperatures reached during deposition or heat treatment high and no oxide layer is found on the substrate surface. The diffusion coefficient is defined in *Eq. (2.1.)* as:

$$D = \exp \frac{-E_A}{k\,T} \qquad\qquad (2.1.)$$

where E_A represents the activation energy, T the absolute temperature and k is the Boltzmann constant (1.38·10^{-23} J·K^{-1}).

Chemical adhesion occurs at the moment of the particle impact, when the substrate and the feedstock creating a chemical compound. The chemical bonding can be mathematically defined and is dependent on the melting point of the material and the effusivity. Such phenomena were observed in iron particles hitting a preheated

aluminium substrate forming $FeAl_2O_4$ [42] or YSZ lamellae impacting stainless steel [43].

Mechanical adhesion in thermal spraying happens by roughening the substrate, commonly by grit blasting. The force develops on the contact surface as the splats shrink by cooling on the substrate. The adhesion is dependent on both the distance between the highest points and the amplitude of the peaks and valleys. Adding deoxidizing substances in the feedstock helps also increasing the active zone and therefore the adhesion of the coating to the substrate. Grit blasting preheating is commonly enhancing the adherence of the coating to the substrate by a factor of 2 to 4 [44].

A current development direction in the area of adhesion was pursued by *Kromer R.* [45,46]. A finding concluded that during APS sprayed coatings a large contact area increases the energy release at the coating-substrate area during failures [45]. Another research concluded that the adhesion is dependent on the powder size and especially the morphology of it [46].

Internal stresses can be also introduced in the coating, with grit blasting being one of the possible causes. Internal stress generation in TS is categorized into:
- Quenching stress, happening through the lamella solidification
- Stress induced by the torch movement
- Cooling stress, generated immediately after the deposition process
- Phase-transformation stress, due to the crystallinity changes happening in the coating during cooling.

Although understanding the coating formation mechanisms is crucial to obtain a high-end product, without effectiveness during the deposition, a large scale implementation is not possible. In thermal spraying, in accordance with the standards DIN EN ISO 14917 [25] and EN ISO 17836 [47] to determine the deposition efficiency, the mass of the fed spray material has to be first considered. This is defined as:

$$m_{sm} = f_r \cdot \frac{t_s}{60} \qquad (2.2.)$$

where m_{sm} (g) is the mass of the spray material, f_r $(g \cdot min^{-1})$ the feed rate and t_s (s) is the spray time. Considering *Eq. (2.2.)*, the process deposition efficiency applicable for all the techniques is therefore defined as:

$$\eta_D = \frac{\Delta m_{tp}}{m_{sm}} \cdot 100\% \qquad (2.3.)$$

where the deposition efficiency η_D $(\%)$ equals to the ratio between the mass difference Δm_{tp} and the mass of spray material m_{sm} (g). Furthermore, for a more in depth view, the target deposition efficiency can be also taken into account. This characteristic is attributed to the component and depends on the geometry of the part and on the gun movement [22].This concept still represents an actuality subject, *Toma et al.* recently highlighting that the cost-effective coating preparation is mainly dependent on the deposition efficiency and layer thickness [48].

By knowing the coating processes, by being able to choose the right technique for the given application, by understanding the functioning of the technology and by managing to implement the research outcomes in the industry, a company can comfortably establish itself as an important player on the market with a considerable development potential.

2.2.   Pre-spray processing

The parts arriving at the coating department are mostly new but in some cases they can be also coated or present defects. Even supposing that most of the parts are new and made out of metal alloys, they are still generally covered in grease or oil to prevent corrosion. Anyway, grease or any kind of layer or imperfection on the surface to be coated has to be removed before the deposition. An activation of the surface is as well commonly performed. A general pre-spray processing of the substrate can be seen in *Figure 2.5*.
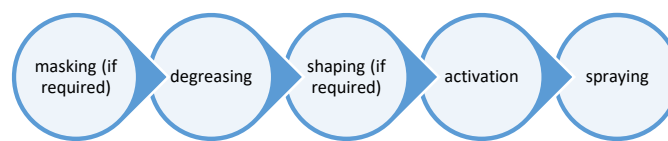
Figure 2.5 General pre-processing of surface before thermal spraying

Coatings are sometimes not entirely covering the substrate. Masking is a process applied to the surface of a part to properly protect the surface against grits from the activation stage or hot particles during spraying. Several types of masking are available from plastics or rubbers, metallic or glass fibre tapes which can be cut to desired dimensions [26] to commercial liquids like Metco Anti-Bond™ [49]. The masking method depends mostly on the geometry of the part and on the application.

Degreasing of metal substrates can be done using organic solvents such as methyl alcohol acetone. The parts should comply to the *Sa 3* class of cleanliness according to EN ISO 8501-1 [50]. As for large pieces the use of solvents is not a convenient method, hot water or clean and dry air at regulated pressure can be an alternative. The process should be performed in a separate clean room used only for this purpose. The operator handling the pieces should have the respiratory system and the hands protected for both health and part contamination purposes. Nevertheless, due to the use of different chemicals, surface cleaning can present major disadvantages with regard to health of the operator or protection of the environment. The removal of grease can be done through turning but specialized techniques like immersion of ceramic coating in molten potassium hydroxide [51] or vacuum electric arc removal [52] have been also reported. Those chemical processes compared to classical turning have the advantage of being fast but special equipment has to be purchased as well.

Shaping, when needed, is a crucial step in assuring a high quality coating on the entire surface of the part. The process, besides bringing the samples to their dimensional specifications, is also necessary to prevent sharp angles or ends where it is difficult to spray. Because of the high concentrations of thermal stresses in such places, the adherence would become lower and these points would become vulnerable starting points in defect generations.

For substrate activation, a certain degree of automation is recommended, as the process has to be repeatable. Although the abrasive grit blasting is the most widespread, processes like water-jet treatment, chemical attack or laser ablation are also employed. Water-jet treatment is mostly used in biomedical application, when contamination-free coatings are required. Such activations have been used in

suspension plasma spraying (SPS) of Inconel alloys [53,54]. Chemical etching with diluted nitric, hydrochloric or sulphuric acid is also possible for surface activation [26]. However, because of environmental standards and advancements in the manufacturing project, activation through chemical etching tends to lose ground. The single step pulsed laser activation marketed under the name PROTAL[TM] has been developed and it is partially used in APS spraying [55], although the high costs attached to this method though make it less attractive in the industry.

The most used activation method, grit blasting, uses grits (metal grits of steel or cast iron of irregular or spherical shapes or ceramic particles with irregular shapes) agglomerated in a nozzle, accelerated in an air stream and projected towards the substrate surface.

Table 2.2 Substrate roughening grit size recommendations [26]

Grit	Grit size (µm)	Application
Coarse	-2000 +600	Best adherence coatings, thicker than 250 µm
Medium	-1400 +425	Fair adherence coatings, smooth surface, thinner than 250 µm
Fine	-600 +180	Coatings used in as-spray condition, thinner than 250 µm

The substrate roughening grit sizes recommended by the reference book of *Pawlowski L.* [26] can be consulted in *Table 2.2*. Although European standards like DIN EN ISO 13507 [56] or EN ISO 12679 [57] suggest only that the roughness of the surface should be decided by all the involved partners and permanently controlled, the American Navy Standard MS 2138 [58] recommends values in the range 70-100 µm to favour a good adherence. Successful DOE methodology was also performed by *Varacalle et al.* [59] in order to determine the best grit blasting material and to determine the optimal roughness for a certain application. *Bobzin et al.* [60] investigated the effect of different parameters (particle size, blasting angle or distance) while three grit blasting materials (aluminium zirconia, steel shot and corundum) are impacting the substrate. Some of the conclusions were that the distance between the mean width between the peaks of the elements is not constant and should not be taken into account, the air pressure greatly influences the particle velocity and consequently the surface roughness, and the durability of the steel shots and aluminium zirconia is superior to the ones of alumina). On the other hand, *Begg et al.* [61] concluded that for their study, when using a mechanized robot for grit blasting, the flow rate and stand-off distance have little effect on the Ti-6Al-4V substrate roughness. Recent research [62] determined that superior contact angle and adhesion was obtained for Mo particles hitting the environmentally friendly dry-ice sand blast as it roughened the Al and steel substrates.

Looking at the numerous standards and studies about pre-processing and the preparation of substrates before coating, the importance of the process in order to obtain satisfying products appears clearly.

2.3.   Fundaments and techniques of post-spray processing

Post-spray processing has been identified in the last two decades [63] as an important factor for obtaining quality in the coatings industry. In response to a need to standardize the numerous developed techniques, the first norm of post-processing technologies in thermal spraying was created in 2002. For this reason, corroborating the DIN EN 14924 [64] standard and other reference books in the domain of thermally sprayed coating [26,65], the main identified techniques of post-treatment and finishing are:

- Mechanical finishing
- Sealing
- Heat treatment (electromagnetic remelting, furnace remelting, combustion flame, hot isostatic pressing)
- Other processes (chemical transformation, paintings, diffusion annealing, friction stir processing, laser engraving, sol infiltration).

Mechanical finishing in thermal spraying is not unusual, as the roughness of the coatings in the as-sprayed state can fluctuate generally between 3 μm and 40 μm [6,65,66]. Turning and grinding are also used to bring a part to specific tolerances, the application being the determining factor for the finishing process. Mechanical finishing is also used to bring the final part to a specific roughness. The challenges during the finishing processes can arise from: a porosity that can lead to pull-out of the coating, debonding caused by the lamella structure of the coating, lower machinability of some hard materials like cermets or penetration of coolant towards the substrate [65]. The companies or institutes have also to take care of the mechanical properties and the corrosion and wear behaviour as they can be altered through mechanical finishing. The presence of slight defects on the surfaces can lead to penetration of liquids in the coatings, which can create surface corrosion. Some defects can be repaired by using sealing materials. Sealing materials are generally in a liquid form and they can be simply applied on the coating [65]. The sealer solidifies immediately on the piece. The most used organic sealers in the industry are: epoxy, phenolic or silicone resins, polyurethanes or waxes. [67]. Inorganic sealers like aluminium-phosphate or sol-gel techniques or impregnation can be also used, but they are employed mostly for high-temperature applications.

The electromagnetic heat treatment is usually subdivided into: laser remelting, electron beam remelting, TIG remelting, spark plasma sintering and microwave [26,65]. However, as laser and electron beam remelting are the most widespread, only these processes will be briefly described. Laser remelting is employed because of the possibility to control the heating and the melting. The coatings are further built up by a one-step laser deposition technique (1SLD). The powder is melted and forms a coating similarly to the plasma transferred arc technique [68]. One of the most popular developments of 1SLD is the rapid prototyping [26]. Applications for 1SLD come from corrosion and wear resistant, biomedical or thermal barrier coatings and remelting became extremely employed in the industry. Electron beam is employed in the industry due to the unique possibility to treat spot sized areas [69]. The generation of a small sized electron beam is nevertheless extremely expensive and requires high vacuum ($<10^{-4}$ Pa). Therefore, it is less used on a large scale. The technique is sometimes found in the areas of high power industries, semiconductors, machining or drilling applications [70].

Furnace remelting is an important technique for material fusion. It is employed in specific industries, and it presents advantages but is also challenged by several problems [6]. Furnace remelting playing an important part in the present work, a detailed overview of the technology will be presented in the following subchapter.

Combustion flame remelting is largely used for self-fluxing Ni-based and Fe-based self-fluxing coatings [26,71,71–73]. The treatment is carried out at temperatures about 1300 K depending on the chemical composition of the material [26]. Oxyacetylene or propene are often used as gases. The torch is heated up and travels over the part multiple times depending on several parameters like the geometry of the part or the thickness of the coating [65]. Sometimes, the component can be preheated up to 760-870 °C [65]. An important aspect and a challenge of the process is the temperature control [6].

Hot isostatic pressing (HIP) is a technique that requires a simultaneous usage of temperature up to 2000°C and pressure that can reach 200 MPa. It can be employed both as a manufacturing or post-processing process. An advantage of HIP is that highly complex shaped products with homogeneous densities can be manufactured [74]. The applications in HIP are in the area of diffusion bonding, powder metallurgy healing of castings or coatings. In thermal spraying, HIP is used as a post-processing technology and it can influence pore size distribution, physical properties and microstructure of the coatings or can eliminate cracks. HIP can be used for the post processing of several materials like hydroxyapatite, TiAlV alloys, ZrO_2 or TiB_2 [75–78].

Less commonly used post-spraying processes include: chemical transformation, paintings, diffusion annealing [64], friction stir processing, laser engraving or sol infiltration [65]. The so-called chemical transformation process after DIN EN ISO 14924 [64], is a technique employed for esthetical purposes where metallic, thermally sprayed coatings can be chemically treated. By spreading with suitable solutions, a colouring of the metallic sprayed layer can be achieved. Although close to the methods previously described, the painting is meant to both improve the visual aspect and increase the corrosion protection of coatings [64]. According to EN ISO 12944-5 [79] for aluminium sprayed coatings that have in their composition organic components, the painting must be applied within four hours after thermal spraying. In special circumstances, thermally sprayed coatings can be post-processed by diffusion annealing, an adhesion by diffusion takes place between the coating and the component material. The process should be carried out in a vacuum chamber or in a controlled inert gas atmosphere to avoid oxide formation in or on the coating. Friction stir processing (FSP) can be placed in the category of solid state thermomechanical surfacing process. The principle in FSP is that a pin is rotated along a specific path on the surface of the component. Heat is therefore produced and the surface of coating is plastically deformed from the pin action. Microstructural and grain, homogenization or mechanical properties changes occur at the surface of deposited coating [80]. FSP is nevertheless a niche technology and its usage in the industry is limited. By laser engraving, specific patterns can be produced on APS ceramic coatings by vaporisation on specific places on the surface [81]. CO_2 laser is the most employed in the industry [65]. Research on APS sprayed Al_2O_3-Cr_2O_3 coatings deposited on Al_2O_3 was performed by *Marple et al* [82]. The coated specimen was immersed in 25% Si_2O_2 ethyl silicate solution. Remarks regarding the sintering stresses on cracking behaviour of coatings designed for elevated temperature environments were made.

Norms and well-known books in the industry deal with post-spraying processing of coatings. Some of the techniques are extensively used in the industry

like mechanical finishing, electron-beam or flame spraying remelting and others like sol infiltration or laser engraving are less common. However, each of them can be crucial to obtain a good quality coating for a certain type of material.

2.3.1. Vacuum furnace treatment

Although the etymology of the word *vacuum* is originating from Latin meaning „empty" or „empty space", such a concept in science cannot be produced nor exist. In technology, a space is considered „vacuumed" when it has a highly reduced gas density. Such a space is achieved by removing through a pump system the air and other gases from the space that as to be vacuumed. The quality is quantified by the degree of gas density reduction [83]. Terms like „controlled" or „protective" are also often used. They come from the fact that the atmosphere is characterized by its contamination level. The classification of vacuum quality is shown in *Table 2.3*. In the steel industry, the practice shows that a vacuum level of 1.3 Pa to $1.3 \cdot 10^{-1}$ Pa is sufficient [83].

Table 2.3 Pressure ranges of each vacuum quality

Quality of vacuum	Pressure range (Pa)
Low vacuum	$1 \cdot 10^5$ to $3 \cdot 10^3$
Medium vacuum	$3 \cdot 10^3$ to $1 \cdot 10^{-1}$
High vacuum	$1 \cdot 10^{-1}$ to $1 \cdot 10^{-7}$
Ultra high vacuum	$1 \cdot 10^{-7}$ to $1 \cdot 10^{-10}$
Extremely high vacuum	$<1 \cdot 10^{10}$

In spite of the fact that vacuum furnaces were created for electron tube materials and refractory metals in the aerospace industry, the technology extended in brazing, sintering, thermochemical treatments or diffusion of metals.

Vacuum treatment has some specific advantages [84,85] like:
- Keeping a clean surface and preventing partial oxidation or decarburization
- Adding a substance to the surface of the part resulting in a thermochemical process
- Removing contaminations like residual traces from fabrication
- Joining possible components like metals, coatings by brazing or diffusion bonding
- Removing O_2 diffused on metallic surfaces.

In spite of all the benefits, the operation of vacuum furnaces can be complicated and unwanted effects can occur such as accelerated diffusion or evaporation of volatile alloying elements [86]. Another drawback is that heat can be transferred only by radiation and not through conduction, thus the treated parts will get warm and cool down slowly and unevenly [86].

2.3.1.1 Comparison of atmosphere and vacuum heat treatment

The clearest differences between atmosphere and vacuum heat treatment probably lie in the cleanliness and impact of the environment on the parts during post-processing. In the majority of the heat-treating techniques, a reaction takes place between the part to be treated and the normal atmosphere. In order to reduce and eventually eliminate such reactions, heat treatments in the presence of inert gases can be performed. The dependence of the level of oxygen in an inert gas environment furnace can be seen in *Figure 2.6.*. When examining the atmosphere in a vacuum furnace at medium vacuum quality of 0.1 Pa it was observed that less than 0.1% of the air was still present [85].
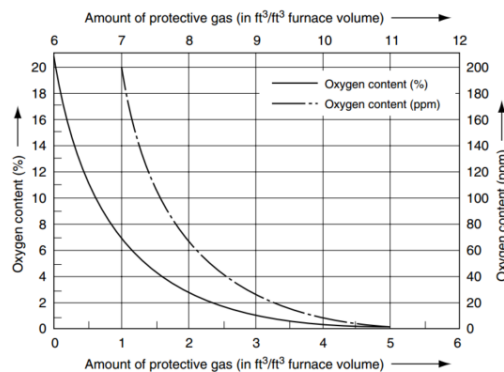
Figure 2.6 Oxygen level reduction in a vacuum furnace by purification with the aid of controlled atmosphere [83]

Vacuum furnaces do not create fumes or other gases, don't involve flames and are generally cold. The visual aspect of a treated steel part is distinct as well. Parts submitted to atmospheric heat treatment have different colours while the ones treatment in reducing atmospheres remain shiny, smooth and bright. The difference is due to the low levels of pressure accomplished in a vacuum atmosphere, resulting in oxide reduction on the surface. A controlled atmosphere furnace can additionally carry out thermochemical treatments. Employing gasses that create high mass transfer like propane, ethylene or acetylene, certain surface modification can be performed [87].

2.3.1.2. Vacuum furnace equipment

Although conventional atmosphere furnaces can be adapted with additional parts to develop vacuum for purposes like heat or thermochemical treatments, equipment especially designed for this purpose is generally employed. Vacuum furnaces can be broadly categorized in: hot wall (without exterior wall cooling) and cold wall (with cooled walls) [88]. Vacuum furnaces can be also classified by their design: top-loading (pit), bottom-loading (bell), or horizontal-loading (box) furnaces [85].

Vacuum furnaces are machines with complex components and detailed descriptions and proper selection of parts can be done using valuable literature like *Hoffman et al.* [89], *Fabian* [90] or the handbook of *ASM* regarding heat treatment [85].

Regardless of the type of furnace, every piece of equipment should consist of:
- A chamber with opening for a proper vacuum generation
- A vacuum pumping mechanism
- Components that can handle various temperatures, heating and cooling rates
- Precise tools to observe, check and control data from the furnace.

Hot wall furnaces have been the first designed. The entire vessel system in this type of furnace is heated by external means, using either burners or electric parts [90]. Bell or pit type furnaces have been progressively replaced in the industry because of their limited capabilities and notably their incapacity to realize significant progress in the temperature range, to heat or cool quickly and to generate high vacuum. [85]. Nevertheless, when working with temperatures that do not exceed 900°C and with heating and cooling rates that don't need to be fast, those types of items can be employed. One application can be found in the copper industry where coils, sheets and wires are annealed in such furnaces [88].

By far the most widely employed, the cold-wall furnace features vessels that are water-cooled, which maintains through the whole system excepting the chamber at ambient temperature. As the vessel is not affected, this type of units can be particularly adapted for big parts and high operating temperatures. In this type of furnaces, the heating and cooling can be precisely controlled. A lot of progress has been made in the cooling of furnaces by increasing the amount and velocity of inert gases, which can evacuate the hot gasses filling the chamber [90]. The cold-wall furnaces can be further split in batch and semi-continuous. In the batch type furnace, the piece stays in the chamber during the treatment. The semi-continuous furnace has the possibility to move the part in the vacuum between different chambers. In the batch one, extremely high heating rates and temperatures can be used, the heat being almost fully transferred by radiation. Batch cold-wall vacuum furnaces have some advantages like reliability, repeatability, effortless control of the environment or capacity to treat alloys without creating oxides. Semi-continuous furnaces are more complex structures with several chambers, each of them having usually their own pump and a carrier system. They also offer advantages like higher productivity, longer life cycle, and automatized process. The selection of the proper equipment for each university, institute, company and application is an important decision as such a unit is usually a costly investment. Where a high volume of similar or identical parts needs to be treated, a semi-continuous furnace may be advisable. For testing, single-piece lots or laboratory purposes, a batch type equipment may be more suitable.

Design considerations have to be also taken into account like part geometry or the size of the equipment. Just like any other complex machinery, furnaces need as well regular maintenance. In a modern piece of equipment, plenty of sensors are installed to avoid operating it when damaged for both safety and prevention of permanent damage. Nevertheless, it is important to regularly check the parts of the apparatus for leaks or dirt that could contaminate the vacuum pump.

As the application range of the technology greatly widened in the last decades, numerous standards are recommended when using a vacuum furnace (regarding the pumps, valves, vessels, insulations, *etc.*) [91]. Among the numerous norms developed in the fields, documents like DIN 28400 [92] dealing with definitions, units, basic principles, components, accessories or DIN ISO 10012 [93] concerning the quality assurance can be considered as reference literature. Regarding recent performed research, a high temperature cold-wall vacuum furnace was one of the pieces of equipment used by *Pascal et al.* in the brazing area to study the

electrochemical corrosion behaviour of W-Co-NiP and the characteristics of WC-Co-NiCrBSi functional coatings deposited on a 16MnCr5 steel substrate [94,95].

2.3.1.3. Future of the vacuum technology

A growth of 6% in the vacuum industry is forecasted in the following years. An increased use of the technology in the copper processing industry in nations such as India and China has been reported. Due to the absence of emissions during the operation, the vacuum furnace heat treatments are used by more and more nations to reduce their environmental footprint [96]. Leading technological vendors like ALD Vacuum Technologies, Ipsen International or Seco/Varwick offer a wide range of solutions for almost any type of applications. Stimulated by the economic health of this sector, technological developments are continuously made. For example, in 2016, *Liang* filled an application for patent that has not approved yet [97] for a new type of gas discharging nozzles that can be arranged in several rows for cooling the vacuum furnaces. Using a finite element method (FEM) simulation, *Xaohua et al.* recently proposed [98] a model for an approximately 1 m^3 vacuum furnace tested at a temperature of 835 °C that can improve the volume of heating zone and temperature uniformity, therefore enhancing the production efficiency. Scientific reviews state forecast increase in furnace life cycle, reduction in energy consumption and production costs [99,100].

2.4.   Design of experiments in thermal spraying

As in any industrial process, in thermal spraying finding the right parameters for a given operation is a crucial step to ensure the effectiveness and maximize the win of the commercial entity. The design of experiments (DOE), introduced for the first time by *Fisher R.A.* [101], is an approach in which through the control of one or more input parameters a mathematical output model helps the optimization of an analysed process [102]. In DOE, the resulted prediction aims at controlling the initial working parameters. For this to happen, a calculated number of experiments have to be run before reaching the optimum values. The statistical approach strongly concentrates on ensuring validity, reproducibility and reliability. DOE is used in research and industry in the fields of natural or social sciences, marketing and engineering and research to both optimize systems and learn how they are working [102]. Models are currently generated through dedicated software where it is generally required to go through certain well-defined steps in order to reach a solution. The general steps of an optimization model are represented in *Figure 2.7*.
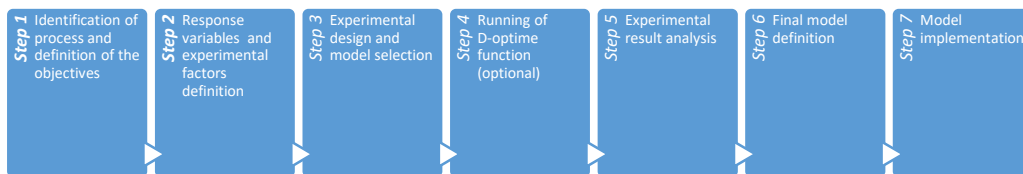
Figure 2.7 General steps needed to undergo in a typical DOE analysis

The programs greatly rely on theoretical models that were continuously developed through the last decades, the most notable improvements being brought

by *Fisher R.A., Taguchi G., Montgomery D., Myers R., Box G., Hunter W., Hunter J.S.* and *Barrentine L.B.* [101–106].

DOE is considered as an important optimization method in thermal spraying [107,108]. As it makes it possible to take into account several factors and analyse their interactions, it doesn't carry the same limitations as classical optimization models varying a single parameter. In the coating technology, as in any model design, the first step is to define the object. Several optimizations can be done in this field starting from material loss, coating properties or post-processing and finishing. In thermal spraying, it is not uncommon to find as many as 50 parameters to analyse and vary [109]. Input variables in thermal spraying can relate to:

- Process: feed rate, spraying distance, gas stoichiometry or flow rate [26,110]
- Material: size distribution of powder, morphology, internal porosity [111]
- Post-processing: temperature, time.

Through a polynomial regression equation the properties of coating (responses) take the following mathematical form [102]:

$$Y = b_0 + \sum b_j X_j + \sum b_{ij} X_i X_j + \sum b_{ijk} X_i X_j X_k + \varepsilon \tag{2.4.}$$

i, j, k representing the number of variables, b_0 being the mean of all responses of the experiment, b_0, b_{ij}, b_{ijk} being the regression coefficient that represent the effects of the X_i, X_{ij}, X_{ijk} variables and ε a general error of the equation.

After defining the input and response variable the model design has to be chosen. The models and experimental plans that can be employed [112] are summarized in *Table 2.4.*

Table 2.4 Design selection guideline

Number of factors	Comparative objective	Screening objective	Response surface objective
1	1-factor completely randomized design	-	-
2-4	Randomized block design	Full or fractional factorial	Central composite or Box-Behnken
5 or more	Randomized block design	Fractional factorial or Placket-Burman	Screen first to reduce number of factors

The types that are the most used in thermal spraying are [111]:
- Placket-Burman screening design
- Two-level full (2^k) and fractional (2^{k-m}) response surface objective factorial designs
- Other response surface methodology (RSM) designs.

The Placket-Burman (Hadamard) optimization method is done by varying a large number of X_i factors (*i>4*) that can influence the *Y* response. To the factors are generally attributed minimum and maximum correspondents (-1 to 1) [105]. To find the influence of the factors, a first degree polynomial degree equation is usually performed [111]:

$$Y = b_0 + \sum b_i X_i \tag{2.5.}$$

Ramkumar et al. found out with the aid of a Placket-Burman design that for a Ti-6Al-4V/10B$_4$C sintered composite the specific wear rate of the alloys is at the lowest value with 10% B$_4$C and is decreasing with the increase of the wt. % of the reinforced particles [113]. On the other hand, Thirumalaikumarasamy et al. concluded on the base of a constructed screening objective design model that for plasma sprayed alumina coatings on AZ31B magnesium alloy, the plasma input power has the biggest effect on the Young's modulus proceeded by the stand-off distance and feed rate [114].

By far, the most employed category of designs in the applicative area is the RSM one. The response surface methodology represents a group of techniques used to improve, develop and optimize processes [104]. As the effect of input variables is used to measure certain characteristics of a product or process, the RSM design constitutes the most important optimization class of models. The response function Y, which can take a complicated form correlating the input and response variables, can be mathematically described as [104]:

$$Y = f\ (X_1, X_2, \ldots, X_k) + \varepsilon \qquad (2.6.)$$

defining X as the process variable and ε as general error of the equation that can represent mismeasurements or sources of variability not attributed to the Y function. The Box-Behnken and two-level full factorial (2^k) and full fractional (2^{k-1}) are typically operated in the optimization in the thermal spraying field.

The Box-Behnken design incorporates the middle points of a k factor cube. Such centre point is needed for the orthogonality of the design and in this way a better standard deviation is obtained, which reduces the error degree in the process. A Box-Behnken design was carried out by Liu et al. [115] to investigate the influence of the argon and hydrogen flow rate and the arc current on the velocity and temperature of La$_2$Ce$_2$O$_7$ thermal barrier coatings during supersonic atmospheric plasma spray. Both Rico et al. [116] and Salavati et al. [117] used as well the same design to find the best possible results for their analysis. The latter researched the effect of the gun parameters and the powder spray conditions during a twin wire arc spray process for the production of porous metallic coatings. Therefore, it was concluded that for a wanted porosity of 20% a voltage around 28 V was needed and a polyester feeding rate of 26 l m^{-1} was recommended.

The two-level full factorial design (2^k) is employed to assess the interaction between the X_i and X_j factors from the polynomial regression equation. Using this solution, Candidato et al. determined the optimal spray parameters for hydroxyapatite coatings deposited by solution precursor plasma spraying (SPSS) on sandblasted stainless steel [118]. The research established that the surface temperature determined greatly the coatings crystallinity and that the spray distance affected the most the temperature during the deposition. For the two-level full fractional design (2^{k-m}), the number of runs is incremented by the increase of k [111]. If a big value of k is employed it might make it necessary to run a large number of experiments. Nevertheless, by running a D-optime function, a part of the runs can be eliminated by using a specialized software. In this way, a higher effectiveness of the design is obtained. This type of model also helped Rico et al., who used a full fractional design to optimize the process parameters of APS sprayed Al$_2$O$_3$-50wt%Cr$_2$O$_3$ coatings [116]. Using a (2^{k-1}) fractional design with k=6 it was reported that by operating with high power of the equipment, coatings with an agglomeration of hard phases, high hardness values, but a short life cycle are obtained. When operating with low power values, small hardness is achieved but more durable coatings are reached.

Selecting the right design model is important in order to understand the problematic, to realize the correct dependencies between the input and response variables and to generate valuable data for further analysis. The data generated by the attributed design model can take the form of an analysis of variance (ANOVA) table, Pareto chart, correlation matrix or different kind of plots (power, variance dispersion graph, fraction of design space, desirability or prediction variance or profile). In the field of thermal spraying ANOVA tables, Pareto charts, desirability, deviation or perturbation plots are frequently used [113–118] in the optimization of different parameters like deposition of the coatings, influence of different reinforcements on the matrix or certain applied post-processing.

2.5. Theoretical aspects regarding the materials

As presented in the motivation, the work concentrates on thermally deposited fused reinforced self-fluxing alloys. Considering this aspect, the dissertation will focus from now on less on general theoretical principles and more on the specificities of the topic.

2.5.1. Substrate material

A long list of materials can be used as substrates starting from wood, paper or glass and ending with more conventional ones such as metals or metal alloys [37]. The present work will focus on metallic substrates. A good knowledge of the alloy is essential in order to select and perform an appropriate pre-spraying treatment.

Several material properties have to be taken into account when selecting and preparing a deposition. Substrates which do not exceed 45 HRC can go through the common standard procedure of cleaning, roughening and spraying. For materials surpassing the hardness value of 40-45 HRC usually a common grit blasting is not enough and depending on the application special procedures should be implemented [37]. As in brazing, more complex metallurgical reactions happen and the adhesion can become problematic [119]. These metallurgical bonds during the process can create defects like internal stresses or micro-cracks. Another important factor that has to be kept in mind is the coefficient of thermal expansion (CTE). The big difference between the CTE of the substrate and the coating can influence the quality through residual stress generation. Materials like steel or Cu, Ni, or Co alloys are considered easy to use as a substrate. Al, W and Mo alloys are materials considered of medium difficulty to be used as substrates whereas materials considered difficult are ceramics, glasses or for example Ti or Zr alloys [119].

More attention should be paid when handling materials that are susceptible to oxidize quickly. In this situation, the preheating of the substrates should not exceed 65°C and an immediate spraying should be performed. Components that are casted, sintered or produced through methods that may induce internal porosities need to be specially cleaned.

Little attention is paid in the research field to the substrate. Most of the research in the substrate-coating region is given to grit blasting, splat formation or blasting methods [59–62]. Nevertheless, for W coatings deposited by APS and vacuum plasma spraying (VPS) *Kovářík et al.* recently concluded that the substrate influenced the porosity, the hardness and the thermal conductivity of the coatings [120].

2.5.2. Coating material

There are several methods for classifying coating materials. The first categorization of coating materials can be done according to the form of the materials to be deposited: powder, wire, suspension, and solution [25]. The characterization and the technical supply of powders is normed through ISO 14232-1 [121]. Another classification regarding the importance of spraying powder properties depending on the spraying process and material group [121,122] is presented in *Table 2.5*:

Table 2.5 The importance of spraying powder properties in regard to the TS process and material group

	Chemical composition	Powder size distribution	Powder form	Bulk density	Flowability	Microstructure	Phase composition	Working temperature
Pure metals (Mo, Ni, *etc.*)	+++	+++	++	+	+	-	-	-
Metallic alloys (self-fluxing, MCrAlY, *etc.*)	+++	+++	++	+	+	-	+	++[3]
Carbide-metal composites (WC-Co, *etc.*)	+++	+++	++	+	+	++	++	-
Oxides (AlO$_3$, Cr$_2$O$_3$, *etc.*)	+++	+++	++	+	+	+	+	-
Organic materials (ethylene, *etc.*)	+++	+++	+	++	+	-	-	++[1]
APS/VPS	++	+++	++	-	+	-	++[2]	-
FS	++	+++	+	-	+++	-	-	+++
HVOF	++	+++	+++	++	+	-	++[2]	+

+++	highly important
++	moderately important
+	less important
-	without importance
[1]	during the usage of organic materials, the decomposition temperature, the oxidation resistance of the melt and the toxicological behavior has to be particularly considered
[2]	exact required information at deposition of carbides and oxides
[3]	for self-fluxing alloys

Probably the last important method of classification can be done according to the properties that will be needed from the coatings when implemented [6]. The coatings during operation can be damaged caused by abrasive and adhesive wear, atmospheric and immersion corrosion, cavitation, electrical resistivity and conductivity, fretting, hard bearings and surfaces, heat and oxidation, machine element clearance control, or particle erosion. Considering the large number of damage possibilities, knowing the field in which the coatings will be used is extremely important.
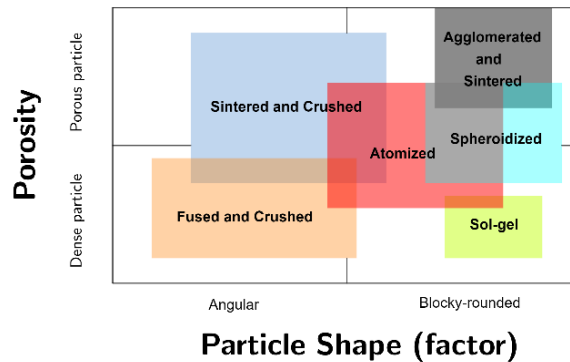

Figure 2.8 Powder characteristics, porosity and shape as a function of their manufacturing process [22]

The production of the powder is a very important aspect when choosing the depositing materials. Some very important characteristics like density, shape, fineness or porosity are defined during the fabrication process. The main technologies are presented in *Figure 2.8* [22]*.*

The usual manufacturing process for a powder is seen in *Figure 2.9* and can be split in five big steps: manufacturing, particle size determination, blending, quality control and packaging.

A normal range of powder size produced through the techniques mentioned above is between 5 μm and 120 μm depending on the application [6]. A particular attention will be given to atomisation as the Ni-based powders are produced by the main vendors through this process [123–126]. However, the other main processes will be briefly described as well. Crushing and milling have mostly the purpose of breaking a bigger particle into smaller ones through a mechanical force. Usually, the resulted material has an irregular shape, which could lead to flowability problems in the feeder. This process can be applied to brittle materials, for example ceramics or oxides. Sintering is a process of compacting a material under pressure and temperature. The sintering temperature does not reach the melting point of the material. The internal porosity of the material decreases using this process. Powders with a high melting point like tungsten or molybdenum alloys can be fabricated through this process. Agglomeration is a technique consisting in introducing in an atomizer raw powder, a binder and water. Through a drying under heat, the water evaporates and the powder is formed. Materials like oxide alloys, nitrides or cermets can be produced. Spheroidization can be used in combination with other processes to create a better flowability of the powder in the feeder and to create a homogeneous melting of the particle. The spheres however need to be optimized to avoid formation of internal porosity. The sol-gel is a chemical process during which a solution enables reactions subsequently forming distinct particles. The technique is used to form ceramic powder, mainly oxides.

Mechanical alloying is also a relatively novel method. As it is used to obtain smaller quantities, especially in research and laboratory work, this method is not integrated in *Figure 2.8.* Alloys and mixes of cermet and composite structures can be produced. In a special equipment, heat is formed allowing the particles to plastically deform [26]. There, it is possible to obtain agglomerates with a distinct lamellar geometry.
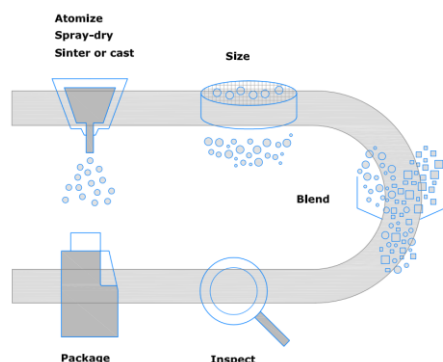

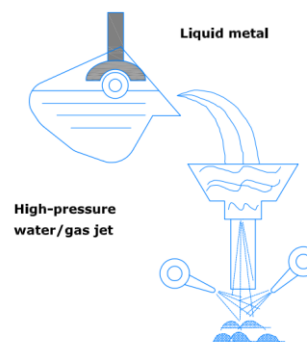Figure 2.9 Usual manufacturing steps for a powder

Figure 2.10 Schematics of the atomisation production process

As previously mentioned, the atomization process is used by large vendors in the TS industry to produce Ni-based powders. Schematized in *Figure 2.10* the technology is split in four categories: gas, water, centrifugal and mechanical atomization. Out of these, by far the most used are the gas and water ones. The two processes work with the same principle, in which a liquid material stream is broken into small pieces with the help of either a gas or a water jet. The water atomization gives to the particles an irregular geometry unless a large degree of heat is given to the metal, whereas the gas atomisation tends to form spherical particles. Regarding the size of the particles, the process using water results in coarser dimensions between 150 μm and 250 μm while the process using water results in coarser powder sizes between 25 μm and 100 μm. The water atomisation is advantageous when a fast production is necessary. However, the gas process results in a very clean powder, especially when an inert gas is used. This technology is employed especially for reactive materials like titanium, titanium alloys but also for other composites like cobalt-chromium, nickel-chromium, copper, or aluminium. Recent research [127] in the production of NiCrBSi powders showed that a high cooling rate using gas atomization formation of unstable Ni-based phases may be possible.

Characterization of particles is also an important step of quality evaluation. Numerous methods have been developed like powder sampling, particle size determination by image analysis or sieving, scanning methods (stream or field) [128], surface area determination, or pore size and distribution [129]. US standard guides for powder particles [130] or test methods for particle size analysis are also available [131].

An important feature to consider is also the powder feeding of the material as it can decisively influence the coating quality. Although spheroidized powders generally have a good flowability, feeding irregular shaped powder in an improper feeder can create problems. A normal feeder hoper can carry usually 10 kg of powder but if the worker happens to create saltation (overloading of the feed tube) an obstruction of the system would be caused. Another example of harmful matter could be caused by an overdose of the carrier gas.

The potential negative impact of the size and chemical composition of the particles should also be stressed. Once inhaled, a penetration in the tracheobronchial tree is possible. The exposure to powder feedstock and subsequently dust are the most dangerous for the human health [22]. A recent study of *Viana et al.* showed concentrations of ultra-fine powders intakes among the employees in the case of atmospheric plasma spraying, which unfortunately did not decrease significantly outside the workplace. Health protocols with special attention to powder are recommended [132]. *Galey et al.* proposed in 2018 an approach regarding aerosol measurement for engineered nanoparticles [133]. The method combines several factors including real-time measurements, particle sampling or development of safety measures.

Ni-based powders and coatings, have as any complex structure plenty of particularities to take into account. The heating of the alloy can produce phase changes in the coating and can create fusing problems or undesirable influence of elements on the final product.

Self-fluxing alloys, derived from the Latin *flux* meaning flow, contain elements that help purifying, deoxidizing and cleaning the materials. The known self-fluxing alloy categories are Fe-based, Co-based or Ni-based [138], [139]. By having in the composition elements like boron or silicon which, when exceeding 1.5% alone or in combination help pushing oxides trapped in the coating towards the surface [6]. Boron and silicon in combination, depending on their quantity in the chemical

composition, can help lowering the melting temperature by a few hundred degrees [6]. Boron can as well aid act as hardener for Co- and Ni-based alloys. Like in many applications, chromium is added to improve the wear and corrosion resistance of the alloy.

The as-sprayed alloy is not employed in the industry as it presents a high and interconnected porosity, low adhesion, weak particle cohesion and poor corrosion and wear resistance. Hence, post-processing techniques like fusing and mechanical finishing are widely performed. The fusing process for the Ni-based alloys starts at 760-870°C [136], reaching the range of 1000°C-1120°C [6,136–138] in order to obtain satisfactory properties. The temperature control is crucial to obtain good results with the coating. The high temperature helps creating metallurgical diffusion that significantly increases the bond strength in the coating-subtrate region. Another advantage of the fusion, regardless of the temperature is the effect of oxide removal towards the surface. A CrBFeSiCNi alloy in which Si and B are used as deoxidizers results corresponds to an equation that could take the following form [136]:

$$(FeCr)_x O_{x+y} + 2B + 2Si \rightarrow xFe + xCr + B_2O_x + B_2O_xSiO_y \qquad (2.7.)$$
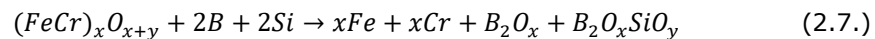
The resulted $B_2O_xSiO_y$ borosilicate during the fusion process is brought to the surface and is usually removed by mechanical finishing. The mechanical post-processing processes aid as well in the hardness of the coating [139].

As any process, the fusion as well has drawbacks. When a complete melting, fluxing or wetting is not reached, a so-called "under-fusing" can happen. Overheating or under-fusing are negatively affecting porosity and are particularly likely to happen when working with large parts. A high content of lead, sulfur or selenium in the base material are usually causing porosity related problems as well [66]. A failure of match in terms of expansion coefficient between the substrate and coating can lead to cracks. As for any thermal spraying technology and material, in self-fluxing alloys as well, cracks are formed when the coating is brittle. A certain control of crack propagation can be achieved by uniform heating and cooling.

Material inhomogeneity and residual porosity can be eliminated by a solution proposed in the patent of *Harada* and *Shin* [140] which consists in coating a second coating on top of the already fused self-fluxed material. Therefore, the material can produce better results and the uniformity of the coating by eliminating the rest of the oxides and pores can be improved. Laser-selective fusion of self-fluxing Ni-based alloys using diode lasers recently performed by *Chun et al.* [141,142] show that Cr_5B_3, M_7C_3 or $M_{23}C_6$ type carbides and borides form in the coating microstructure and improve the hardness of the part.

The phase composition is strongly linked to the chemical composition of the material, the fusing process and the temperature control of the post-processing. The generation of the binary and ternary systems, which are further presented, have a base in the so-called "CALPHAD method" [143]. Using this methodology, parametric equations are used to represent the Gibbs energies of the phases. Crystallographic information and thermodynamic parameters are used to identify the phases, potentials or enthalpies. All the identified phases are represented in the situation in which the system contains equal concentrations of Cr, Ni and B.

The Ni-Cr-B alloys are a major interest group in the self-fluxing and brazing research. Looking at the partial reaction scheme represented in *Figure 2.11* [144], one can observe that around 1025°C the Ni, Ni_3B and CrB solid solutions start forming. At 1050°C the solid solution starts melting. Reaching the 1096°C point, formations of L+Cr_5B_3+CrB (L standing for liquid) or liquid Ni_3B+Ni_2B+CrB can be observed.

Reaching the temperature of interest of approximately 1100°C a liquid solution of Ni_3B+CrB can be found. Going further the CrB phase transforms depending on the temperature in Cr_5B_3, Cr_2B turning at about 1250°C into a solution of Cr_2B and Cr. Ni splits from the Ni_3B phase 1200°C, remaining alone in the melt. One should take in account that adding Si and B in the self-fluxing alloy and remelting it, a coating shrinkage up to 20% can be produced [6,66,136].

The isothermal B-Cr-Ni diagram in *Figure 2.12* [144]*, shows the Cr_xB_y and Ni_xB_y type phases at 1000°C. This temperature is important as the fusing of self-fluxing alloys is performed around this value. One can observe that at approximately 60% at.% Cr the Cr_2B is formed and the important structures are highlighted until 20% Cr. Between the two phases highlighted other important ones like Cr_5B_3, CrB and Cr_2B_2 can be found. On the other hand, looking at the B interaction with Ni, at about 25% concentration of Ni, the Ni_3B solution is formed. All the important phases in the Ni-B interaction are formed until the Ni-B 50-50% ratio. Between these two values, in the ternary diagram phases like Ni_3B, Ni_2B are mentioned. No important phases in the Cr-Ni interaction are shown.

Cr-Ni	B-Cr	B-Cr-Ni	B-Ni
	2080 — p_1 : $l + CrB_2 \rightleftharpoons Cr_3B_4$	?	
	2050 — e_1 : $l \rightleftharpoons CrB + Cr_3B_4$	?	
	1890 — p_2 : $l + CrB \rightleftharpoons Cr_5B_3$		
	1850 — p_3 : $l + Cr_5B_3 \rightleftharpoons Cr_2B$		
	1830 — e_2 : $l \rightleftharpoons CrB_2 + (B)$	?	
	1600 — e_3 : $l \rightleftharpoons (Cr) + Cr_2B$		
1336 — e_4 : $l \rightleftharpoons (Ni) + (Cr)$		1258-1390 — e_5(max) : $L \rightleftharpoons (Ni) + Cr_2B$	
		1258 — $L \rightleftharpoons (Ni) + (Cr) + Cr_2B$ — E_1 ; $(Cr)+(Ni)+Cr_5B_3$	
		1220 — $L + Cr_2B \rightleftharpoons (Ni) + Cr_5B_3$ — U_1 ; $Cr_2B+(Ni)+Cr_5B_3$	
		L+(Ni)+Cr$_5$B$_3$; ~1110 — e_6(max) : $L \rightleftharpoons Ni_3B + CrB$	1111 — e_7 : $l \rightleftharpoons Ni_3B + Ni_2B$
		1096 — $L + Cr_5B_3 \rightleftharpoons (Ni) + CrB$ — U_2 ; Cr$_5$B$_3$+(Ni)+CrB	1093 — e_8 : $l \rightleftharpoons Ni_3B + Ni_2B$
		L+Ni$_2$B+CrB ; 1096 — $L \rightleftharpoons Ni_3B + Ni_2B + CrB$ — E_2 ; Ni$_3$B+Ni$_2$B+CrB	1035 — p_4 : $l + (B) \rightleftharpoons NiB$
		L+(Ni)+CrB ; 1050 — $L \rightleftharpoons (Ni) + Ni_3B + CrB$ — E_3 ; (Ni)+Ni$_3$B+CrB	1025 — p_5 : $l+Ni_{4-x}B_{3+x} \rightleftharpoons Ni_{4+x}B_{3-x}$
			1018 — e_9 : $l \rightleftharpoons Ni_2B + Ni_{4+x}B_{3-x}$
			1018 — e_{10} : $l \rightleftharpoons Ni_{4-x}B_{3-x} + NiB$

Figure 2.11 Partial reaction scheme of the Cr-Ni, B-Cr, B-Cr-Ni and B-Ni systems [144]
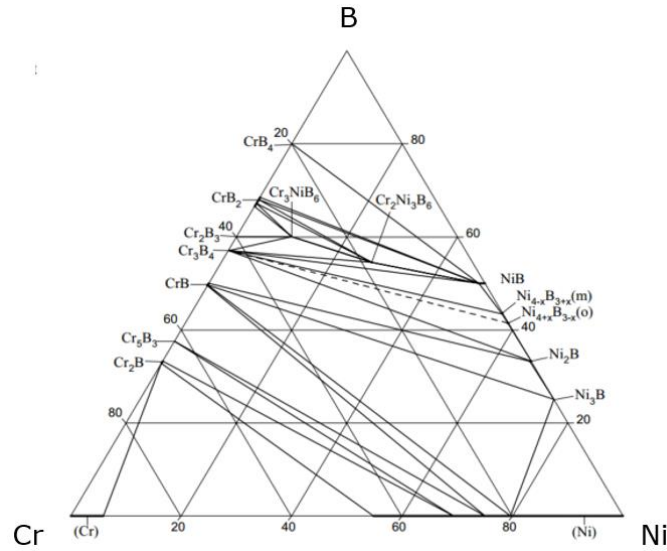
Figure 2.12 B-Cr-Ni - isothermal section at 1000°C [144]

Another important component to consider in the alloy interaction is Si. The Ni-Si phase alloy diagram is represented in *Figure 2.13* [145]. One can see that until 35% Si, phases like γNi_3Si, βNi_3Si, δNi_2Si are observed. At about 35% Si, the lowest melting point of the NiSi alloy is identified and after this point, Si rich phases start to be dominant. A Ni-Si phase diagram has been also calculated by the *Korea Research Institute of Standards and Science* [146]. Additionally, the institute identified the $Ni_{31}Si_{12}$ and θNi_2Si phases as well.
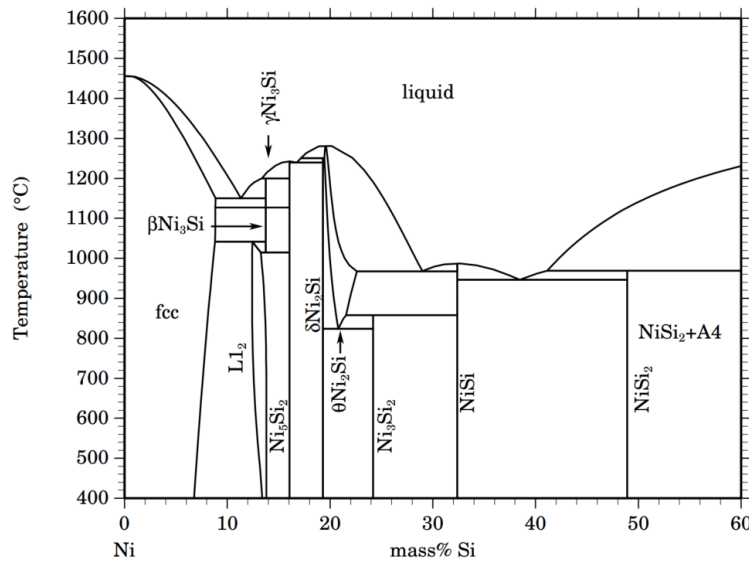
Figure 2.13 The Ni-Si binary system [145,146]

One should keep in mind that the partial reaction scheme and both binary and ternary diagrams are calculated in the situation in which the components have the same at.% proportions, namely B-Cr-Ni 33,3% in the three-component diagram and Ni-Si 50% in the two-component one. Nevertheless, the formed phases provide important information in the phase identification and analysis of alloys that are composed mainly of these elements.

Several researches confirmed the phases identified in *Figure 2.11, Figure 2.12* and *Figure 2.13.* As an example, for laser cladded samples produced by *Guo et al.* [147] for both self-fluxing and WC reinforced self-fluxing alloys the γNi, CrB and Ni_3B phases have been identified. When investigating the surface microstructure of flame sprayed NiCrBSi powder, Cr-B and NiB have been identified [148]. As a normal process when working under normal atmosphere, oxides like Cr_2O_3 or Cr-B-O can be found [148]. The γNi phase is predominant in the same work. A recently employed TEM mapping for a high Cr content self-fluxing sample produced through laser-assisted selective fusing performed by *Chun et al.* [142] revealed lamellar structures of Ni-based phases. High content of Cr and Fe have been as well detected. When looking at the microstructure analysed by the same group of authors [141] before the remelting process, non-homogeneity in the coating could be seen and Cr-based borides and carbides have been identified. After homogenization at 1150°C, the microstructure evolved into a lamellar one composed of γNi and Ni_3Si with smaller than <5 μm carbides and borides.

2.5.3. Reinforcing material

Composite materials are acknowledged to be a combination of two or more materials that partially or totally blend. The resulting material is heterogeneous although an interaction happens. A clear interface can be most of the time identified between the components that have separate properties (*e.g.* physical, chemical, mechanical) [6].

Particles and whiskers have been mainly introduced to reinforce the matrix material and increase properties and behaviours under different conditions. Some of the most used reinforcements are WC, Cr_3C_2 or TiC. Particles or whiskers can be blended with the base material through several methods *e.g.* mechanical mixes, coinjection, doping. The reinforcements can vary from 10% to 90%, the metal matrix becoming a binder.

For the thermal spraying technology, the manufacturing of reinforced composites through mechanical, thermomechanical or chemical means is possible**.** An exemplified process of a composite powder is illustrated in *Figure 2.14*. In the representation both matrix and reinforcement can be seen as separate structures.
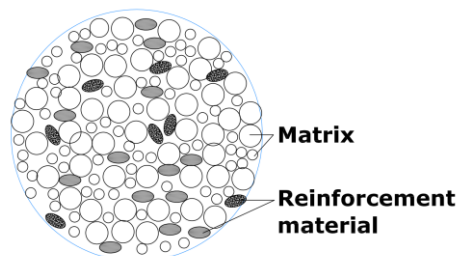

Figure 2.14 Representation of a composite powder

During the deposition and post-processing, phase changes are occurring in the structure, material properties and behaviour in different environments. Heterogeneous coatings can be also produced by material segregation during handling, shipping or equipment feeding [149]. Spheroidization, which can be performed through several techniques, can lead to numerous advantages in thermal spray. Some of the improvements are homogeneous melting, densification or flowability, all of them leading to a quality increase of the final product [150,151]. Another process to improve composite powder is agglomeration. Alloys can be agglomerated with organic binders to promote a better adhesion to the substrate [149]. Nevertheless, the agglomerates are affected by the viscous jets of the thermal spraying process, leading to powder breaking. However, powder agglomeration still retains a 4-8% of internal porosity [152]. The last composite powder production that will be considered here is performed at elevated temperatures and called SHS (self-propagation synthesis). The SHS process produces large bulk pieces that have to be further processed. Problems regarding the shrinkage or volumetric growth of powders such as TiC-Me still occur. The behaviour and its macrostructure have been recently studied by *Korosteleva et al.* [153]. Comprehensive overviews of the SHS manufacturing technique and power usage in the thermal spraying industry can be found in the recent scientific literature [154,155].

Borides are believed to be in the industry one of the most important and widely used refractory materials. *Serebrykova et al.* realized a classification of them after their atom size in and found approximately 80 binary systems out of which 60 react with metals [156]. The structures from Me_2B to MeB_{12} to $MeB_{66 \cdot 100}$ with a particular attention to the diborides represent one of the most interesting series for research because of their electron configuration. TiB_2 is a material of interest as it presents a few attractive properties like high hardness 25-35 GPa at room temperature, good creep resistance and thermal conductivity ($\approx$ 65 W m^{-1} K^{-1}) and good chemical stability [157]. It is therefore predictable that the material will have lower density and have a higher hardness than WC-Co systems. Nevertheless, a relatively low fracture toughness and the sensitivity of crack growth come as disadvantages of the material. In order to understand the compound better the Ti-B binary phase diagram should be studied. The phase diagram can be found in *Figure 2.15* [158].

TiB_2 is an intermetallic composite with an orthorombic TiB and Ti_3B_4 and TiB_2 structure [157]. It can be observed that the solubility of B in αTi is reached at about 880°C and the one of βTi at 1540°C. The melting of the TiB_2 phase can be observed at 3225°C. A peritectical decomposition of TiB and Ti_3B_4 is also happening at 2180°C [157]. The homogeneity of the TiB_2 phase has been reported between 65.5 and 67% [158]. The grain growth can be avoided and the densification improved for the TiB_2 phase by the addition of C, CrB_2, C, Ni, NiB or Fe composites [159]. Research concluded [159] that the addition of a mass fraction up to 10% in Ni compounds for a sintering at about 1700°C for 1h can lead to properties enhancement of the material. The same work stated that a further solubility of B in Ti can be obtained by rapid quenching (10^6 K·s^{-1}) of Ti-rich eutectic alloys. Hardness, electrical conductivity and fracture toughness are all increased when the diboride is added to Al_2O_3 or Si_3N_4 matrixes [160].
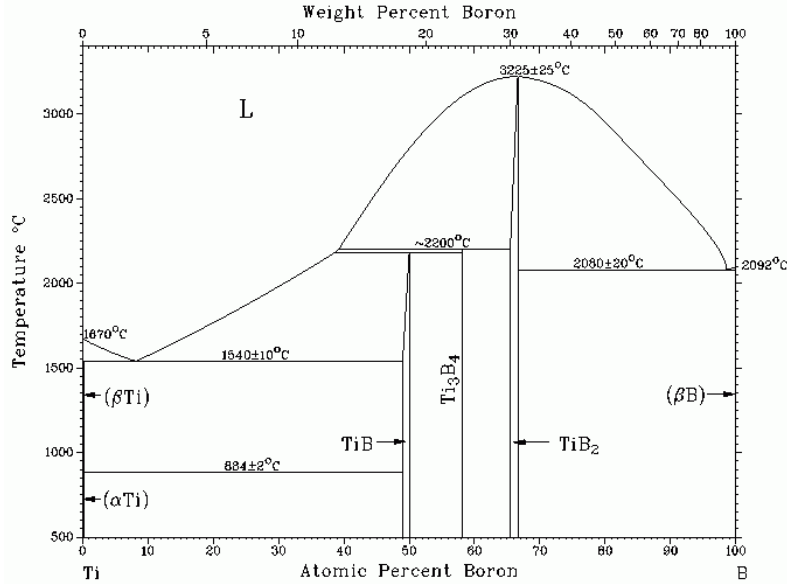
Figure 2.15 The Ti-B phase diagram [158]

The evolution of some of the studied [159] mechanical properties at room temperature and at 1000°C can be consulted in *Table 2.6*.

Table 2.6 Some mechanical properties of polycrystalline TiB$_2$ compound having a mass fraction of ≥98% and density of ρ=4.5±0.1 g·cm^{-3} and grain size of g=9±1 μm

	Bulk modulus (GPa)	Density (g·cm^{-3})	Elastic modulus (GPa)	Flexural strength (MPa)	Friction coefficient	Hardness (GPa)	Wear coefficient (10^{-3})
20°C	240	4.5	565	400	0.9	25	1.7
1000°C	228	4.3	534	459	0.6	4.6	

It can be observed that small or insignificant decreases for bulk modulus, density and elastic modulus occur at elevated temperature. The hardness has unfortunately at high temperature a big decrease from 25 GPa to 4.6 GPa. Nevertheless, with an increase of the friction coefficient and flexural strength a decrease of wear rate and lower stress coatings could possibly be obtained.
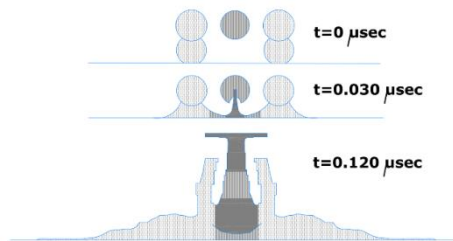
Figure 2.16 Sequence of deformation and impact of multiple Ti droplets on a substrate [161]

Liu et al. [161] realized a numerical simulation of the thermal spraying technology at the impact of molten Ti, Ni, and W particles with a flat substrate. The particle impact is one of the most neglected parts in thermal spraying. As previously mentioned, the droplet interaction with the substrate affects especially the microstructure, porosity and adhesion of the coatings. In *Figure 2.16* the impact of multiple Ti droplets on the substrate is represented. The particles have a diameter d=30 μm and have been accelerated with a velocity v = 200 m·s^{-1}. At the time t=0.030 μs the droplets reach the substrate but the plastic deformation does not yet occur. When the bottom particles reach the substrate, they start deforming and creating adhesion on the substrate. At t = 0.030 μs the lateral jets produce a rebound of the coming particles due to their velocity when interacting with the already impacted particles. Reaching the maximum speed of t = 0.120 μs the liquid spreads, forming layers on the top of each other. The particles rebound continues at the surface of the coating. In the moment when the piece is rotated or the gun moved, the ejected liquid separates from the stream, a solidification process takes place and defects like void may unfortunately occur. A post-processing in which the material reaches the glass transition temperature can be performed. This would generate the elimination of the existing pores and create a metallurgical interface bonding.

Looking at TiB$_2$ as a stable material with favourable crystallographic structure for wear applications at high temperature, having a clear view regarding the Ti droplet impact with a flat substrate and presenting interesting mechanical and thermal properties, the compound in combination with a Ni-based alloy can represent a highly attractive research subject.

2.6.   Applications

The combination of conception, materials, technologies is a critical factor to assure performant products [162]. Coatings are used as solutions for applications that require wear, corrosion or tribocorrosion resistance. In this way, the lifespan of the coated machine parts is prolonged and the general maintenance is drastically reduced. For the Ni-based alloys, and especially the NiCrBSi, the chemical composition represents an important role in obtaining high quality products.

Boron and silicon in combination, depending on their quantity in the chemical composition, can help lowering the melting temperature by a few hundred degrees [6]. The presence of Cr, B, Si and C form hard phases and when they are homogeneously distributed in the Ni-matrix, the coating shows reasonable hardness. The Ni matrix provides ductility to the coating and Cr protects against corrosion [6,163]. The hardness and the wear is improved by reinforcing the Ni-based powder for example with WC [95,119,147,164] or TiC particles [165].

The reference book in thermal spraying by *Davis* [6] lists plenty of industries where Ni based coatings are used. Some of these are: agriculture, automotive engine, chemical processing, defence and aerospace, electric utilities, food processing, forging, hydro-steam turbine, iron and steel manufacturing, oil and gas exploration, paper and printing equipment or steel roll mills.

Among the classic machine parts where these types of coatings are applied are shafts and sleeves of pump seals, rotary airlocks and feeders, or conveyor screws. Japanese automotive companies applied NiCrBSi coatings on valve seats. Cr$_3$C$_2$+NiCr coatings have been employed against wear and abrasion resistance for piston rings of diesel engines [26], while Mo+NiCrBSi have been used for parts of a gasoline engine [6]. Restorations are also largely performed using self-fluxing alloys. A

particular successful example is the restoration of expensive and large pump housings.

Although the vast majority of the self-fluxing alloys find applications in the steel industry where wear resistance is needed, they can be also used spraying thermoplastics [136]. Applying multilayer coatings is as well possible with such materials.

TiB_2 ceramics is mostly used as a reinforcement for different materials. The combination of different properties makes the material a good candidate for various applications. In the review made by *Vallauri et al*. [166], the TiC-TiB_2 material is given as an example for industries like cutting tools, armour material or electrode materials in metal melting. The ceramic has attracted as well attention in the area of high temperature structural materials or reinforcement to steel matrix composites because of the density, melting temperature and good wettability. TiB_2 is expected in these kind of materials to improve the wear resistance of the steel because of its mechanical properties like Young modulus or hardness [167]. A producer of highly performant materials [168] recommends the TiB_2 to be used in applications for electrically conductive composites like Al evaporation boats, complex sinterable shapes, additive for producing ceramic composites or thermal management materials.

All in all, both self-fluxing alloys and TiB_2 appear to be used in a large number of industries and specific applications. The combination of these materials could lead to new application fields for part protection or restoration.

2.7.   Testing and characterization of thermal sprayed coatings

Characterization is a crucial part in materials science to predict the behaviour of the parts in real life applications. Simulations, analysis or testing in order to define certain properties are all important parts of material research.

2.7.1.   Microstructure and image analysis

In many instances it is necessary to examine the structural elements or defects that influence properties of materials. Macroscopic observation is possible, but most of the time it does not offer enough information to come to a conclusion. After careful metallographic preparation and etching with a chemical reagent grains, their boundaries or defects can be easily observed using a light microscope [169]. Material contrast, chemical composition analysis, element quantification or topography can be all determined using a SEM or TEM at considerably higher magnifications. There is plenty of research on the microstructure of Ni-based alloys [71,73,138,138,139,141,148,164] and as new studies are performed, they will be all very likely submitted to similar characterization techniques.

Due to the rapid development of computational power, more and more performant software has been as well created. This kind of software is used by researchers to deepen their knowledge in the material characterization. Nevertheless, by misinterpretation, errors can occur. An image with a high pixel resolution gives the possibility to perform a large number of analysis. Quantitative analysis for coating thickness measurement [170], porosity determination [171] or different kind of contour plots or mappings for mechanical characterization [172] all represent important techniques in materials science and surface engineering.

2.7.2. Phase composition

Phase composition is classically performed with an X-ray diffractometer. This method allows to interpret the atomic and molecular structure in solids and powders. The diffraction is based on Bragg's law, which is grounded on electromagnetic radiation. Electron backscatter diffraction (EBSD) is a crystallographic technique to study either crystalline or polycrystalline materials. Using this technique, the structural properties, texture, defects or deformations can be all investigated. Wide angle X-ray scattering (WAXS) is a more recently developed technique usually employed to study the crystalline structure of polymer materials. Small angle X-ray scattering (SAXS) is used for scattering samples at a nanoscale level. Typical examples where phase identification is performed are: identification of phase in geological samples (can lead to the explanation of the formation of the planet), nanomaterials or pharmaceutical industry. Whether it is about XRD, EBSD, WAXS or SAXS, all have their importance and are successfully used in the research in coating technology [72,166,173].

2.7.3. Hardness properties

In the mechanical characterization of thermal sprayed coatings, a large variety of properties like elastic moduli, toughness, tensile properties or hardness can be identified through indentation tests. Macroindentations help defining some of the general mechanical properties of the material. When the grains are large or the coatings are relatively thick, microindentations are possible. Nanoindentations are largely employed to characterize mechanical properties of grains, determine the hardness in the interface regions or in the thin films industry. In the coating and self-fluxing alloy technology the mechanical characterization is largely employed [135,164,174] and new developments are constantly made.

2.7.4. Friction and wear

Friction and wear are two of the most important mechanisms against which a large part of the thermally sprayed coating should be protecting.

The fundamentals of friction are represented in *Figure 2.17a*: a normal force F_N is exerted over two bodies. When a tangential force F_T is applied on the top body, a relative motion starts [175]. The result of the simultaneous action of the F_N and F_t generates the friction force F_f. The coefficient of static friction μ_s is defined as the ratio of tangential force F_T with the normal force F_N. The coefficient of kinetic friction is created by keeping the movement between the two bodies with a certain velocity. Both of the factors versus time or sliding distance are represented in *Figure 2.17b*. The coefficient of kinetic friction (COF) is defined as:

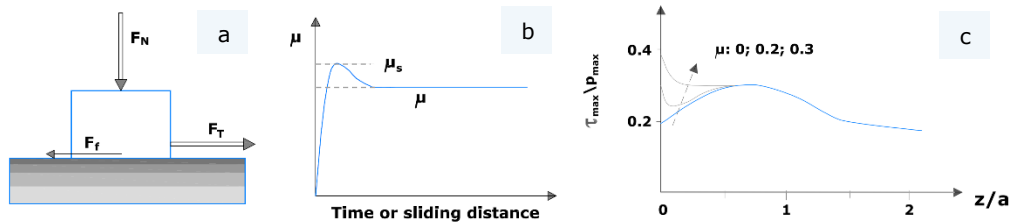$$\frac{F_T}{F_N} = \mu \qquad (2.8.)$$

Figure 2.17 Schematic of the (a) force needed to move the bodies, (b) resulted ideal COF (μ) vs. time/sliding distance and (c) maximum shear stress (τ_{max}) evolution against the depth for an application [175]

The COF induces two main consequences [175]:

    (1) A shear stress τ_{zy} which is defined as $\tau_{zy} = \mu \cdot \rho$ where ρ represents the Hertzian pressure (the pressure excerted by the contact of two bodies) [176]

    (2) A contact compression stress $\sigma_t^`$ is formed at the beginning of the contact between the two bodies and a tensile stress at the end of it.

It can be concluded that the evolution of the COF μ starts with a compression stress $\sigma_t^` < 0$ followed by a shear stress $\tau_{zy}$ and ending with a tensile stress $\sigma_t^` > 0$.

The maximum value of the compression stress $\sigma_t^`$ [177] is given by:

$$\sigma_t^` = 2 \cdot \mu \cdot \rho_{max} \tag{2.9.}$$

A relative motion between two bodies is considered in *Figure 19c*. The friction coefficient τ_{max}/ρ_{max} in the given situation is a function of *i.e.* the depth. The peak value of elastic deformation is reached at approximatevely z = 0.7. When the friction value exceeds the 0.25 value, the sheer stress is superior to the subsuface value having a great consequence on the elastic-plastic deformation of the material. After reaching the maximum value COF the plastic deformation starts.

Wear is a term which relates to the removal of undesired material from a surface as a consequence of a mechanical action. A large number of variables can influence the creation of such processes and controlling them requires a solid knowledge in tribology. There are numerous books, norms and scientific papers trying to classifiy wear mechanisms either generally or in relation to the thermal spray technology [175,176,178–183]. Although opinions vary, most of the literature agrees on four distinctive mechanisms:

- Adhesive wear
- Abrasive wear
- Surface fatigue
- Tribo-oxidative [175] / corrosive wear [176] / tribochemical [178] / high temperature oxidation or corrosion [179] / oxidational wear [180] / flow [181]. In spite of being diferently named, they all have in common the same fundamental mechanism. In the following work the term "tribochemical" will be used.

Fretting, ploughing, rolling contact or erossive wear are considered in a large part of the literature as particular cases of the four phenomena named above but a minority of experts mention them as distinct mechanisms.

The most common types of wear mechanisms that can take place on the surface of a thermally sprayed coating are represented in *Figure 2.18*. Before briefly describing each phenomenon, it is important to note that a wear mechanism can only occur if the two following conditions are: a normal force F_n has to be exterted from a counterpart on the thermally sprayed coating and a movement with a velocity v_x of at least one part has to be applied. As the F_N is exerted on at least one of the parts, a tangential force F_T is generated and a wear mechanism starts damaging the surface of at least one part.
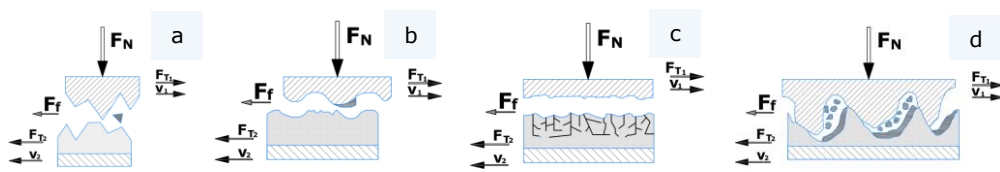

Figure 2.18 Schematics of the (a) adhesion, (b) abrasive, (c) fatigue and (d) tribochemical wear mechanisms

Adhesive wear, represented in *Figure 2.18a*, occurs when the motion of two components in contact that have different velocities induces a damage at the interaction surface creating wear fragments. The theory developed by *Archard J.F.* represented the fundaments of adhesive wear theory. Since then, a lot of development has been made in the domain. Specialized literature [183] mentions that it is important to make a clear distinction between the wear behavior of ductile and brittle materials.

If the brittle materials (as the ones considered for the present work) have a low enough fracture fatigue toughness, as a consequence of the contact, wear fragments can be formed. In the case in which micro-cracks are formed on the contact surface possible brittle fracture can as well happen.

Thermal spraying contributed in protecting surfaces against adhesive wear in various applications. A few examples are: piston rings coated with Mo or Mo/self-fluxing by flame or APS, large cylinders coated with Fe-Mo material, US Navy approved HVOF coatings for hydraulic rods [179].

Abrasive wear, represented in *Figure 2.18b*, takes place when an external particle from the system enters between the contact surface of two parts causing damage. The phenomenon happens as well when the contact of two components with significantly different hardness causes scratches and leads eventually to material removal [119].

The abrasive wear of brittle materials is commonly attributed as a consequence of the Lawn and Swain mechanism [184]. This states that the depicted material is resulted from a microindentation between the two surfaces in interaction. In the case in which the generated particles are round-shaped, brittle fractures can occur [175].

In industry, WC-Co are generally used for low temperature application (400°C-500°C), NiCr-Cr_2C_3 for high temperature applications (800°C-900°C). Although APS Cr_2O_3 coatings have a higher hardness (RC 70) than WC-Co coatings (RC 65-68), the abrasive wear of WC-Co is 30%-40% higher [179].

Fatigue wear, represented in *Figure 2.18c,* is considered happening when a surface damage and removal is performed by cycling contact between two parts. This

type of mechanism provokes damage generally in large assemblies where the numerous components in contact work at a very high intensity or frequency [185].

When fatigue in combination with wear occur in a system, pits, cavities or cracks on one or both surfaces are very likely to appear. The damage produced in the coating, especially cracks, acts as stress concentrator and fractures the material [186].

The technology of thermal spraying is frequently used for protecting parts against fatigue wear [16]. Recent research [187] has been done on applying shot peening as a post-treatment of SPS sprayed steel coatings on steel surface. After bending fatigue test, it has been observed that crack initiation does not start at the interface as in the not processed sample but rather on the surface and only after a long time. The shot peening has been observed to reduce as well the residual stress of the coating. Further developments are recommended, especially in the field of the kinetics and process-microstructure of the thermal spray technology [16].

Tribochemical wear, represented in *Figure 2.18d,* happens through an unlubricating film built by chemical interaction on the parts in interaction creating damage on one or both the components [94]. The most frequent type of phenomenon is the one of tribo-oxidation where a built harmful oxide is encouraged by the system and results in debris damaging the surface.

Specialized literature [175] divides the mechanism in tribochemical wear at high temperature and tribochemical wear at low sliding temperature. In the first case, the surface temperature alone promotes the formation of unwanted particles and films that start harming the material. Intensive research [175] concluded that the wear at low sliding temperature is formed as a consequence of the adhesive wear by trapping the dislocated asperities between the parts in interaction. The constituents are hardened, fractured, oxidized, forming finally a film and ending in irreversible damage of at least one component. Tribochemical wear at low sliding speed can occur for example when the temperature is not high enough to form oxidation of the surfaces in contact. Such type of wear can also be developed when load and sliding conditions are intense and a compact layer of asperities is built.

Recent research [16] reported that cylinders in contact, that tend to form destructive films, can be protected with plasma VPS or LPPS (low-pressure plasma spraying) by applying high concentration Ni-alloys containing Si, Mo or B.

Historically, *J.F. Archard* calculated the wear volume W_c as the wear coefficient K multiplied with the sliding distance s and the ratio of the normal force F_N and the yield stress H:

$$W_V = K \cdot \frac{F_N}{H} \cdot s \ (mm^2) \qquad (2.10.)$$

The wear rate k can be further calculated as:

$$k = \frac{W_v}{F_N \cdot s} \ (mm^3 N^{-1} m^{-1}) \qquad (2.11.)$$

2.7.5. Corrosion behaviour

According to the DIN EN ISO 8044:2015-13 [188] norm, corrosion is defined as "the physiochemical interaction between a metal and its environment that results in changes in the properties of the metal, and which may lead to significant impairment of the function of the metal, the environment, or the technical system, of which these form a part". The standard lists over 50 types of corrosion. However, only a part of them are frequently occurring in thermal spraying.

In the corrosion process, a dissolution of metallic elements happens as in the following reaction:

$$M \rightarrow M^{n+} + n\,e^-$$
(2.12.)

where M is a metal, M^{n+} is positively n times charged ion, and e^- is an electron.

The main types of corrosion attack for coatings represented in *Figure 2.19* are generalized (uniformed) corrosion affecting about 30% of the failure and localized types of corrosion (galvanic, intergranular, intragranular and pitting) corresponding to approximately 70% [136].
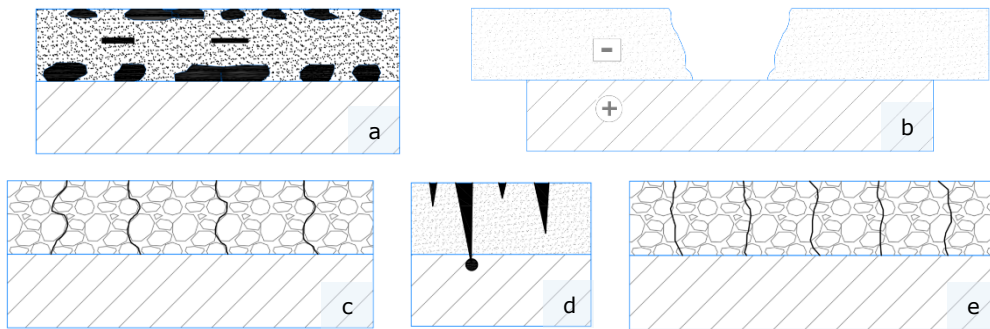

Figure 2.19 Schematics of the main corrosion mechanisms found in thermal spraying: (a) generalized, (b) galvanic, (c) intergranular, (d) pitting, (e) intragranular

Briefly, the main types of corrosions are described as:
- *Generalized corrosion,* represented in *Figure 2.19a,* or uniform corrosion is a form of damage causing material loss on a considerable size through the interaction of the part with a harmful environment [189]
- *Galvanic corrosion,* represented in *Figure 2.19b*, is a material degradation process happening preferentially to one metal when in contact with another and it takes place when two criteria are simultaneously occurring: two dissimilar material have to be present (with two considerable different corrosions potential) and a conductive electrolyte has to move ions from the more anodic to the more cathodic material [136]
- *Intergranular corrosion,* represented in *Figure 2.19c,* is a localized type of corrosion generally occurring when a chemical element is removed or a material defect is present, creating the possibility for the electrolyte to provoke damage in the material especially at the grain boundaries
- *Pitting corrosion,* represented in *Figure 2.19d,* is a form of localized corrosion where pits (holes) are formed in the material. The pit cavities behave as stress generators irreversibly damaging the coating or/and the substrate

- *Intragranular corrosion,* represented in *Figure 2.19e,* is a form of corrosion happening due to residual stress or an external factor, the coating being damaged transgranularly letting the conductive electrolyte catalyse the corrosion process.

Stress corrosion cracking (SCC) is an important form or material destruction happening due to several complex processes. SCC is defined as "a cracking owing to a process involving conjoint corrosion and straining of a metal because of residual or applied stress" [190]. In thermally sprayed coatings, SCC can appear due to several reasons [136,190]:
- imperfections in the coatings which can introduce physical defects.
- wrong material selection for the intended purpose.
- unintentional variations in the system *e.g.*, environment chemistry, stress or temperature.
- high tensile stress in the coating.

Some of the most important mechanisms to explain the stress corrosion cracking in thermal spraying are [190]: slip dissolution (because of local strain, a rupture of a passive film occurs and material loss will continue through the coating due to oxidation), anodic reaction-enhanced fracture (plastic flow induces anodic reactions to create and advance a cracking process) and hydrogen embrittlement (hydrogen atoms caused by corrosion enter the coating and diffuse at material defect sites generating cracking when a critical combination of hydrogen content, microstructural sensitivity and stress is achieved).

Corrosion resistance depends largely on the conditions of exposure, on the environment and on the material. The corrosion rate of the material is an important parameter which gives the opportunity to measure the provoked damage to the material and is defined as [119]:

$$rate\ of\ corrosive\ attack = \frac{corrosivity\ of\ the\ environment}{corrosion\ resistance\ of\ material} \qquad (2.13.)$$

There are numerous practical applications in the industry where corrosion attack has been prevented by using TS coatings. Using thermal barrier coatings, large pillars of the Tokyo Bay Aqua-Line Highway have been protected [191]. Applications exposed to marine environment are another example where HVOF coatings are successfully used. Corrosion has been and will continue to be a very important scientific topic in the TS area [18,35,94,171].

Both wear and corrosion, their forming mechanisms and rates are among the phenomena against which a coating should be protecting. When a substrate is not protected against these types of damages the coating is frequently losing its main functions. Therefore, a careful preliminary analysis is very often performed against both wear and corrosion before the scientific outcomes reach the industry.

3.   Methodology and experimental procedure

3.1.   Equipment and materials

The most important equipment used to complete the experimental work were:
- Manual powder mixer
- Deposition gun (Methaterm MPP-85 - 5PII Type)
- Thermogravimetric analysis instrument (STA 449 F1 Jupiter, Netzch)
- Vacuum Furnace (HITERM 80-200, HITEC-MATERIALS)
- Cut-off machine (Discotom-2, Struers)
- Hot mounting press (Pronto-Press-20, Struers)
- Grinding and polishing machine (Rotopol-V, Struers)
- X-ray diffractometer (X'Pert, Philips)
- Light microscope (DMRME, Leica)
- Confocal laser scanning microscope (VK-X260K, Keyence)
- Scanning electron microscope equipped with SE, BSE and EDX detector (ESEM XL 30, Philips)
- Universal testing machine (KB, 250 BVRZ)
- Micro Vickers hardness tester (ZHVµ-M, ZwickRoell)
- Pin-on-disc arrangement (TRB, CSM Instruments)
- Potentiostat/galvanostat (VoltaLab PGP201, Radiometer Analytical)
- Thermostated electrochemical cell (CEC/TH, Radiometer Analytical).

The essential materials used in the experimental program were:
- S235 JR commercially available substrate material
- NiCrBSi powder (LSN Diffusion)
- TiB_2 powder (H.C. Starck)
- Hydrochloric acid, HCL 38% purity (Sigma-Aldrich)
- Sodium chloride, NaCl, ≥99,5% purity (Carl Roth)
- Ethanol, 96% (VWR Chemical).

The software used to process the results were:
- STA 449 F1 Netzch Data Collector
- Proteaus Thermal Analysis, Netzch Data Processing
- iTools Engineering Studio
- X`Pert Data Collector, XRD Philips
- X'Pert High Score 3.0, PANalytical
- LAS V4.6
- Statgraphics Centurion XVI
- VK Recording Module
- VK-X Analyzer, Keyence
- TestXpert ZHVµ
- TriboX 2.7
- ImageJ
- VoltaMaster 4, Radiometer Analytical
- OriginPro
- Microsoft Office Package.

3.2. Powder characterization, mixing and deposition

3.2.1. Thermogravimetric analysis

Thermogravimetric analysis (TGA) is a method that permits the analysis of the mass of a material as a function of temperature or time while the specimen is subjected to a controlled thermal program in a controlled atmosphere. In a TGA equipment, the material to be analysed is placed in a high precision balance and heated or cooled with a predefined program. The mass changes of the specimen during the experiment are carefully monitored. The analysis is performed in the presence of a protective gas [192].

The differential thermal analysis (DTA) is a method where a difference between the sample and a material taken as a reference by the means of a thermocouple is plotted against time or temperature. An empty reference and one containing the material to investigate are placed in the apparatus and submitted to the same program [119]. Using DTA crystal structure changes, a glass transition temperature or melting can be measured without mass loss.

The thermal behaviour and the melting temperature of the materials have been determined using TGA and DTA analysis with a Netzch STA 449 F1 Jupiter® apparatus. The equipment operates using a top-loading system with a temperature that can reach 1600°C. The nanometric digital resolution of the system allows operating with samples weighing up to 5 grams. The equipment works in a protective gas atmosphere with heating and cooling speeds that can vary between $1 \cdot 10^{-3}$ K·min^{-1} and 50 K·min^{-1}. The information provided from the equipment has been saved using the STA 449 F1 Netzch Data Collector software. The results have been interpreted using the Proteaus Thermal Analysis software.

3.2.2. Powder mixing

The material has been blended using a specialized tool produced for thermal spraying powder mixing. The matrix and different vol.% of the filler have been prepared. They have been placed at the two ends of the manual powder mixer. Afterwards, a mix between the two materials has been performed. The procedure has been executed at each volumetric fraction for 600 s. The resulted powders have been deposited in different containers in order to have them ready to use for further material analysis and thermal spraying.

3.2.3. Powder deposition

The importance of the pre-spray processing has been already highlighted in the theoretical part of the present work. Degreasing, cleaning or grit blasting all represent important steps for a proper adhesion of the coating to the substrate. For the coating of the material, the substrate has been carefully cleaned and grit blasted with chilled iron grit. As a consequence of the pre-treatment process, the substrate should reach a roughness of minimum 75 µm. The stand-off distance has been selected at 120 mm and the deposition has been made through the translation of the gun over the sample.

The deposition of the four manually mixed powders has been performed using a Methaterm MPP-85 - 5PII Type spraying gun. The gun has a powder feeding rate of 2.5 kg·h^{-1}. The material has been fed in the gun through a gravitational system propelled towards the nozzle using purified air. The stoichiometry between the gases generating the flame has been set to C_2H_2:O_2 1:2. For a better adhesion of the

coating, the substrate has been warmed at approximately 120°C while the spraying temperature reached approximately 2600°C. The two temperatures have been set considering the fusion and composition of the two blended materials. The particles velocity used during the flame spraying was around 100 m·s^{-1}.

3.3. Vacuum furnace heat treatment

The heat treatment of the samples has been performed in a HITERM 80-200 water cold wall vertical controlled atmosphere furnace. The used vacuum has been set at $3.5 \cdot 10^{-2}$ Pa. The maximum service temperature of the furnace is 2000°C and it can be performed in an ≈ 140 cm^3 volume chamber. The apparatus is equipped with an oil sealed rotary pump and a turbomolecular pump. The parameters can be adjusted so that the heat treatment can be done with a high precision. The iTools Engineering software is the user interface for heat-treatment program development.

3.4. Optimization of chemical composition and vacuum furnace parameters

A high performance is needed in the majority of the engineering areas. Simulations, tests and experiments can be performed to understand the product better.

Once a product or process has been designed, it is important to evaluate its performance. Therefore, a set of "runs" is performed to measure this performance. A multitude of orderly runs is considered an experiment. In DOE, "controllable" factors are considered the inputs corresponding to the variables during the experiment. The "responses" in optimization are known as the chosen outputs or measured results of the runs. The systems in engineering are in most cases "noisy" as the same input parameters can produce responses that are not perfectly identical. "Sampling variability" is the technical term used for the difference between responses produced by the statistical experiment. By regulating as many controllable factors as possible and measuring a significant number of responses during the optimization process, the noisiness and sampling variability can be significantly reduced. A "designed experiment" is an experiment where the runs are planned in advance. In other words, an experimental design is defined as a set of test value for the chosen controllable factors [193].

The performance of the experimental part of the current work was maximized using the method of response surface methodology (RSM) developed by *Box and Wilson* [105] where a series of experimental analysis and optimization techniques are used. The main idea of the RSM is to optimize an unknown number of noisy functions by approximating functions that are accurate just for a small area using designed experiments. The flowchart of an RSM procedure can be seen in *Figure 4.1*.
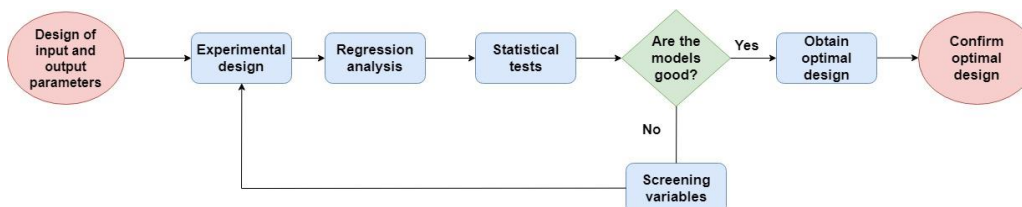

Figure 3.1 Flowchart procedure of response surface methodology

As the computational power advanced, an awareness for the creation of optimization software grew. The software used for the present work in order to find the best values for the controllable factors was Statgraphics Centurion XVI.I. Evidently, the created model tried to be an accurate representation of the studied system. The implementation in the real system was performed by using the responses delivered by the modelled experimental design.

Experimental RSM models have been created by making the best possible decisions using the intuitive software. The statistical analysis has been performed by following the steps from *Figure 4.1*. Through the recommended runs, a series of responses have been collected and further analysed. By calculating the desirability of each model, a final decision regarding the optimal design has been made.

3.5. Morphological, chemical and physical characterization

3.5.1. Metallographic preparation

In order to have a complete view of the performed coatings, metallographic samples have been prepared. Although metallography is a basic step in materials science analysis, it has to be performed very carefully to introducing foreign particles that could affect the later performed investigations. The samples have been prepared exclusively with equipment from the Struers company. Following a cross-sectioning of the material using a Discotom-2 cut-off machine, an embedding of the specimens has been performed with a Pronto-Press-20. Afterwards, a grinding using SiC paper of 320 μm, 800 μm and 1200 μm has been performed followed by polishing with diamond suspension and lubricant. The last process in the metallographic preparation has been cleaning the samples with distilled water and ethanol followed by drying under hot air.

3.5.2. Light microscopy and image analysis

The light microscope is a fundamental equipment in materials science and many other areas of technical research. For this study, a Leica DM-RME light microscope has been used. The working temperature of the equipment should not exceed the range of 10-36°C. The magnifications varied between 25x and 1000x while the working frequency was between 50-60 Hz. The LAS V4.6 software helped for the electronic acquisition of the micrographs [194].

The porosity is a measure of the void space in a material. The pores distribution, shape and their complexity led to the development of several methods of porosity measurement. Methods like Archimedeans pycnometry, mercury porosimetry and image analysis are just some of them. As often in scientific research, each method has pros and cons. Archimedeans pycnometry is considered a cheap investigation method but no information can be obtained regarding the shape, diameter or distribution. Mercury porosimetry is a destructive method but it is used to detect open porosity and for comparisons because of its wide range of applications. Recent research [195] dealing with the comparison of different measurement techniques concluded that for samples having >30% porosity the Archimedean method provides the best results while for sample with <30% porosity the image analysis is recommended. In thermal spraying a very used method is the image analysis. Using this technique, the shape, distribution and quantification can be

performed. Image analysis software do not allow unfortunately to distinguish between open and closed porosity [195].

For this work, the image analysis method was chosen. The porosity analysis and measurement was performed with the ImageJ v1.50i open source program. ImageJ, formerly known as NIH Image, is a program largely used in materials science and crystallography [196]. For the porosity analysis, micrographs taken from both light microscope and SEM have been used. For reproducibility five micrographs taken at the same magnification have been analysed. The images have been first scaled from pixels to μm. They have been afterwards transformed to 32-bit grayscale images to prevent the different shades of colours from altering the results. The threshold has been afterwards measured and the result exported and analysed.

3.5.3. Scanning electron microscopy

A scanning electron microscope (SEM) is a highly performant tool used in a large number of research areas and in materials science as well. Bulk materials, coatings, wet and dry samples, chemical composition or crystallography can be all analysed using an SEM. The fundamental operation to obtain an image using such a microscope, schematically presented in *Figure 3.2.a*, is by scanning an electrically conductive sample with a finely focused electron beam emitted from an electron source. The energy of the beam, E_0, varies typically between 0.1 keV $< E_0 <$ 50 keV. The emitted beam is modified by apertures, lenses and coils until it reaches a thinness of under 10 nm. The modified thin electron beam will finally hit the sample [197].
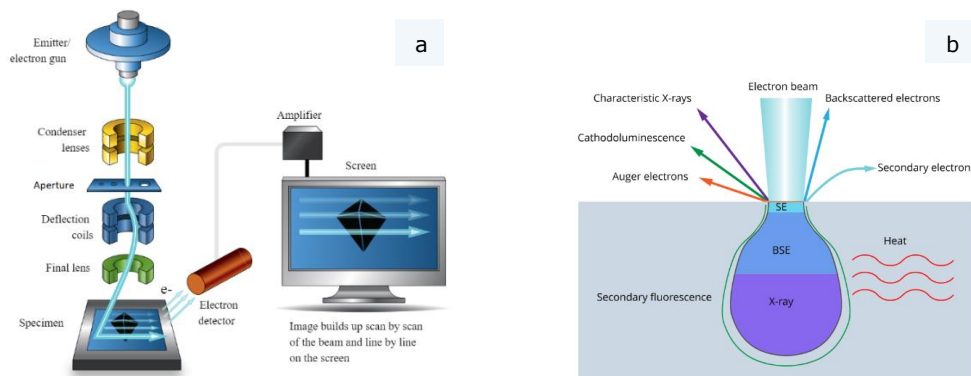

Figure 3.2 (a) SEM layout and function and (b) the outcomes of the electron beam interaction with the sample [198]

By the interaction of the high energy electron beam with the sample, schematized in *Figure 3.2b*, several products are resulted:
- Heat generated by the photon excitation
- Characteristic X-ray radiation
- Cathodoluminescence (visible light fluorescence)
- Auger electrons by the bounce of the outer shell electrons
- Continuum radiation also called *bremsstrahlung*
- Backscattered electrons (BSE)
- Secondary electrons (SE).

The present experimental program was conducted using a Philips XL 30 ESEM TMP equipment. The technical book of the equipment [199] provides all the necessary information in order to set the equipment up for the analysis of TS samples. The microscope uses a point-source tungsten cathode which has a ZrO_2 layer. The resolution of the equipment is 2 nm in a high-vacuum mode (10^{-4} Pa) while the chamber vacuum pressure can go up to $26 \cdot 10^2$ Pa. The robust four-axes (x, y, z and rotation) 50 mm stage of the SEM, on which a stage adapter is mounted, allows the recording of stable micrographs. Although the magnification of the device can go up to 250 000x, the maximum needed was 10 000x. Self-evidently, for using the microscope in the ESEM mode (which was not necessary for the present work) other settings have to be made. A built-in camera is allowing the monitoring of the position of the sample in the chamber. All three equipped detectors (SE, BSE and EDX) of the apparatus have been used.

The backscattered electrons (BSE) after their scattering by the electric fields of the atoms in the sample are deflecting from the specimen with a large fraction of their incident energy usually exceeding 50 eV. When the beam hits an atom with a higher atomic number, the collision likeliness is also increased due to the higher cross-section area. As the number of the collided atoms in this case is bigger, a brighter area will be displayed on the screen.

The secondary electrons (SE) escaped from the sample have a significantly lower energy than the BSE ones, reaching a maximum value of 50 eV [197]. The low value is obtained by the low transfer of the kinetic energy, most of them having even under 5 eV. The negatively charged electrons are caught in a Faraday type cage. The high electrically charged cage is able to generate flashes of light causing a video or, after a conversion, a digital image [200].

3.5.4. Characteristic X-rays. Energy dispersive X-ray spectroscopy

The characteristic X-Ray generation is schematically shown in *Figure 3.3* and excellently described in the reference book of Goldstein et al. [197]. In the primary stage, the nucleus presents a well-known number of electrons on its K,L,M etc. shells, depending on the element. These electrons are bound to the nucleus due to a critical excitation ionization energy. An external stimulation in the form of an electron beam with an initial kinetic energy $E_{in} > E_c$ can inelastically eject an electron from the K-shell (the ejected electron having the energy E_k). The total transferred kinetic energy can be as much as the half of the incident electron one. The outgoing beam E_{out} suffers an energy loss simply mathematically described in the *Eq. 3.1.*

$$E_{out} = E_{in} - E_k \qquad (3.1.)$$

The ionized atom is therefore left with a vacancy on the *K*-shell, which is immediately filled with an electron found in the immediate vicinity on the *L*-shell. The energy difference can be expressed in one of the two routes:

- The inter-shell transition energy difference E_k-E_L is brought to an *L*-shell electron and afterwards ejected from the *L*-shell electron with a certain kinetic energy E_{kin}. The ejected electron is called Auger electron and is forming the fundaments of the Auger spectroscopy.

$$E_{kin} = E_K - E_L - E_L \qquad (3.2.)$$

- The X-ray photon, which carries the transition energy E_v between the shells, is mathematically described in *Eq. (3.3.)* and is known as the characteristic X-ray energy.

$$E_v = E_k - E_L \tag{3.3.}$$

Although having a very small range of just a few electronvolts, the characteristic X-ray energies are well defined and can be identified for all the elements having an atomic number $Z \geq 5$.
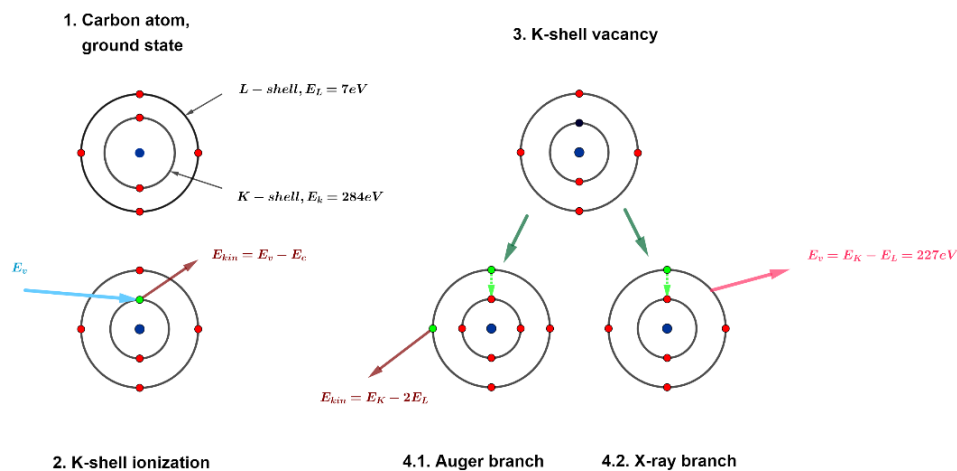

Figure 3.3 Schematic diagram of X-ray generation process for a carbon atom

The Philips XL 30 ESEM TMP is equipped with an EDX detector with an ultra-thin window. The working software of the detector can perform qualitative and semi-quantitative point, surface, linescan and mapping analysis. The system permits the acquisition of information in both high vacuum and ESEM mode [199].

3.5.5. Confocal laser scanning microscopy

The confocal laser scanning microscope (CLSM) is a device similar to the SEM in the sense that it scans as well the sample. The fundamental difference is in the nature of the beam and that by placing a small pinhole in front of the detector the micrograph acquisitioning mode changes. The CSLM theoretical principle is presented in *Figure 3.4*. The light source in a confocal microscope is composed preferably from several laser beams to generate a range of wavelengths. The light source is focused by the objective on the specimen. The reflection is imaged back through the same objective to the pinhole. Outside the focus plane, reflected photons can still be found as not all of them have been captured in the pinhole. In a conventional microscope this light source would generate a blurry image while the confocal microscope manages to eliminate these unneeded outside pinhole photons. A full 3D image is created from a collection of series of overlapped micrographs taken at different focus. The recent specialized software creates different views of the sample [198].
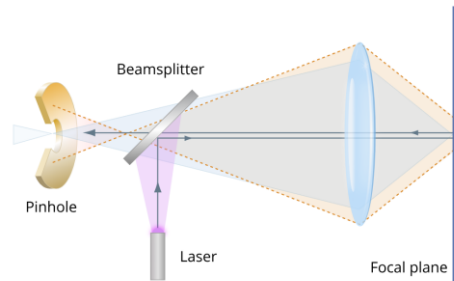
Figure 3.4 The fundamental principle of the confocal laser scanning microscopy [198]

The quality of the resulted micrographs can nevertheless be altered by several factors. Some of them can be the alignment or the instability of the laser unit, distortions of the scanning system, the cleanliness or chromatic aberrations of the objective, alignment of the pinhole, noise of the detector or the malfunction of other optical components (mirrors, filters, *etc*.) [201].

For this work, a Keyence VK-X260K CSLM was used to perform several analyses. The microscope is equipped with four standard CF EPI Plan objectives that have 10x, 20x, 50x and 150x magnification. The depth of field varies between 0.45 µm for the 150x lens to 4.53 µm for the 10x one. The device has incorporated a 16-bit photomultiplier that can generate a 408 nm violet laser beam of a 0.5 nm resolution. To receive the best possible results, the ambient working temperature did not exceed the range of 18°C and 23°C, the humidity was kept constant at approximately 40%. The VK Recording Module and the VK-X Analyzer are the two programs that helped for result examination and interpretation [202].

3.5.6.   X-ray diffraction

X-ray diffraction is an important and widely used method in materials science to obtain data on the atomic scale of different materials in different states. The diffraction phenomena can be understood as coherently reflection waves constructed in the moment in which an incident wave beam encounters an obstacle. The main concern in X-ray diffractometry is to determine the conditions in which the incident and the scattered X-rays are completely in phase and therefore reinforcing each other. The *Figure 3.5* might be of use. The most familiar method is given by the Bragg's law according to which two necessary conditions have to be fulfilled:

•   The angle between the incident X-ray beam and the normal to the reflection plane is always equal to that of the normal and the diffracted X-ray beam

•   The value of the angle between the transmitted and the diffracted X-ray beam is always 2θ, forming the so-called "diffraction angle".

If an incident X-ray of wavelength λ strikes a crystal where the atoms are found in a periodical well-defined array with an interplanar spacing d, the diffracted beam is detected just in the situation in which:

$$2d \sin \theta = n\lambda \qquad\qquad (3.4.)$$

where *n* is called the reflection order and equals the number of wavelengths in the path difference between the diffracted X-rays from the next crystal planes. The equation is called the *Bragg's law* or *Bragg condition* [203]*.*
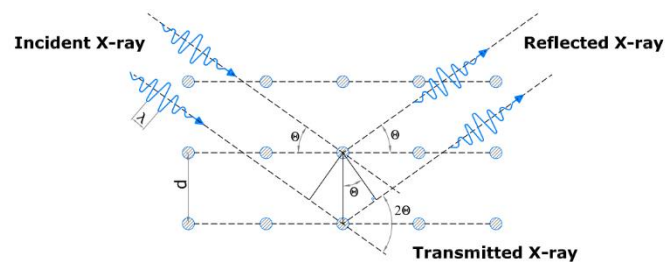

Figure 3.5 Schematics of X-rays diffraction by a crystal (Bragg condition)

For the crystallographic analysis in this work, a Philips X`Pert MPD system was used. A high resolution goniometer is equipped on the device. A Cu anode is also found in the apparatus. It is one of the most used target materials for a single-crystal diffraction. The device can reach up to 3 *kW* and 60 *kV*. The software XRD Philips X'Pert High Score 3.0 (PANalytical) and X`Pert Data Collector is the user interface to, on one hand, set the equipment for the measurement and, on the other hand, collect the data [204].

3.6.   Mechanical testing

3.6.1.   Micro Vickers hardness testing

In steel and steel related industry the hardness of a material is often a very important indicator that needs to be taken in account when designing an application. It is well known that in different parts of the industry different measurement units are preferred. Nevertheless, conversion charts are available when comparison is needed.

Microhardness is an approach to determine the penetration resistance of a material when the specimens or areas to be analysed are thin or small. Precise information can be obtained for fine, multi-phase, non-homogeneous or crack susceptible surfaces.

A ZwickRoell ZHVμ-M micro Vickers and Knoop hardness tester [205] equipment was used to provide valuable information for the experimental part of the current work. The apparatus work in respect to the DIN 4545 [206], DIN 6507 [207] and ASTM E384 [208] Vickers and Knoop microindentation testing norms. The load steps of the equipment range between 10 gf and 2000 gf. Four objectives and one Vickers and one Knoop indenter can be simultaneously mounted. The indenting time can be set between 5 s and 60 s. The control of the x-y 100 mm x 60 mm table can be done through two micrometers mounted on each of the two axes. A high resolution 2.5x objective lens connected to the PC-installed TestXpert ZHVμ software allows performing the measurements in a comfortable medium.

3.6.2. Friction coefficient and wear measurement

Tribological characterization delivers valuable information about the friction and wear under controlled conditions. There are several wear testing methods to deliver such information like pin-on-disc, block-on-ring, disc-on-disc, four-ball-tribometer, dry-sand rubber-wheel wear test, or pin abrasion wear test.

The test equipment used for the experimental part of the work was a pin-on-disc tribometer. The schematic principle of such a setup is shown in *Figure 3.6.* The main components of such a test configuration are a stationary pin with a cylindrical shape and a diameter of a few millimetres, pressed with a predefined load against a rotating disc. In the case in which the pin touches directly the sample the contact is named "conformal" while when a sphere substitutes a pin the contact is considered a non-conformal one. A strain gauge is installed as well on the tribometer arm for the lateral force measurement [175].

The friction coefficient of the material is immediately generated by such an apparatus. This is resulted through the acquisition of the tangential force to restrain the pin. A thermocouple may be installed on the equipment for temperature information acquisition. Performant installations may have displacement transducers for the measurement of wear depth. Alternatively, wear can be measured using several ways like the mass loss method, profilometers or CLSM installations [175].
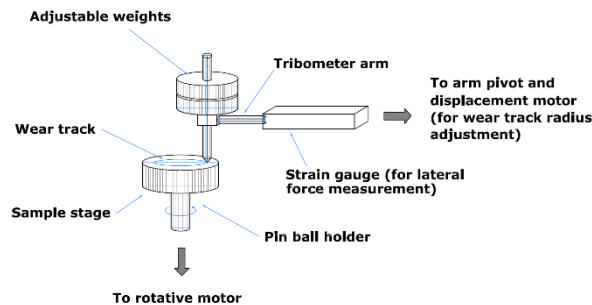

Figure 3.6 Schematics of a pin-on-disc setup

The experimental part of the tribological test has been performed on a CSM Tribometer conform to the DIN 50324 and ASTM G99-17 [209] norms. The load installed on the equipment can vary between 1 N and 10 N. The apparatus contains an adjustable pin positioned at 90° and creates a non-conformal contact with the sample. Subsequently, 6 mm AlO$_2$, WC-Co or 100Cr6 balls have been available for use [210]. The data collected by the equipment is directed to the TriboX 2.7 software where further analysis can be performed.

3.7. Corrosion testing

The manufactured coated parts need most of the time to be used in situations that challenge their corrosion resistance. This is why accelerated corrosion tests are widely used to simulate the behavior of the material in different environments. Whether it is kesternich, salt spray, humidity cabinet or electrochemical testing, all of them provide useful information about the quality of the coatings.

Electrochemical tests are grouped as direct current (dc) or alternating current (ac) depending on the perturbation signal that is applied to take the measurements.

Investigations using both dc or ac have been undertaken to study the performance and the quality of the coating and passive films or to evaluate the surface of a treated part [211]. Corrosion rates (Tafel slope), passivation rates, active/passive characteristics or anodic and cathodic protection can be all investigated through electrochemical tests.

The potential sweep method or linear voltammetry is a widely used electrochemical testing method. This kind of examination often provides additional data regarding the kinetic and the mechanisms of the corrosion process. Linear voltammetry performs the variation of the working electrode potential in time. The current density i is measured by performing a linear scan between an initial E_i and a final E_f value. The electrode cell used in the measurements represented in *Figure 3.7* is composed of a working electrode (WE), reference electrode (RE) and counter electrode (CE). The WE, RE and CE are placed in the cell in an electrolyte solution [119,200].
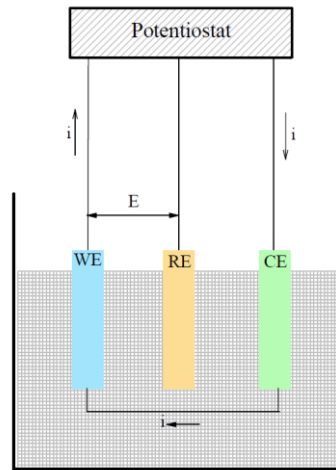

Figure 3.7 The configuration of an electrochemical cell [200]

Materials like platinum, gold or graphite are typically used for the CE as they are inert materials and help closing the circuit. The RE is an electrode with well-defined and known properties and has the role of controlling the system. A saturated calomel electrode (SCE) has been in the present work used as a reference. To minimize the electrolyte resistance a Luggin capillary has been used as a RE. The WE has been the sample mounted in a holder. The active geometry has been 1 cm^2.

The corrosion rate can be calculated as:

$$i = i_0 \left\{ exp\left[\frac{2.33}{b_a}\left(E - E_{eq}\right)\right] - exp\left[-\frac{2.33}{b_c}\left(E - E_{eq}\right)\right]\right\} \qquad (3.5.)$$

where $\frac{2.33}{b_a}$ and $\frac{2.33}{b_c}$ represent the anodic and cathodic slope, b_a and b_c are the anodic and cathodic Tafel plot constants, E_{eq} the equilibrium potential and i_0 the exchange current density.

4. Experiments and results

The main steps for the development of the high temperature NiCrBSi-TiB$_2$ vacuum furnace fused flame-sprayed coatings were:

- Powder designation
- Mechanical mixing of the powder
- Material deposition through flame spraying
- Vacuum furnace heat treatment
- Chemical composition and vacuum furnace parameter optimization
- Characterization of the optimized coatings
- Evaluation of the results and conclusions.

The established procedure is schematically represented in *Figure 4.1.*
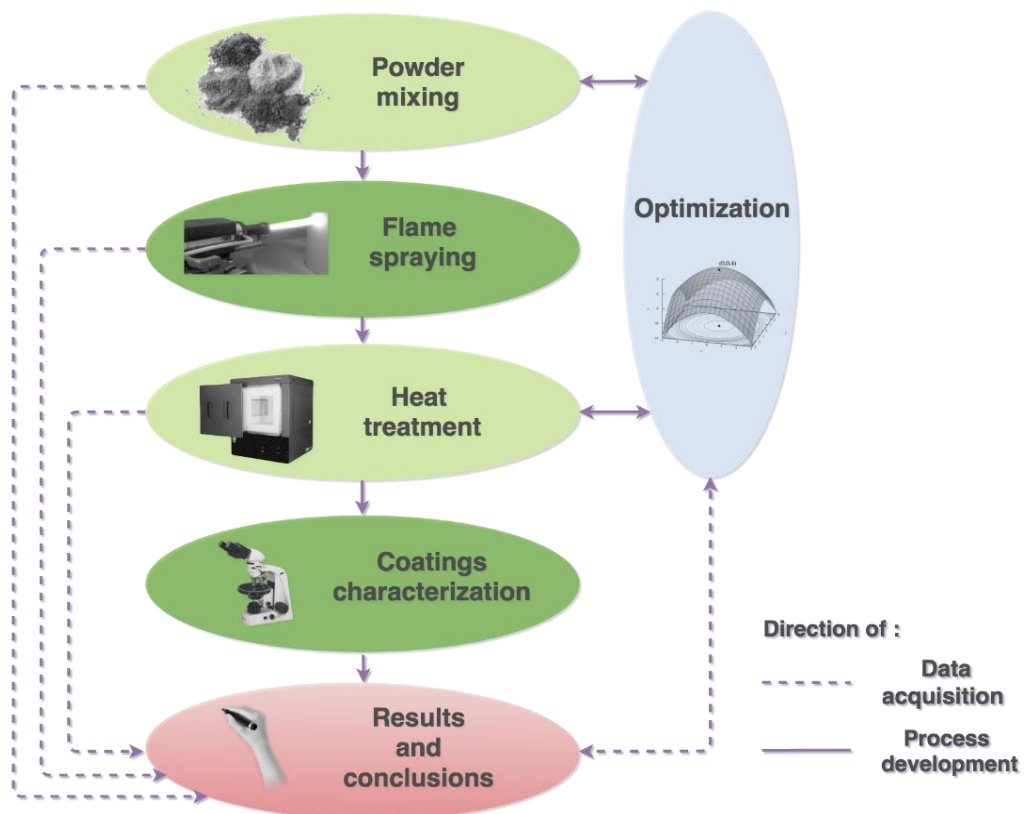

Figure 4.1 Schematic representation of the experimental program

4.1. Materials

Although thermal spraying has a comfortable position in the industry and a large number of materials can be used in combination with a multitude of deposition technologies, there is a lot of room for improvement in the sector. The chosen substrate and coating material influence every aspect of the deposition. Whether or not a substrate should be heated is determined in function of the base and coating material. Other decisions like the method of degreasing, the grit-material or the roughness that should be obtained also have to be made taking into account the coating and substrate materials used. All the coating parameters like *e.g.,* feeding rate, gas stoichiometry or the required temperature of the powder/rod have to be set according to both the material and the chosen technology in order to obtain a high efficiency of the deposition.

Therefore, in order to develop a high-end product, making the right decisions regarding the materials and the technology is crucial. The present section splits in three subchapters that closely analyse the base material, the chosen matrix and the reinforcing material. Aspects like chemical composition, melting points or particle geometries are all important details to consider when a thermal spraying deposition is performed.

4.1.1. Substrate material

The importance of the substrate material is undisputable. The base material has to be perfectly adapted to the application for which it was chosen and the materials to be coated. The subchapter 2.3.1. detailed a few aspects of the base materials of thermally sprayed coatings.

In the current study, the structural steel S355JR was used as a substrate. Structural steels are known to be used in almost all the facets of industry. Their geometries can be extremely different because of the high stiffness in regard to their cross-section. This kind of materials often take the shapes of plates, T, L or C shaped profiles or elongated pipes or railways. Thermally sprayed coatings can be found as deposited on such geometries. The six-part EN 10025:2004 standard strictly regulates the normalized, quenched, tempered or thermomechanically rolled steels with regard to their *e.g.* chemical composition or the thermal and mechanical properties. The chemical composition of S355JR is found in *Table 4.1*.

Table 4.1 The chemical composition of S355JR as regulated by EN 10025:2004

	C max. (%)	Mn max. (%)	P max. (%)	S max. (%)	Si max. (%)	N max. (%)
S355JR (DIN 1.0045)	0.24	1.6	0.035	0.035	0.55	0.012

In the delivery condition, depending on the thickness, the steel has to have a yield strength between 315 MPa and 355 MPa, a tensile strength between 470 MPa and 630 MPa, an elongation in the range of 20-22%, Young modulus 210 GPa, the hardness between 140 HB and 190 HB and an impact strength at 20°C 28J. Regarding the thermal properties of the material, the average CTE between 20°C and 300°C is 12 $\mu m \cdot m^{-1} \cdot K^{-1}$ and the thermal conductivity at room temperature in formatting 40 $W \cdot m^{-1} \cdot K^{-1}$. As the experimental part of this thesis involves working with high

temperatures, it is important to know that the S355JR grade steel has its A_{c1} and A_{c3} temperatures at 720°C and 790°C.

The most favourable substrate geometry for performing the scientific tests has been decided to be 50x20x15 mm. The machining of the samples has been done according to this specification. A degreasing has been first performed to obtain a substrate that complies with the Sa 3 class of cleanliness required by the EN ISO 8501 [50]. A grit blasting has been performed with chilled iron and a roughness between 70 µm and 100 µm has been obtained, as required by the American Navy Standard MS 2138 [58]. To protect the substrate from possible contaminations from the atmosphere, the grit-blasting has been performed in a separate room dedicated only to this procedure. The grit-blasting was the last procedure in the preparation of the substrate. Shortly after this step, the coating material was deposited.

4.1.2. The matrix material

Once deposited, the thermally-sprayed coating should be considered as an integral part of the product. In a thermally sprayed component, several materials have to be compatible with each other for the part to have a long life-cycle.

The quality of the coating hugely depends on the initial feedstock. As in any thermal spraying process, the coating of a NiCrBSi self-fluxing alloy is formed by repeated deposition of molten and/or semimolten particles. Particles that didn't melt during the coating process can unfortunately be trapped in the coating, generating porosity and poor bonding. The compatibility of the coating material with the substrate is essential as unmelted particles are not the only factor that can generate problems. The material properties of the coatings are generally not influenced by the deposition parameters of the equipment when the feedstock is optimized for the specific process.

The Ni-based self-fluxing alloys are known for the good homogeneity of the coatings and their good wear resistance. For the present work, a NiCrBSi powder from the company LSN Diffusion commercialized under the N-330 name has been used. The chemical composition of the material can be seen in *Table 4.2.*

Table 4.2 The chemical composition of the NiCrBSi powder

	Ni (%)	Cr (%)	B (%)	Si (%)	Fe (%)	C (%)
NiCrBSi (N-330)	bal.	6	1	4	1.5	0.3

The manufacturer reported size of the water-atomized powder was -60 +100 µm. In *Figure 4.2a* the SE micrograph demonstrates both the spheroid shape and the size of the material. Advantages like smaller energy input or uniform heating arise when using such powder production technologies. The obtained sphericity is connected with the in-flight particle oxidation. As the present powder is produced through water atomization, the oxidation represents a bigger problem than when the material is produced using inert gasses. The latter case implies a much more expensive powder producing technology as well.
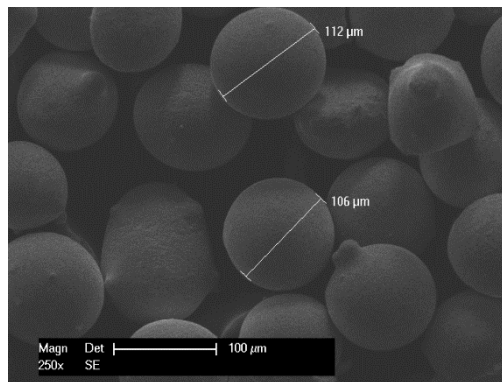
Figure 4.2 Micrographs presenting the topography of the NiCrBSi powder

The flowability of a powder is defined as the capacity of the material to move by flow and is characterized by the flow factor (ff). The NiCrBSi atomized powder has a ff of 16, as presented in *Figure 4.3*, making it a free flowing powder [212]. A high degree of flowability represents an advantage in the thermal spraying technology. For the Ni-based spheroidized atomized powder it means that by having a high consolidation stress σ_1 the material will not agglomerate in the feeding system and flow freely.

Although the powder has all the characteristics for an excellent deposition, other aspects have to be as well considered. A blockage can easily occur when the quantity of powder fed into the system is more than what it can support. An improper storage of the powder, for instance in a humid or sunny environment, can as well decrease the ff of the material.
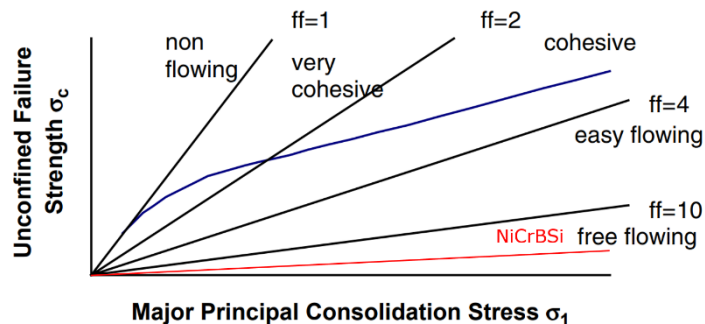

Figure 4.3 The flowability function of the NiCrBSi powder [212]

An EDX analysis of the NiCrBSi powder can be seen in *Figure 4.4.* The balance element Ni dominates the spectrum having the most intense peaks. After Ni, the carbide forming element Cr has the highest peak. Carbides are known to be hard compounds and to have a favourable effect on the wear resistance of thermally sprayed coatings. Si, even though it is found in a small quantity in the chemical composition, promotes, in combination with B, the deoxidation and the wettability of

the coating during the heat treatment. Si tends to form phases with both Ni and Fe, influencing the structure of the matrix in the coating.
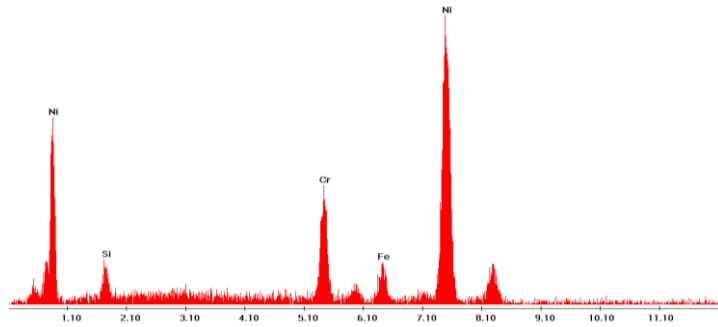

Figure 4.4 EDX spectrum of the NiCrBSi powder

The melting range of the material is a very important aspect in the context of an industrial use. The whole deposition process is adjusted in function of the melting range of the powder, which was in this case determined using a thermogravimeter. Approximately 100 mg of the powder have been placed in a Al_2O_3 crucible. The thermal analysis has been performed between 23°C and 1200°C under N_2 flowing atmosphere with a heating rate of 15 K min^{-1}.

In the thermogram presented in *Figure 4.5* the range of temperature that is relevant is between approximately 920°C and 1150°C. The liquefying point is starting at 1009°C, the material being completely melted at 1068°C. Therefore, this chemical composition of Ni-based powder will have to be deposited and heat-treated at a temperature of at least 1050°C. However, if the chemical composition of the powder is changed, the melting range of the material is shifted and the temperatures of the torch, flame and substrate have to be adjusted accordingly. Si and B are lowering the melting temperature of the matrix material and stabilizing it at the same time [213]. Moreover, the addition of Si in the alloy is increasing the self-flux ability of the material.
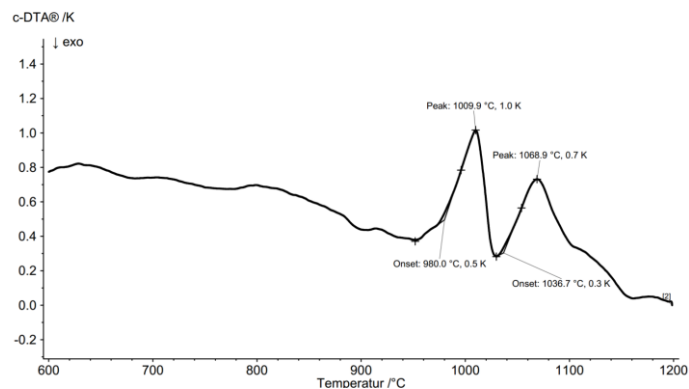

Figure 4.5 DTA curve of the NiCrBSi powder

If possible, it is highly recommended to perform XRD analysis on compounds as complex as NiCrBSi, as the phase composition can vary significantly depending on numerous factors *e.g.* chemical composition or production method. It is important to note that for the applications in which the material is used, the phase composition can give as well predictions and explanations regarding the material behaviour under wear or corrosion tests.

The *Figure 4.6* presents the diffractogram of the NiCrBSi powder scanned between the 2θ angle of 20° and 100°. As expected for the chemical composition of powder, the most intense peak at approximately 45° 2θ angle is identified as Ni. The largest part of 70% of the quantification chart is as well attributed to Ni. The two other following phases are the orthorhombic NiSi and Ni_3B, occupying 14% and 11% of the quantification chart. Those two phases, along with the Fe_2Si, crystallized in this situation in a hexagonal structure and were quantified at 3% of the whole. The smallest quantity of 2%, is the hard Cr_5B_3 phase crystalized in a tetragonal structure. The maximum intensity of the phase has been identified as overlapping with the Ni one at approximately 45° 2θ angle.

The intermetallic compounds dominate the structure of the coating but their properties radically differ from the properties of the single constituent elements. For example, in most of the cases, a Ni solid solution is dominating the microstructure. For flame-spraying processes followed by a flame remelting chromium carbides and borides have been detected. In a flame spraying process followed by laser cladding, additional nickel borides have been found. All these different compounds can affect the microhardness, adhesion, tribological or corrosion behaviour of the coating in different environments [214].
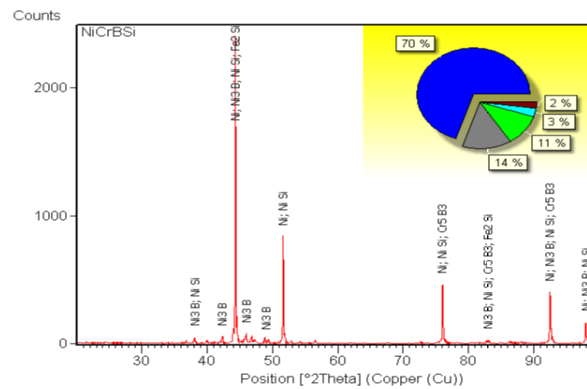

Figure 4.6 XRD pattern of the NiCrBSi powder

Once the powder is deposited, the number, the crystalline structure, the lattice parameters and quantities of the detected phases are considerably altered. Moreover, due to the addition of a reinforcement to this already complex material, the properties of the coating are expected to be radically modified.

4.1.3. The reinforcing material

The vast majority of the thermally sprayed coatings are constituted of a matrix and a reinforcement. The theoretical part of the current work briefly reviewed some of the most important powder production technologies. Atomizing, sintering, agglomerating milling or mechanically mixing, all have their pros and cons. The process has to be chosen according to the materials, the application and naturally, the needed result.

TiB_2 is a relatively studied ceramic in the medical, thin film and aeronautic industries. The high hardness, good creep resistance, thermal conductivity and chemical stability are just some of the properties that make the compound attractive to use in the coating industry. The material can crystallize in an orthorhombic or hexagonal crystalline cell, both structures being an advantage for the decrease of the wear rate of coating containing TiB_2. Another positive aspect in using TiB_2 for the coating industry is that the majority of the properties do not change at room and elevated temperature [157,159].

The TiB_2 powder used for the current work was produced by the German company H.C. Starck. The chemical composition of the powder can be consulted in *Table 4.3*.

Table 4.3 Chemical composition of the TiB_2 powder

	B min (%)	C max (%)	O max (%)	N max (%)	Fe max (%)
TiB_2	min. 30	6	1	4	1.5

SEM micrographs of the compound can be seen in *Figure 4.7.* The particle size distribution of the TiB2 varies between 3.5 µm and 8 µm. As it can be observed in *Figure 4.7a*, the topography of the particle is irregular. On one hand, during the feeding and thermal spraying process, it can be an unfavourable aspect because it can easily create difficulties in the flowing of the material through the powder carrier system. On the other hand, the material being mixed with the spheroidized Ni-based matrix, it creates the possibility of a powerful hooking between the two powders, making it possible for them a flow simultaneously in the feeding system.
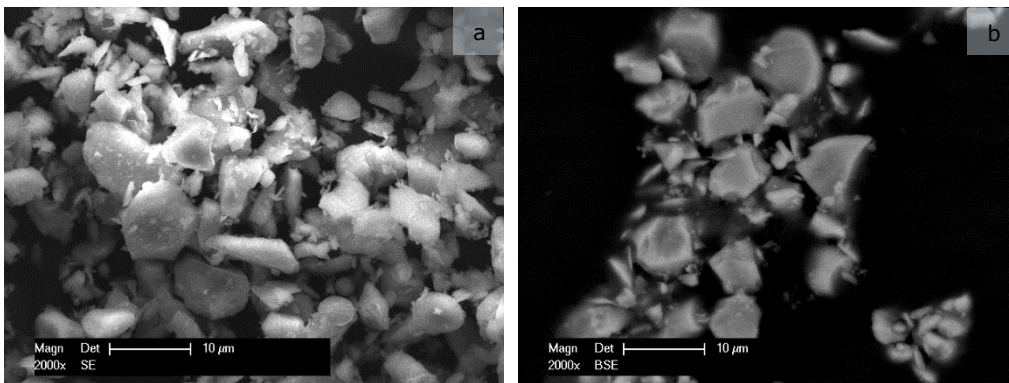

Figure 4.7 Micrographs presenting (a) the topography and (b) the cross-section of the TiB_2 powder

The EDX spectrum from *Figure 4.8* confirms the chemical composition of the delivered powder showing both the principal Kα at 4.51 KeV and secondary Lα 0.41 kEV of Ti. Although having a very low reflected characteristic X-ray energy of 0.18 kEV, B has been also detected.
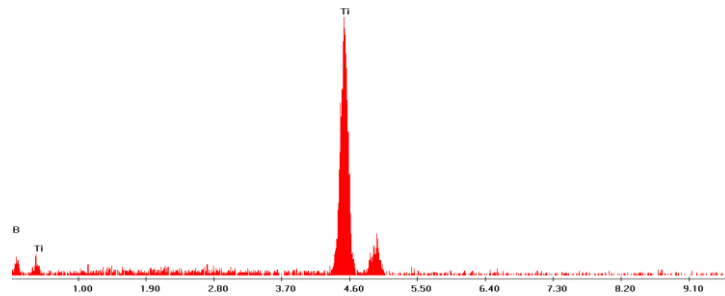

Figure 4.8 EDX spectrum of the TiB$_2$ powder

The powder manufacturer reported a powder size range of -3.5 +10 μm. As expected, in the XRD spectrum of the powder presented in *Figure 4.9,* the only detected phase is the TiB$_2$. The compound crystallized in a hexagonal structure with the maximum peak found at the 2θ angle of approximately 44.46°. Several interesting aspects can be underlined regarding the forming elements of the compound. Ti is a silvery metallic element that typically has a hcp structure transforming to a bcc one at 882°C, 870°C and 1760°C. When heated to high temperature, the element reacts with most of the non-metals. Explicitly because of its easy reactivity, it has an outstanding room corrosion temperature provided by the dense, adherent, self-healing formed oxide film. This property of the Group 3 elements can be an advantage in the case of the thermal spraying coatings. B is a hard refractory solid with rhombohedral as most stable crystalline structure. The element keeps its structure up to temperatures reaching 4000°C [215].
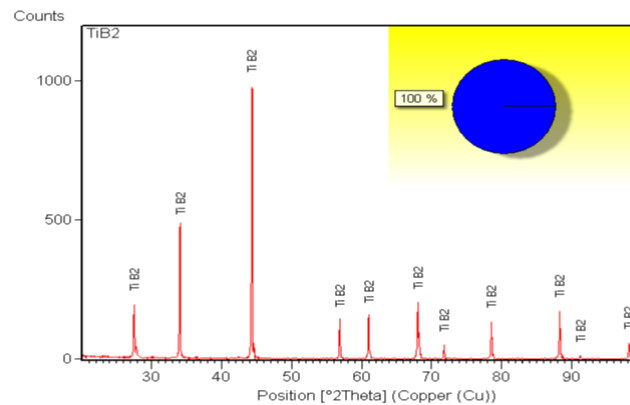

Figure 4.9 XRD pattern of the TiB$_2$ powder

Considering all the analysed aspects of the reinforcement material there are reasons to expect interesting changes when the thermal spraying and post-treatment is performed.

4.2. Powder mixing

The matrix and the reinforcement materials presented in the former two subchapters have been mixed in four different volumetric proportions using a screw conveyer. This type of process, schematized in *Figure 4.10*, relies on the principle of turning the apparatus in a controlled manner with the materials inside of the conveyor. The matrix and the reinforcement are placed in two separate containers found at the two ends of the assembly. Once the two components including the powders are screwed to the conveyer, the equipment has to be completely turned in a controlled way for about 600 s. At the end of the process, the whole amount of the mixed powder should be located at one end of the assembly. The screw conveyer has been afterwards disassembled, the powder sealed and the single containers carefully cleaned. It is important to leave the single parts of the assembly clean so that in a future use of the conveyer no contamination of the material occurs.

Several advantages of the powder mixing technology motivated the decision to use this technology for the present work. The screw conveyors inherently ensure that the NiCrBSi and TiB_2 powders are constantly mixed while the combining of the materials through the rotating spiral eliminates the risk of segregation of the smaller reinforcing material. The cost-effectiveness of the method can as well be a big advantage for powder analysis in the research.
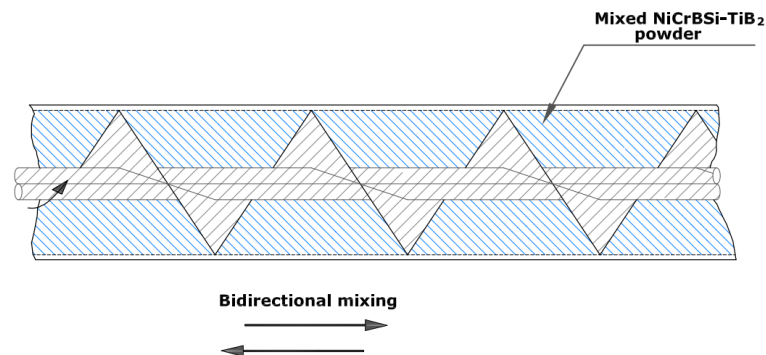
Figure 4.10 Schematic of a screw conveyor

Some preliminary tests showed that the flow of the material through the powder feeder gets extremely difficult when mixing a high volumetric percentage of the reinforcement with the matrix. Consequently, four mixes, presented in *Table 4.4*, have been considered for further investigations.

Table 4.4 The four NiCrBSi-TiB_2 volumetric mixes considered for investigations

Designated name	NTB5	NTB10	NTB15	NTB20
NiCrBSi:TiB_2 vol. %	95:5	90:10	85:15	80:20

Comparing the topography of the NiCrBSi and TiB2 material, presented in *Figure 4.2* and *Figure 4.7a*, it is easy to observe the size difference of the powders. When mixing materials with such a size dissimilarity, maintaining the integrity and

avoiding the degradation of the powders is as well a challenge during the process. It can be observed in *Figure 4.11* that, when using a screw conveyor, the two materials are carefully mixed in a way that makes the small TiB_2 attach as satellites of the much bigger in size NiCrBSi matrix.
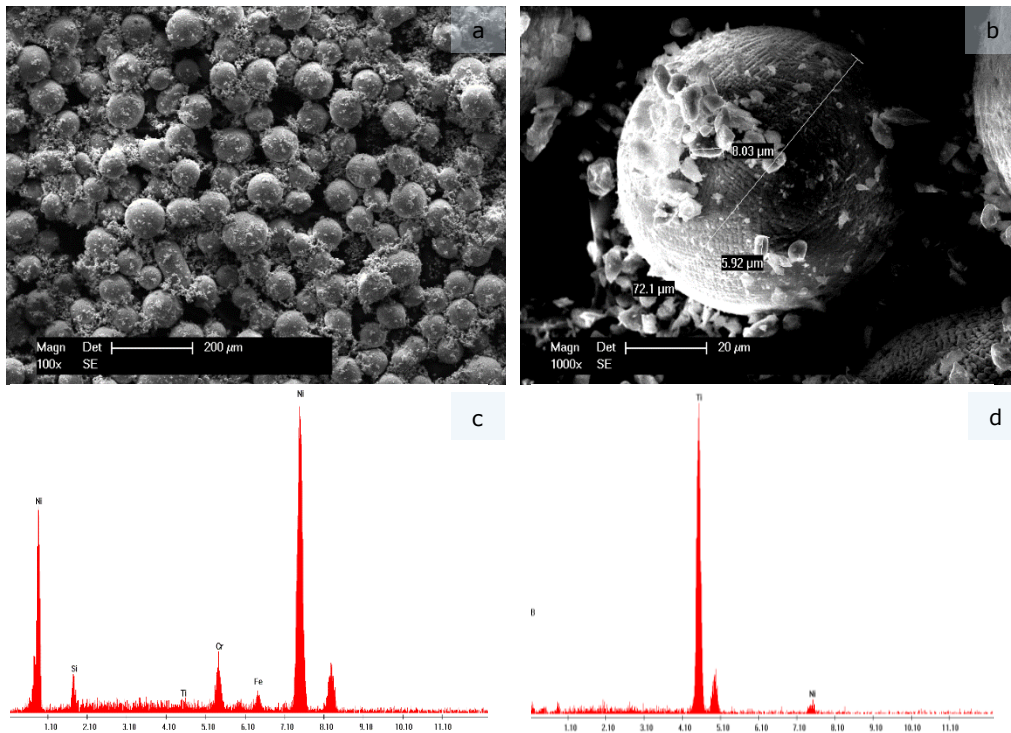
Figure 4.11 SE micrographs of (a) the overview and (b) the detail of the composition and the corresponding EDX analysis of (c) the NiCrBSi and (d) the TiB_2 powder

Although it could be believed that the mixing process does not affect the chemical compositions of the material, a small change can yet be observed. The EDX analysis in *Figure 4.11c* and *Figure 4.11d*, show a small content of Ti and Ni in the matrix and reinforcement material respectively. This phenomenon is a consequence of the material friction and of a minor detachment of microparticles from each material. Part of these bodies attach to the same material and another part on the other one while the rest remains free in the system.

4.3. Powder deposition

The material deposition process is an extremely important step to obtain the desired characteristics of the coating. There are a high number of variables that need to be taken into account *e.g.* the spray pattern, the build-up of the coating, the process variation, the temperature control on both the substrate and coating, or the motion of the torch or substrate, when the thermal spraying is performed. The goal of the thermal spraying was to successfully deposit the mechanically mixed NiCrBSi-TiB_2 powder on the S355JR structural steel. The operating parameters have been attentively set according to the characteristics of both the depositing and the substrate material and they can be consulted in *Table 4.5*.

Table 4.5 The main operating conditions of the thermal spraying process

Parameters	Materials/conditions/values
Sprayed material	NiCrBSi – TiB_2
Substrate material	Structural steel
Surface roughening	
Surface roughening method	Grit blasting
Roughening material	Chilled iron grit
Surface roughness after roughening	min. 75 µm
Flame spraying gun producer	Metatherm
Flame generation	
Fuel gas	Acetylene (C_2H_2)
Secondary gas	Oxygen (O_2)
Flame stoichiometry C_2H_2:O_2	1:2
Substrate temperature	≈ 105°C
Spraying temperature	≈ 2850°C
Fusion temperature	≈ 1100°C
Particle velocity	100 m s^{-1}
Coating deposition	
Powder feed rate	2.5 kg h^{-1}
Stand-off distance	120 mm.
Propelling gas	Purified air
Relative gun motion	Translation over the samples

Before the actual deposition, the substrate has been brought to the cleanliness normed values of the EN ISO 8501 [50] standard through degreasing and water and alcohol cleaning. As the substrate should reach a roughness value between 70 µm and 100 µm [58], the grit blasting with chilled iron grit has been considered a proper technique to use. The chilled iron is an abrasive cast iron material manufactured through atomization. During the blasting process, the material breaks in a way in which a mixture of sharp grit is produced, roughening the structural steel and cleaning it quickly. The blasting was performed in a dedicated room to avoid the contamination of the substrate material. After the grit blasting, the roughness has been measured at an average value of Ra 75 µm, corresponding to the industrial standards [58].

The deposition of the NTB powder has been performed with a Methaterm MPP-85 (5PII Type) gun. This gun has been an ideal choice for the deposition for several reasons. The integrated powder container allowed for a quick and complete cleaning of the air propulsive system to avoid contamination between the NTB powder batches. The gun is equipped with a vibrator that is useful especially for the fine TiB_2 material. Being a combustion flame-spraying device, the system uses oxygen and

acetylene as fuel gasses for deposition. The stoichiometry of the flame has been set to C_2H_2:O_2 1:2, creating an oxidizing flame. The amount of oxygen in this situation increases, the colour darkens and the flame shortens.

The stand-off distance between the torch and the substrate was kept constant during the TS process regardless of the part or torch movement. The chosen 120 mm constant distance ensured the maintenance of the same conditions for the whole spraying process and the deposition of the same thickness of material on the grit-blasted substrates.

In the moment when the deposition is performed, the temperature control of both the substrate and the flame is extremely important. As in the vast majority of the cases, because the coating deposition is performed in normal atmosphere and high temperatures, an inevitable oxidation appeared, eventually giving a darker color to the samples. The heating of the substrate is important for the improvement of the mechanical hooking between the powder and the selected substrate. The critical oxidizing temperature varies for each material but in order to perform a successful TS, the structural steel should be held under 150°C. Considering this aspect, the substrate has been heated at $\approx$ 105°C. In the meantime, the temperature of the flame must be kept above the melting range of the NiCrBSi material, but under the melting point of the TiB_2 particles. The melting temperature of the reinforcing material is around 3200°C. Taking into account those elements, the flame was set and kept at $\approx$2850°C. When those conditions are maintained, a diffusivity between the matrix and reinforcement is assured. Because the flame temperature was under the melting temperature of the TiB_2, the solid particles of the reinforcement material stayed in the matrix and contributed to the corrosion and wear behaviour of the coating.

The velocity of the particles was approximately 100 m s^{-1}, a typical value for the combustion thermal spraying technology. During the coating process, the samples stayed fixed while the gun translated over the sample. The same number of translations has been performed over all the samples in order to obtain the same coating thickness.

4.4. **Vacuum furnace optimization of the fusion process**

Putting it simply, the Design of Experiments (DOE) is a method of gathering the maximum amount of information from samples arranged in a design space by using a minimum amount of probes and invested energy. As each sample is time and resource consuming, it is legitimate to try to limit the needed effort. It is important though to test a reasonable amount of probes as by lowering the runs, the inaccuracy of the system is increasing.

In engineering, the results are instinctively the ones that are giving a hint whether a process is going in the right direction or not. The design of experiment method developed by *Fisher R.A.* [101] focuses on the mean of a process and the one pioneered by *Taguchi G.* (called robust design) [103] tries to correct the loss function (*i.e.* the errors of a system). In a different way of thinking, the response surface methodology (RSM) is a much more intuitive way to increase the quality by employing a cheaper step-by-step approach where fewer experimental runs are required and a high statistical efficiency is reached. For the present work the RSM optimization method has been chosen.

For Ni-based self-fluxing alloys, the thermal post-treatment of the coating is highly important. The post-treatment and its results can largely influence the quality of the entire deposition. For this reason, the optimization process of the heat treatment parameters is strongly recommended. The flowchart of the followed steps of the optimization can be seen in *Figure 4.12.*
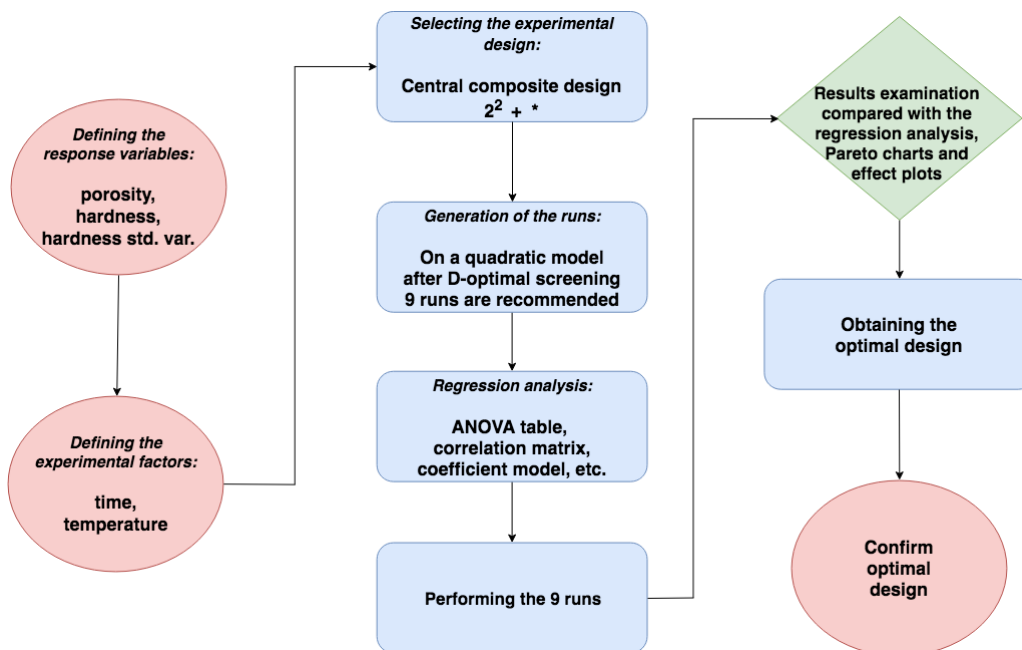

Figure 4.12 RSM flowchart procedure for the optimization of the vacuum heat treatment parameters

To sum it up, the RSM procedure involved:
- Identifying the problem
- Defining the responses that will establish the final working parameters
- Defining the input parameters, the ones that will be varied
- Choosing the experimental design
- Performing a regression analysis to verify the power of the optimization and the correctness of the design
- Running the statistical tests
- Examining the statistical results
- Remodelling the statistical design if the results are not satisfactory
- Obtaining the optimal design
- Confirming the optimal design.

The response variables selected for the present work have been the porosity, the hardness and its standard deviation. These parameters have been extensively used as responses in the optimization of thermal spraying coatings [111,216–218].

The porosity is highly important when it comes to TS. As presented in the state of the art and methodology chapter, the void content, shape and measurement is present in all the technologies and can vary extremely much. An interconnected porosity can be disastrous with regard to corrosion or wear. When it comes to the resistance or machinability of the coating, the porosity plays an important role as well. The microhardness and its standard deviation can give us other hints about the quality of the deposition. The resistance of the material to plastic deformations characterizes the level of strength of the intermolecular bonds. The ductility, the strength or the viscosity are just a few of the elements that depend on the hardness. The standard deviation of the microhardness is a parameter that gives an indication on the uniformity of the coating. Although when performing microindentation, the indented phases exhibit different values, it is essential to measure the same value of the same phase in the whole coating. Considering the importance of these parameters, selecting the porosity, the hardness and the hardness deviation as responses of the design was an obvious choice. The three responses and their considerations can be seen in *Table 4.6*.

Table 4.6 Response variables to be measured

Name	Units	Analyse	Goal	Impact (S) 1-5	Sensitivity	Low (L)	High (U)
Porosity (P)	%	Mean	Minimize	5.0	Medium	0.1	10
Hardness (H)	HV0.3		Maximize	3.0	Medium	200	400
Hardness standard deviation (σ)			Minimize	2.0	Medium	20	100

As stated in *Table 4.6,* the statistical model is built for the mean of the three defined responses. The set goal for the porosity *P* and the hardness standard deviation σ was to minimize the value of the responses as much as possible. In contrast, a high hardness *H* is desired. The impact is referring to the relative importance of one response versus another. In TS, a coating with high porosity, high hardness and low hardness, is generally considered a low quality one. In contrast, one with low porosity, relatively low hardness and high hardness standard deviation can still be easily employed in the industry and resist to wear and corrosion. Therefore, the maximum impact was attributed to the porosity, followed by the hardness and σ. To generate

the statistical model, a range of values that the responses can take has to be defined. The porosity and the hardness standard deviation should be as low as possible and the desired range was set to 0.1 and 20. It is known that the hardness of the Ni-based self-fluxing materials is not necessarily very high [219,220]. Previous work where N-330 powder has been used [221] showed that because of the low content of the alloying elements, the hardness is not very high. Therefore, a range of 200 HV0.3 – 400 HV0.3 for this particular case can be acceptable for the optimization design.

During a RSM experiment, several types of factors can be analysed. Parameters that can be varied are called *controllable factors*. There can be also mixture components where the relative percentage of the components in the mix is changed or noises that are considered uncontrollable factors. The two process factors that are followed in this experimental design, time and temperature, are controllable as they can be regulated during the process in order to enhance the process quality. They can be consulted in *Table 4.7*. In contrast to the categorical type of factors where levels like *e.g.* low, medium and high are attributed, the two experimental factors have been set to be continuous as they can take values over a continuous range. In consequence, A: Time has been set to take between 30 min. and 90 min., values chosen in accordance to peer reviewed literature [222–224], and B: Temperature has to be maintained between 1020°C and 1110°C, based on the melting range of the matrix material determined by the termogravimetric measurements.

Table 4.7 Experimental process factors to be varied

Name	Units	Type	Role	Low	High
A: Time	min.	Continuous	Controllable	30	90
B: Temperature	°C			1020	1110

Depending on the response variables and the experimental process factors, different types of designs can be selected. For continuous factors screening, multilevel factorial, orthogonal array and response surface design can be used. The screening is using the most important factors from a long list. The multilevel factorial is performing an optimization by running a large number of runs and the orthogonal (*i.e.* Taguchi method) design falls in the robust parameter design. As already mentioned, for the present work a response surface design was chosen as it aims at finding the optimal working conditions of the experimental process factors. The details of the RSM model design can be seen in *Table 4.8*.

Table 4.8 Model specification to be fit to the experimental results

Design type	Centrepoints per block	Centrepoints placement	Number of replicants	Total runs	DF [b]	Model type	Final runs [c]
CCD [a] 2^2 + star	2	last	0	10	4	quadratic	9

[a] Central composite design
[b] Degrees of freedom
[c] Number of runs after applying the D-optimal backwards algorithm

The central composite design 2^2 + star consists of several points, each of them being attributed a time and a temperature value. The design is a form of the 2^k CCD (*i.e.* Box-Wilson design) where *k* is given by the number of controllable factors. As

these points take the extreme high-low, extreme and centrepoint values of the experimental factors, the representation of a 2^2 + star design for the vacuum heat treatment would be as represented in *Figure 4.13*. The stars, or centrepoints, are points taken at the centre of the design. This design is considered advantageous as it consists of a relative small number of runs in comparison with a multi-level factorial design.
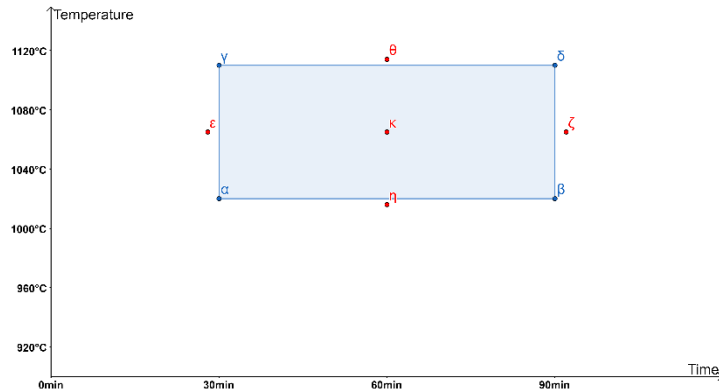

Figure 4.13 The 2^2 + star CCD created for the vacuum heat treatment post-processing

In *Figure 4.13,* the points α,β,γ,δ are found at the high-low levels of the process factors (time and temperature), ε,ζ,η,θ are placed at extreme points, outside of the design, while ι,κ are considered centrepoints.

The design has four degrees of freedom to estimate the error. The measurement of the error is important in order to know the noise in the experimental process. A minimum recommended DF is two, so the four degrees estimated by the design are an acceptable value. Although a randomized design (meaning a randomized order of the runs) is recommended, it has been decided to create one where the centrepoints are placed at the end. After all, the same experiments were run, the advantage in this case being the effortless identification of the point.

There are several model types that can be attributed to a CCD: linear, 2-factor interaction, quadratic and cubic. For this experiment a quadratic model type has been selected. The different model types affect some of the diagnostics the experimental design is generating. The fitted response $\hat{Y}$ of the quadratic CCD model is mathematically described as:

$$\hat{Y} = A_0 + A_0 B_1 + A_2 B_2 + A_3 B_3 + A_{12} B_1 B_2 + A_{13} B_1 B_3 + A_{23} B_2 B_3 + A_{11} B_1^2 + A_{11} B_2^2 + A_{11} B_3^2 \ (4.1.)$$

where the experimental factors A (time) and B (temperature) are considered. The quadratic CCD (Box-Wilson) design $\hat{Y}$ provides typical interactions like the linear and the quadratic factors from the *Eq. (4.1.).* When selecting another type of design, other relationships between the factors are developed and they might influence some perceptions over the regression analysis.

The extracted time-temperature programs that were required for the four batches can be consulted in *Table 4.9*. The first four programs represent the α,β,γ,δ points, followed by the extreme points ε,ζ,η,θ located outside of the rectangle. The values of the ε,ζ,η,θ points have been rounded-up to a two decimal number for practical reasons. The last program is a centrepoint found at the middle of the design

and is practically one program generated from overlapping ι and κ. The elimination is performed by a D-optimal design algorithm. Using a D-optimal backward algorithm is always optional but it is particularly useful to eliminate some runs considered partly or entirely redundant. Using the algorithm is practically a matter of design efficiency.

Table 4.9 The values of the 2^2 + star central composite design

Program no. n	Time (min.)	Temperature (°C)
1	30.0	1020.0
2	90.0	1020.0
3	30.0	1110.0
4	90.0	1110.0
5	28.0	1065.0
6	92.0	1065.0
7	60.0	1016.0
8	60.0	1114.0
9	60.0	1065.0

An evaluation of the design through regression analysis offers a number of possibilities to assess the properties of the selected model.

The correlation matrix (4.2.) reveals any confounding between different effects. The mathematical array is a friendlier interface for the $\hat{Y}$ equation. The matrix helps for analysing the orthogonality of the design. The orthogonality is an important property in the RSM and it allows the individual effects to be independently estimated without confounding. A perfectly orthogonal design shows a diagonal matrix with 1`s on the diagonal and 0`s off the diagonal. Initially, the model generated the 10 runs featuring different time-temperature combinations. However, through the application of the D-optimal algorithm and the rounding-up of the values to an integer number, the perfect orthogonality is lost. The 5 columns that display non-zero correlations are results of the formerly executed actions. In the end, none of the values are equal to or greater than 0.5. It can be therefore concluded that the rounding-up and the application of the D-optimal algorithm were legitimate actions that do not affect the optimization process.

$$
M_C = \begin{matrix}
 & A & B & AA & AB & BB \\
A & 1 & 0 & -0.0467 & 0 & 0.0126 \\
B & 0 & 1 & 0 & 0 & -0.0164 \\
AA & -0.0467 & 0.0042 & 1 & 0 & -0.1432 \\
AB & 0 & 0 & 0 & 1 & 0 \\
BB & 0.0126 & -0.0164 & -0.1432 & 0 & 1
\end{matrix}
\qquad (4.2.)
$$

The ANOVA table presented in *Table 4.10* is showing the experimental error. It can be seen that there are 5 degrees of freedom being used to fit the statistical model. The DF number increased from 4 to 5 after applying the D-optimal algorithm. As mentioned, by using the D-optimal algorithm the design efficiency has been increased but a certain degree of error has been as well introduced. There are 3 DF left for the experimental error. The pure errors come from the replica of the experimental runs. By not performing replica experiments, the pure error will be accordingly equal to zero. There are also 3 DF to estimate the fitting of the experiment in the quadratic model. These lack-of-fit DF will tell if the quadratic model is satisfying for the present

experiment. In general, it is advisable to have as many error degrees of freedom as possible available when testing the statistical significance of estimated effects.

Table 4.10 ANOVA table

Source	Degrees of freedom
Model	5
Total error	3
Lack-of-fit	3
Pure error	0
Total	8

Once the regression analysis was performed, the experimental tests were run. The results of the tests are displayed in *Table 4.11* and *Table 4.12.* The predicted values and variance plot of the generated quadratic central composite design can be consulted in the *Appendix*.

Table 4.11 Results of the experimental program for the NTB5 and NTB10 batches

n	t (min)	T (°C)	$\bar{P}$ (%)	$\bar{H}$ (HV0.3)	σ	D [a]	$\bar{P}$ (%)	$\bar{H}$ (HV0.3)	σ	D [a]
						NiCrBSi+5%TiB$_2$		NiCrBSi+10%TiB$_2$		
1	30	1020	5.99	330	34	0.53	*3.44*	*346*	*48*	*0.71*
2	90	1020	*2.25*	*311*	*34*	*0.71*	3.8	318	78	0.53
3	30	1110	2.08	288	39	0.66	1.28	346	137	0
4	90	1110	1.3	277	42	0.66	1.02	302	89	0.52
5	28	1065	3.88	304	28	0.63	3.94	310	64	0.55
6	92	1065	2.83	352	80	0.59	9.6	366	117	0
7	60	1016	9.96	301	37	0.05	7.7	332	64	0.38
8	60	1114	3.9	315	47	0.61	8.03	289	47	0.25
9	60	1065	6.84	319	89	0.33	13.64	319	89	0

[a] Desirability

Table 4.12 Results of the experimental program for the NTB15 and NTB20 batches

n	t (min)	T (°C)	$\bar{P}$ (%)	$\bar{H}$ (HV0.3)	σ	D [a]	$\bar{P}$ (%)	$\bar{H}$ (HV0.3)	σ	D [a]
						NiCrBSi+15%TiB$_2$		NiCrBSi+20%TiB$_2$		
1	30	1020	5.28	344	52	0.51	4.88	337	51	0.58
2	90	1020	4.25	320	38	0.55	7.23	314	79	0.32
3	30	1110	3.23	344	45	0.63	*1.98*	*351*	*43*	*0.71*
4	90	1110	*1.12*	*321*	*37*	*0.82*	1.41	332	86	0.47
5	28	1065	7.23	320	59	0.35	3.87	344	79	0.51
6	92	1065	3.22	345	40	0.7	1.47	371	142	0
7	60	1016	14.2	325	24	0	5	318	39	0.57
8	60	1114	2	314	24	0.75	1.3	293	62	0.61
9	60	1065	3.46	337	52	0.65	3	335	67	0.58

[a] Desirability

Some exemplifying results of porosity P (*i.e.* the first chosen response to be analysing) from run number 4 can be seen in *Figure 4.14.* The mean porosity $\bar{P}$ for each batch has been calculated as a mean of five calculated values from different regions of the samples. It is necessary to mention that not all the black regions of the micrographs are pores. This aspect will be further detailed and clarified in the microstructural characterisation part of the present work.
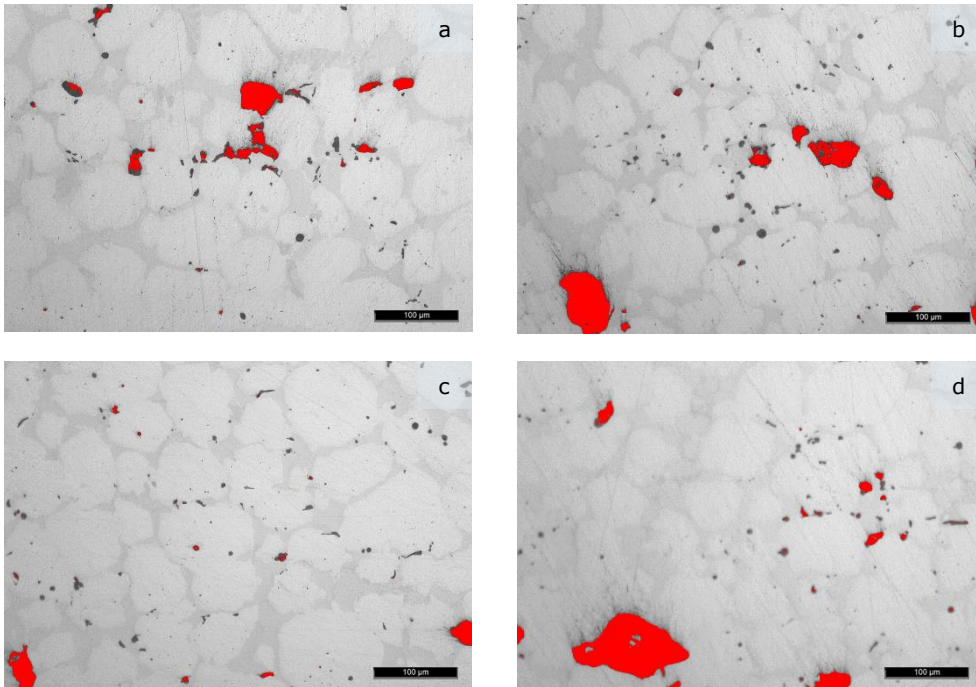

Figure 4.14 Exemplifying porosity measurements through image analysis of the (a) NTB5, (b) NTB10, (c) NTB15 and (d) NTB20 samples

The hardness indentations have been performed close to the middle height of the coating. The distance between the indentations was 200 µm, a value exceeding three times the diameter of a single indentation. The mean hardness $\bar{H}$ for each batch has been calculated as a mean of five calculated values from different regions of the samples.

The standard deviation of the hardness σ has been calculated as:

$$\sigma = \sqrt{\frac{\sum (H-\overline{H})^2}{5}} \qquad (4.3.)$$

where H is the hardness and $\bar{H}$ the mean of the hardness. The sum of the differences has been divided by 5 as there have been 5 hardness measurements for each batch of heat-treated samples.

The desirability D concept*, developed by *Myers and Montgomery,* is a very popular and easy to visualize multiple response method in statistical optimization [104] . The idea behind the concept is that values of a particular process or product must be inside its defined limits. The approach assigns a score between 0 and 1 to

the results of the responses. A complete "undesirability" is reached when the results of the experimental runs of the process are outside its defined low and high limits, the function $d_i(Y_i)$ of the response $Y_i(x)$ taking the value 0. When the desired value of the response is reached through the results of the runs, the function $d_i(Y_i)$ will be 1.

As mentioned in *Table 4.6*, let us define S as the impact, L_i the low and U_i the high value of the responses. When maximizing a response, in the present case the hardness, the individual desirability function is:

$$d_i(Y_i) \begin{cases} 0 & if \ \hat{Y}_i(x) < L_i \\ \left(\frac{\hat{Y}_i(x)-L_i}{T_i-L_i}\right)^S & if \ L_i \le \ \hat{Y}_i(x) \ \le U_i \\ 1 & if \ \hat{Y}_i(x) > U_i \end{cases} \tag{4.4.}$$

When minimizing a response, in the present case the porosity and hardness standard deviation, the individual desirability function is:

$$d_i(Y_i) \begin{cases} 1 & if \ \hat{Y}_i(x) < L_i \\ \left(\frac{\hat{Y}_i(x)-L_i}{T_i-L_i}\right)^S & if \ L_i \le \ \hat{Y}_i(x) \ \le U_i \\ 0 & if \ \hat{Y}_i(x) > U_i \end{cases} \tag{4.5.}$$

The general form of the overall desirability equation with t runs takes the following form:

$$D = \left(d_1(Y_1)d_2(Y_2)\cdots d_k(Y_k)\right)^{1/t} \tag{4.6.}$$

Applying *Eq. (4.6.)* to the present case, the overall desirability function is:

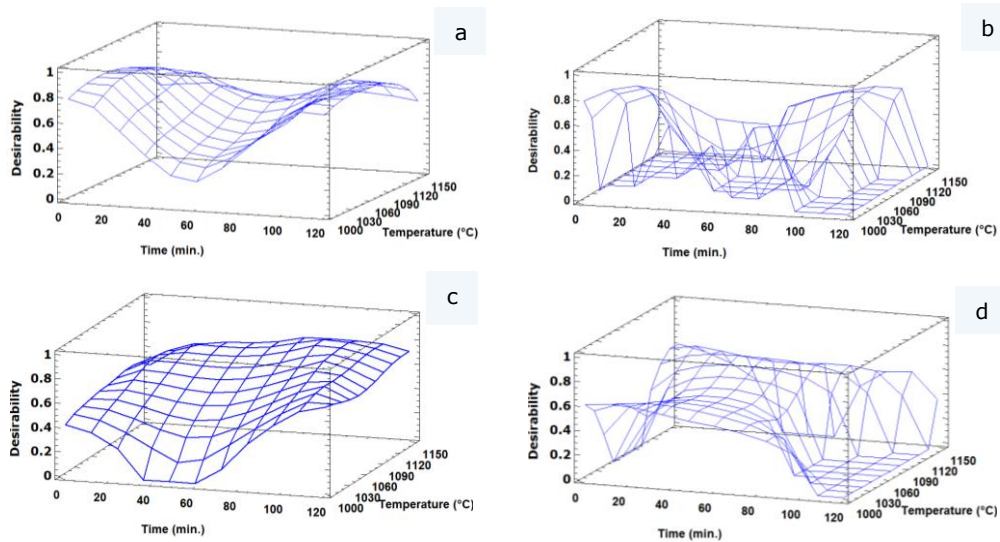$$D = \left(d_1(\bar{P})_1 d_2(\overline{H})_2 d_k(\sigma_k)\right)^{1/9} \tag{4.7.}$$

Figure 4.15 Desirability plot of the (a) NTB5, (b) NTB10, (c) NTB15 and (d) NTB20 samples

The plots of the four batches can be seen in *Figure 4.15*. The desirability is shown as a three-dimensional plot against the time and the temperature. The graph shows the regions where desirable results can be achieved.

An almost symmetrical plot has been obtained in the case of NTB 5. Because of the very low content of TiB_2, it was expected that the plot of the self-fluxing NiCrBSi matrix wouldd take a similar shape. Compared to all the other plots, the NTB5 graph does not present points reaching outside of the experimental factors limit. The batch containing 10 vol.% of TiB_2 presents the most 0 desirability points of all the graphs. The biggest regions where 0 points are found are at a maximum temperature and minimum time and at minimum temperature and a long holding time. The highest desirability value of 0.82 was obtained for NTB15 in the region of 90 min. and 1110°C. It can be observed that after reaching the two points, the desirability is decreasing even when a higher temperature and a longer time is applied. The NTB20 batch is presenting a region of 0 points until a temperature of approximately 1100°C after which a fast increase can be seen.

As general remarks, it can be observed on one hand that at medium combination of the two responses a decrease is occurring in the plots. On the other hand, the highest peaks for all the plots are achieved at high temperatures and long holding times. Every plot of each batch reached a maximum desirability of over 0.7. Nevertheless, the only one crossing a 0.8 desirability point is the NTB15 batch.

Conclusively, it can be stated that in order to obtain optimum results for a vacuum heat-treated thermally sprayed NiCrBSi-TiB_2 sample, a combination of 85 vol.% matrix and 15 vol.% reinforcement should be used. The post-processing with a vacuum furnace at a holding time of 90 min. at a temperature of 1110°C should deliver the best results.

The heat-treatment program for the optimal parameters can be seen in *Figure 4.16.* The program shows a three-interval heating, the first being performed with 10°C min^{-1} up to 200°C. At this temperature the water and other possible compounds evaporate. The second heating ramp is performed with 10°C min^{-1} until 950°C. The temperature is under the melting range of the matrix material but high enough for a soaking of the material. A 10 min holding time should be enough for soaking as the samples are relatively small in size. A slow heating of 5°C min^{-1} has been performed followed by the holding of 90 min at 1110°C as determined by the optimization program. A slow cooling until 950°C has been performed to avoid introducing internal stresses. The last cooling ramp was at 10°C min^{-1} until the ambient temperature of 23°C was reached.
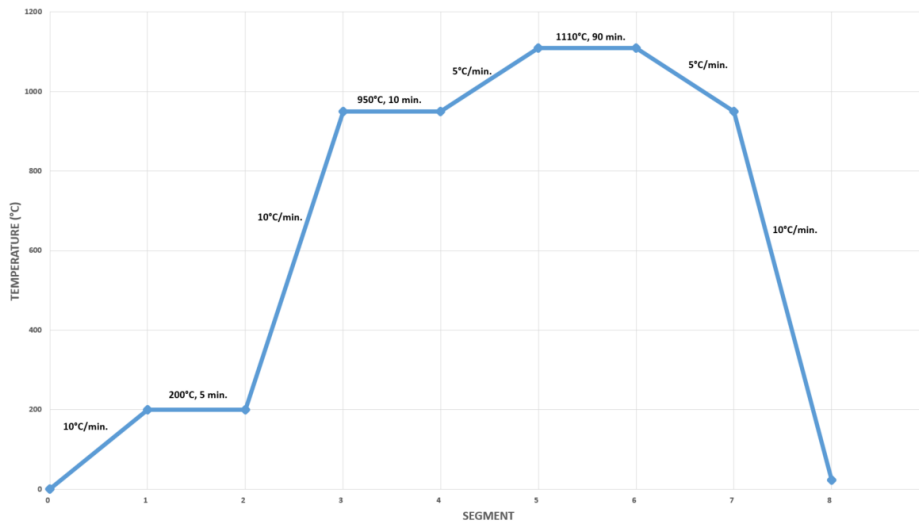
Figure 4.16 Optimized vacuum heat-treatment process parameters

The as-sprayed and vacuum furnace heat-treated samples can be seen in *Figure 4.17*. The sample on the left presents a darker colour and a visibly higher roughness. The colour of the samples is due to the oxides formed during the spraying. In contrast, on the right, the vacuum furnace heat treated sample is much shinier because of the oxides extraction from the sample and it visibly presents a much more sealed coating, having a good chance to present favourable wear or corrosion behaviour. Starting from this point of the research, the only TiB_2 containing coating used for characterization and testing was the NiCrBSi - 15% TiB_2 optimized with the program previously showed.
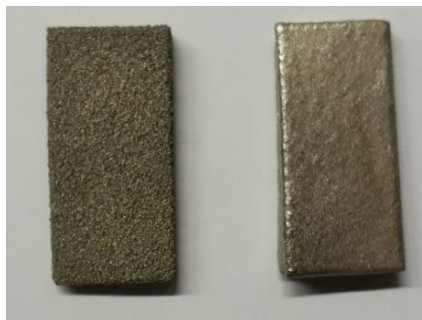

Figure 4.17 Thermally sprayed samples as-sprayed (left) and
vacuum furnace heat treated (right)

4.5. Dissociation and degassing

In the heat-treatment of the thermal spraying coatings, the use of vacuum furnaces if recommended by DIN EN ISO 14924 [64]. Features like volatilization, dissociation and degassing of compounds represent one of the biggest advantages of such equipment. Ni, Cr, B, Si and Ti have different behaviours when heated up to high temperature in a controlled atmosphere. The Ellingham diagram is a chart represented in *Figure 4.18* and shows the stability of some of the most important oxides at different temperatures and pressures. However, research concluded that decompositions of metal oxides tend to rely more on temperature than on pressure [85].
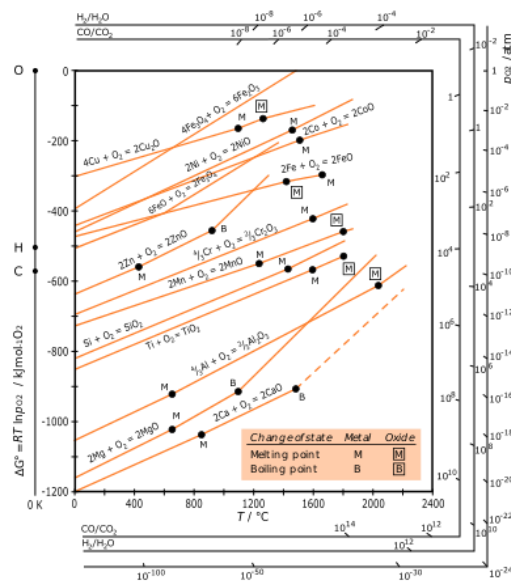

Figure 4.18 The Ellingham diagram of the most important oxides in metallurgy [225]

Because of the high temperatures involved in the thermal spraying process, the feeding material inevitably forms oxides in contact with the combustion gasses. Nevertheless, at elevated enough temperatures and high enough vacuum levels, such compounds can dissociate, the coatings can evacuate gasses and leave a smooth and shiny surface.

The decomposition takes place following *Eq. (4.8)* [226]:

$$\frac{2}{y}M_xO_y = \frac{2x}{y}M + O_2 \qquad (4.8.)$$

In thermal spraying, reactions like *Eq. (4.8.)* are desired as the porosity is reduced, a metallurgical bonding is formed and a compact coating is obtained. The adhesion strength of the coating can be therefore improved through the applied vacuum treatment [227]. It has to be nevertheless taken into account that the working environment is argon. The reduction in an inert gas atmosphere is slightly shifted but the diagram is one of the most important tools to predict the decomposition of the compounds.

Looking at the diagram it has to be known that the lower the line, the higher the oxygen affinity. It can be observed that for the oxides formed from the main constituent elements of the coating, the lines for TiO_2, SiO_2 and Cr_2O_3 are positioned lower than that for FeO or NiO. This means that the first mentioned oxides will decompose as they need a much lower oxygen partial pressure and temperature than the latter ones.

Even though generally the elimination of oxides is desired, it is always important to analyse their presence as they might also help for example by lubricating the coating thanks to their hexagonal structure.

4.6. Characteristics of the vacuum fused optimized coatings

4.6.1. Microstructure, porosity and phase composition

Several aspects need to be taken into account when characterizing a thermally sprayed coating. Thickness, porosity, phase composition, hardness or the interface quality are all features of greater or lesser importance depending on the industrial application of the coating. Various piece of equipment were needed to outline the most important elements of the coating. For immediate microstructural characterisation and quick image acquisition, a Leica DMR light microscope has been used. The porosity has been calculated through image processing with the free-ware ImageJ. The crack propagation analysis has been performed with a Keyence VK-X260K confocal laser scanning microscope. The more in depth microstructural analysis combined with elemental analysis has been performed with an EDX equipped Philips XL30 ESEM. The phase composition has been determined with a Philips X'Pert diffractometer while microhardness indentations have been performed with a ZwickRoell ZHVµ-M equipment.
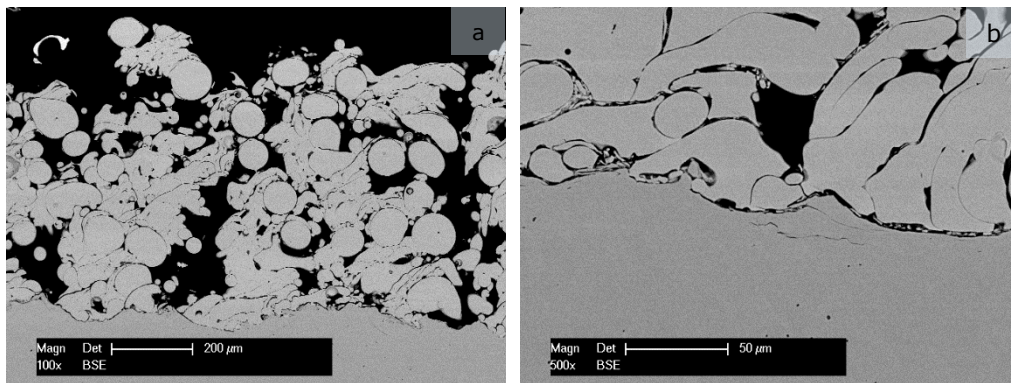

Figure 4.19 BSE micrographs presenting (a) an overview and
(b) a region of the interface of the as-sprayed coating

The BSE micrographs in *Figure 4.19* present two regions of interest of the as-sprayed part. Although these coatings are meant to be post-processed, in a case of disparity in regard to the expected results it is always important to know the starting point of the analysis. *Figure 4.19a* displays an overview of the deposited material. The coating presents an inhomogeneous structure with a high roughness. The calculated porosity by image processing exceeded 20%. The interface from

Figure 4.19b shows regions where the coating is visibly not adhering properly to the substrate. The two micrographs demonstrate that as expected, the present deposited coating needs a post-processing in order to be considered for further investigations.

An overview of the heat-treated NiCrBSi-TiB$_2$ coating in cross section optimized with the program from *Figure 4.16* can be seen in *Figure 4.20a*. The BSE image can be considered a multi-phase structure with a heterogeneous distribution of the dark phase. The adhesion of the coating to the structure appears to be as well of a good quality.
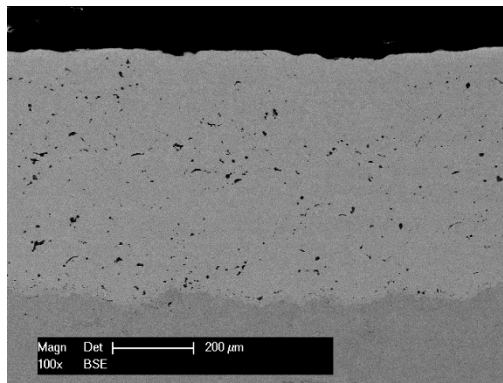

Figure 4.20 BSE micrographs of the coating in cross-section

For a thorough microstructural characterization, a correlation between SEM micrographs, EDX chemical composition analysis and XRD diffractograms was necessary.

From the overlapping of the XRD spectra (*Figure 4.21)* of the NiCrBSi-TiB$_2$ powder after the TG analysis, the as-sprayed and the vacuum heat-treated coating, numerous phase changes can be easily noticed. The first overlapping peak at 26.9° is a hexagonal SiO$_2$. The second peak at 2θ 44.4° contains the Ni solid solutions and the TiB$_2$ reinforcing material while at 51.7° transformations occur only in the Ni$_3$B and Ni matrix structures. Confirming the peer reviewed literature [228,229], during the thermal treatment, the Ni$_3$B is transformed to a Ni$_2$B and a rest Ni phase. The γ-Ni partly stays as a solid solution, does not transform and keeps its cubic crystal system while the rest Ni dissipates in the matrix forming compounds with other alloying elements.
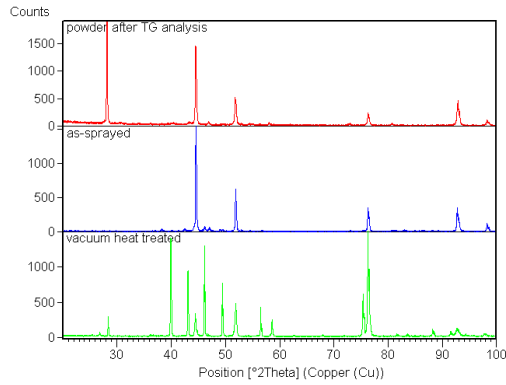
Figure 4.21 Overlapped XRD diffractograms of NiCrBSi-TiB$_2$ powder after TG analysis, as-sprayed and the vacuum heat-treated coating

The last two overlapping regions at 76.1° and 92.4° include phase transformations mostly in the CrNiSi. The solubility of the phase increases in the latter case because of the longer exposure of the sample to high temperatures. For the same reason, oxides of Si and Ti have been observed as forming in the as-sprayed and vacuum heat-treated samples. With so many changes observed, a close correlation of the microstructure of the vacuum treated coating with its XRD spectra can be of a great help to better understand the behaviour of the coating.

Figure 4.22 presents a detail of the NiCrBSi-TiB$_2$ sample in cross-section. The dark TiB$_2$ phases can be seen as heterogeneously distributed in the matrix. The non-homogeneous distribution is a consequence of the mixing process, the high melting point of the TiB$_2$ [230] and subsequently its ability to resist to solubility at the service temperature [231].
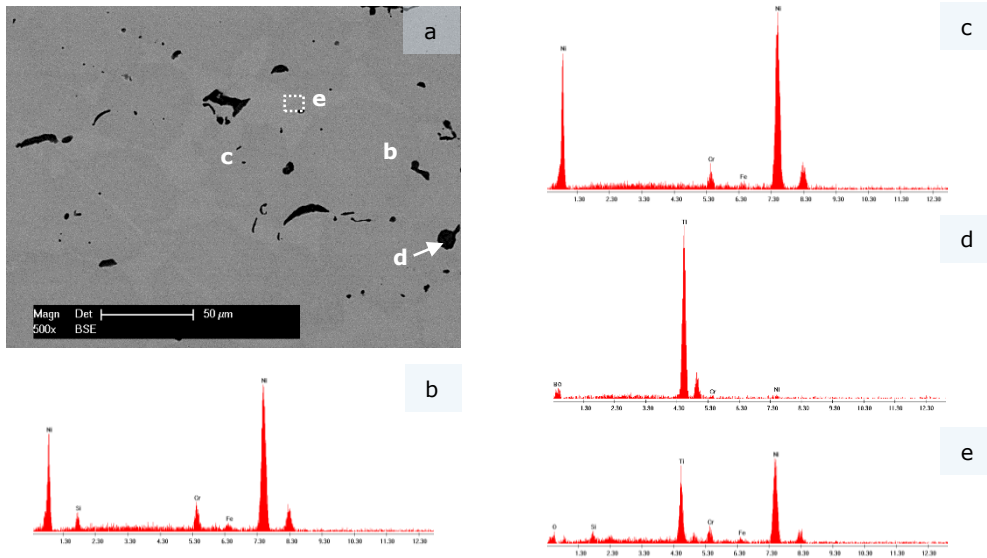

Figure 4.22 (a) SEM micrograph of NiCrBSi-TiB$_2$ sample along with the corresponding (b),(c),(d),(e) EDX spectra

The EDX spot analyses from *Figure 4.22b, Figure 4.22c, Figure 4.22d and Figure 4.22e* correspond to different regions of the coating represented in *Figure 4.22a*. Corroborating the EDX spot analyses with the XRD spectra from *Figure 4.23*, the matrix noted with *b* in *Figure 4.22a* consists mainly of the tetragonal BNi_2 and the cubic γ-Ni. These eutectic structures are often detected as matrix in Ni-based thermal sprayed coatings research [138,214,232,233]. Another component in the matrix is the cubic σ-$Cr_3Ni_5Si_2$ phase. *Schuster et al*. [234] reported that the forming of the σ phase is favoured by the low Si content (4% in the present work). This structure can be consulted as well in the ternary Cr-Ni-Si diagram.
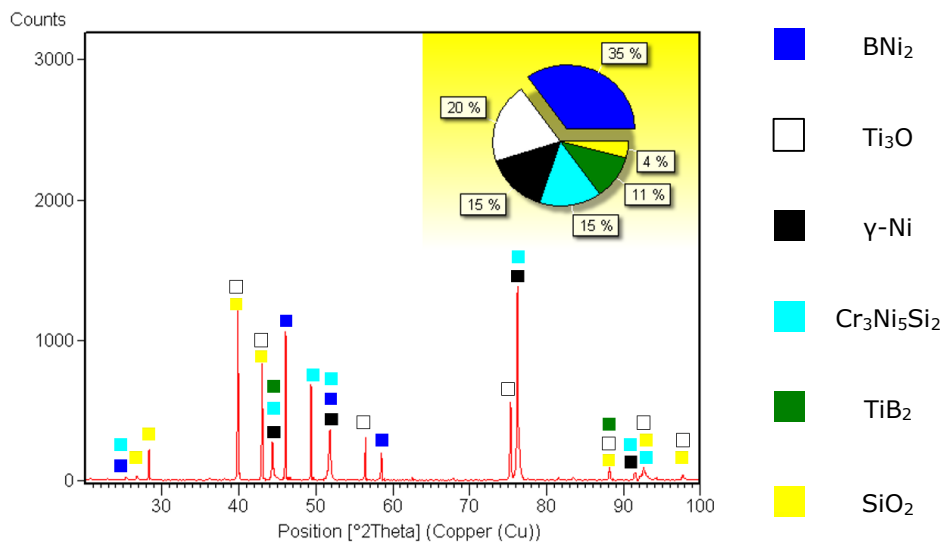

Figure 4.23 XRD diffractogram of the NiCrBSi-TiB$_2$ vacuum furnace heat-treated sample

A sign that the post-processing program was well defined is that Cr is detected in the σ-$Cr_3Ni_5Si_2$ phase and is not diluted in the Ni matrix forming minor constituents [235]. The rest γ-Ni/BNi_2 phase is found in the region *c* of *Figure 4.22a*. The area *d* on the SEM micrograph corresponds on one hand to the hard TiB_2 phase that is expected to aid the wear resistance of the coating [236,237] and on the other hand to the Ti_3O.

The operating pressure of the vacuum pump is 10^{-6} mbar and the elimination of the majority of the oxides and gases is successfully done. Nevertheless, Si and Ti both have a high susceptibility of forming oxides until an oxygen partial pressure of about 10^{-23} mbar [238] according to the Ellingham diagram. Therefore, the formation of SiO_2 and Ti_3O is inevitable.

The porosity is an important aspect to follow in surface engineering as important damage can be produced to coated parts due to an improper sealing. Two representative software processed micrographs can be seen in *Figure 4.24.* An average value of around 1% has been calculated for the NiCrBSi-TiB$_2$ sampled. The results aligns to the state of the art porosity values present in the research of self-fluxing thermal spraying depositions [239–241]. The micrographs reveal that the porosity is distributed in the matrix, mainly near the TiB_2 phases. This can be an effect of the mixing process of the powders. As no strong bond between the matrix and the

reinforcement is realised, the voids are more susceptible to form in the contact area of the two materials at the moment of the coating build-up.
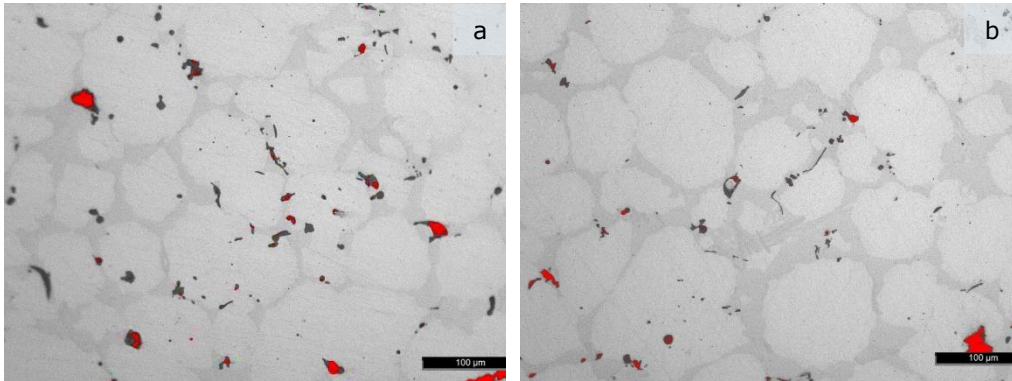

Figure 4.24 Software processed micrographs highlighting the porosity of 1% on the left and 0.6% on the right of the NiCrBSi-TiB$_2$ sample

The homogeneity and the qualitative assessment of the elemental composition of the sample are shown in *Figure 4.25.* The EDS mapping of the sample has been performed in the cross-section of a polished sample. The image acquisition has been performed on approximately 450 μm^2 by exciting the surface of the sample with a beam accelerated at 25 kV. The time of exposure for the map generation has been 2.9 h.

The selected area to perform the mapping included the coating, the interface and a small part of the substrate. A strong presence of Ni and B has been identified in the coating region, which confirms that the matrix contains BNi$_2$ and Ni. Previous research [229] demonstrated that the wear resistance of the depositions grow with the content of B in the coating. As B is seen as clearly distributed in both the matrix and reinforcement, a good tribological behaviour of the coating is expected. The formation of the high boron content BNi$_2$ phase instead of the BNi$_3$, classically found in self-fluxing TS alloys, is supposed to aid as well against the wear of coated parts. A comparison of the Ni, Cr, Si and Ti maps shows that Si and Cr are similar in the superior part. The strong diffusion of Si towards the substrate bypasses problems of coating adhesion by creating a strong metallurgical bonding at the interface region between the coating and the substrate.
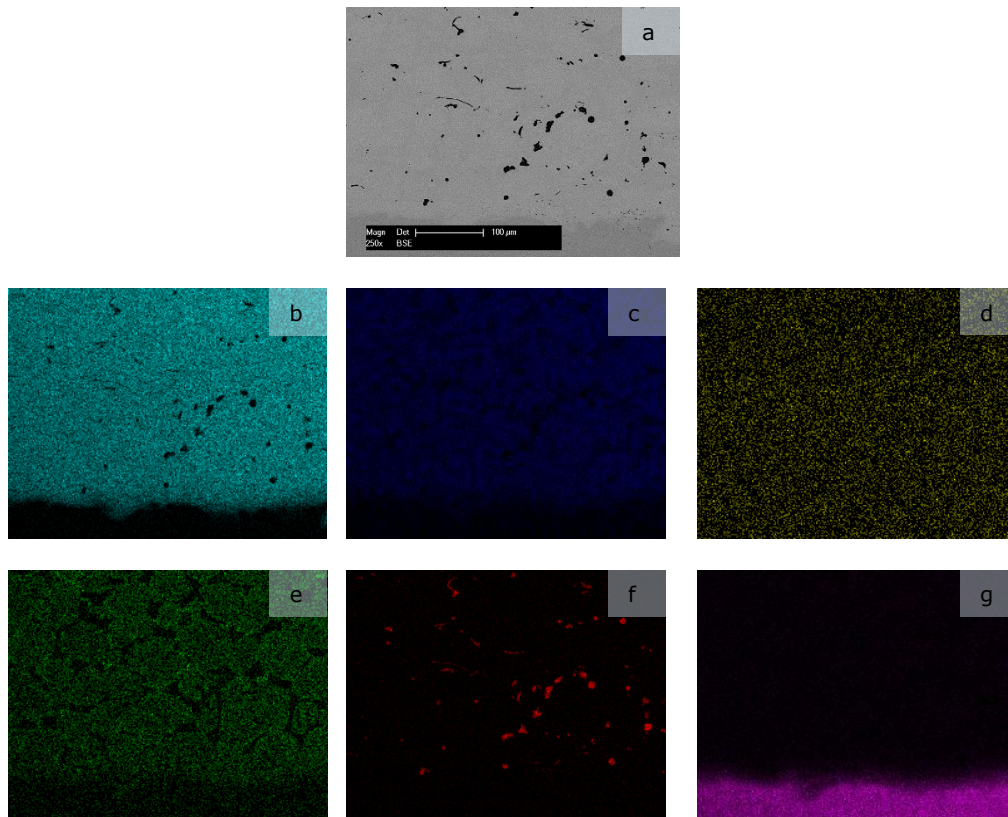
Figure 4.25 Mapping of the most relevant chemical elements of the (a) NiCrBSi-TiB$_2$ coating (b) Ni, (c) Cr, (d) B, (e) Si, (f) Ti and (g) Fe

4.6.2.   Hardness and adhesion

Adhesion or hardness are considered very important data that characterize coatings in service. Hardness is not included generally in the category of intrinsic property of a coating or material and it can take different values depending on the testing method [136] or in the case of coating on the tested direction (cross-section, surface, interface, *etc.*).

For the present work, the following measurements have been performed:
- Surface hardness
- Cross-section hardness
- Interface toughness measurements.

Surface and cross-section hardness have been tested using a Zwick/Roell ZHVμ-S machine. The results have been outputted with the TestXpert ZHVμ user interface of the equipment. The interface toughness measurements have been performed using a KB 250 BVRZ universal testing machine. A special care has been given to the sample preparation to make sure that the measurements are correctly performed. For the surface evaluation, flat and grinded post-treated samples have

been used. For the cross-section and interface toughness measurements, metallographic samples have been prepared. The samples have been cut in cross-section, grinded and polished. The indentation has been performed on coatings thicker than 250 μm to make sure that the results are not influenced by the substrate. In order to make the results statistically relevant a number of at least seven indentations have been done.

The results of surface and cross-section hardness measurements are displayed in *Table 4.13.*

Table 4.13 Values of indentation hardness measurements of the NiCrBSi- 15% TiB$_2$ sample

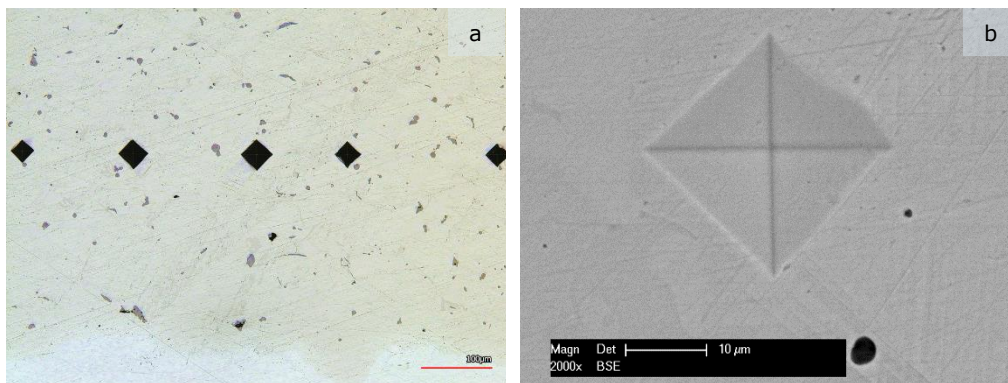| No. of measured point	1	2	3	4	5
Surface indentation HV3	330	534	~~276~~	368	673
Cross-section indentation HV0.3	550	356	~~298~~	410	493

Figure 4.26 Micrographs representing a) a series of cross-section measurements and b) a BSE close-up of an indentation of the NiCrBSi-TiB$_2$ post-treated sample

The loads used to measure the hardness of the coating were ones often used in the coating research [219,221]. When testing the coating at 0.3 kgf and 3 kgf, the load did not create plastic deformation on a large enough surface to be able to correctly measure the hardness of the entire coating, but only in single phases. The measurement of the capacity of the material to resist to plastic deformations has been extensively evaluated in the optimization part of the present work. Neither the values of the matrix nor the reinforcement present any unexpected results. The matrix powder respects its delivery specification maintaining a hardness of approximately 350 ± 20 HV. As already explained in the subchapter 4.1., the reinforcement maintains the large majority of its properties but unfortunately loses from its hardness. The hard reinforcements present lower values than the ones of the material but still reach values between 450 HV and 600 HV. The variation of the values measured for the surface and the cross-section corresponds to the hardness of the indented phases and cannot be regarded as a general value of the whole coating. Considering the extensive range of tested samples for the optimisation of the post-treatment of the coating, a minimum value of about 350 ± 20 HV could be attributed for the general coating, but not for the reinforcement.

The fact that the microindentations do not present cracks can be attributed to the ductility and low internal stresses of the coating. Low residual stresses and the capacity to withstand cracking propagation are conferred by the ability to carefully control the vacuum furnace and especially the 3-4 segment of the program, where a detensioning and a coating homogenization occur.
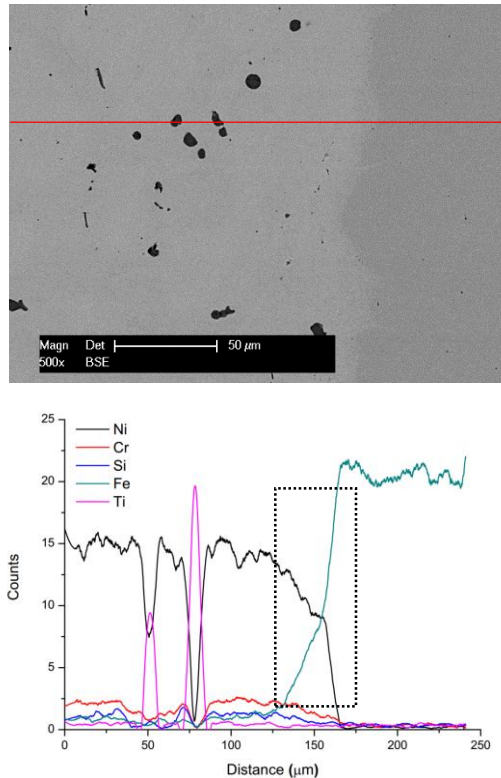

Figure 4.27 BSE micrograph of the interface and
the corresponding line-scan graph

The performance and the quality of a TS coating is dependent on the coating-substrate adhesion. A possible debonding would inevitably result in a collapse of the whole system. The bonding mechanisms in thermal spraying depend on the contact between the splats and between the splats and substrate.

By analysing the line-scan at the interface in *Figure 4.27,* an area between 125 μm and 175 μm can be observed where the content of Ni decreases and the one of Fe is increasing. It can be stated that in the approximately 50 μm region a metal-to-metal bonding is formed, one that should be much stronger than the typical mechanical interlocking found in thermal spraying. The adhesion of a coating can be assessed from the point of view of fracture mechanics as the necessary amount of energy to initiate and propagate cracks. The evaluation in this case is made through fracture toughness. By exceeding a critical value of a strain energy release rate stated in $J \cdot m^{-2}$, a crack propagation occurs and results inevitably in a failure.

A polished cross-section of the NiCrBSi-TiB$_2$ coated sample was indented with Vickers and Brinell indenters by applying different loads in a space where the diagonal of the indent coincides with the coating-substrate interface. As defined by *Lesage et al.* [242], the interface fracture toughness is defined as:

$$K_{ca} = 0.015 \frac{P_c}{l_c^{3/2}} \left(\frac{E^`}{H}\right)_i^{1/2} \tag{4.9.}$$

The quantity $\left(\frac{E^`}{H}\right)_i^{1/2}$ can be expressed as:

$$\left(\frac{E^`}{H}\right)_i^{1/2} = \frac{\left(\frac{E^`}{H}\right)_S^{1/2}}{1+\left(\frac{H_S}{H_C}\right)^{1/2}} + \frac{\left(\frac{E^`}{H}\right)_C^{1/2}}{1+\left(\frac{H_C}{H_S}\right)^{1/2}} \tag{4.10.}$$

where K_{ca} is the interfacial toughness fracture, P_c the function of the critical load, l_c the length of the crack, E the elastic modulus and H the apparent hardness.
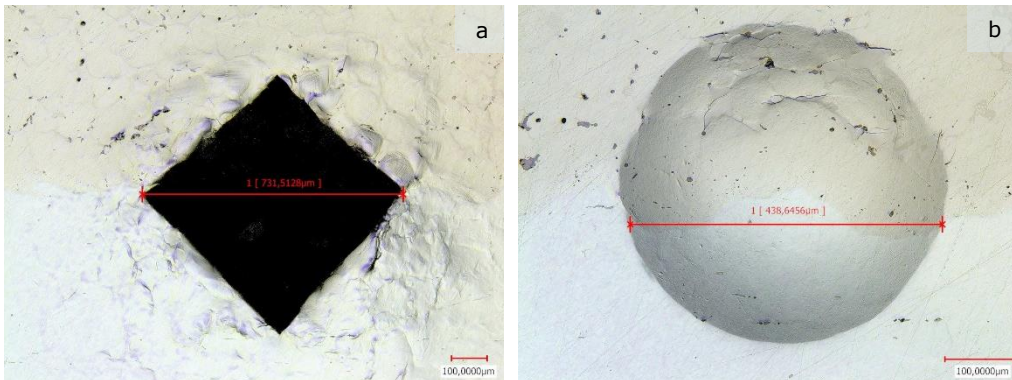

Figure 4.28 Micrographs showing the imprints of the a) Vickers and b) Brinell indentations
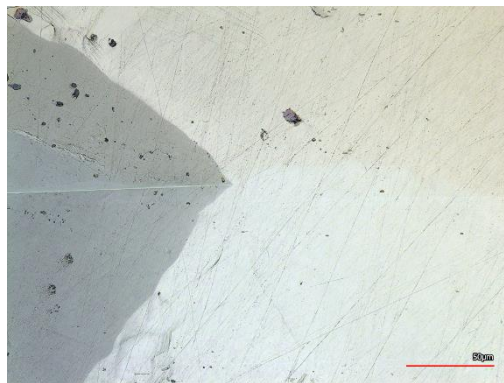

Figure 4.29 Detail of the tip of the Vickers indentation in the interface region

Several indentations have been performed until a load of 50 kgf on the HV scale and 62.5 kgf on the HBW scale was reached. Although large indentations have been obtained, no visible cracks could've been observed at the tips of the indenter. The results denote an excellent interface adhesion, low internal stresses and a high interfacial fracture toughness. The crack free area indicates also a good choice of a series of interdependent factors in the coating building like: the substrate material (roughness, cleanliness), the operating conditions or the feedstock morphology and particle size distribution.

4.6.3. Tribological behaviour

The functionality of the coating is a very important aspect for the applied research. The interest in the self-fluxing thermally sprayed coatings is strongly related to the mechanical properties that lead to a high wear resistance of the part. Wear behaviour related analysis of WC-Co, Cr_2O_3 or sub-microsized particles containing coatings showed that reinforcements can increase abrasion resistance [243], promote formation of protective layers [244] or stabilize the depositions in the case of tests performed at high temperatures [245].

Several tools and determined values have been used and compared in order to perform a comprehensive analysis. Vacuum remelted NiCrBSi coatings deposited with the same matrix material have been used as comparison sample with the NiCrBSi-TiB_2 sample. The result analogy is extremely important as it can give an idea of how the developed coating is behaving in the same conditions as one that is already used in the industry.

Theoretically defined as the ratio of two loads acting parallel and perpendicular to an interface of two bodies that are in relative motion, the pin-on-disc is an easy to measure method that allows observing which component slides over the other in a certain environment. The used setup to measure the dimensionless quantity was a pin-on-disc tribometer with a non-conformal contact. The part in motion in the laboratory setup is represented by the coated sample while the ball serves as the static partner. Several 6 mm 100Cr6 steel and WC-Co balls have been used to perform reproducible tests. The samples and the counterparts have been cleaned with acetone prior to the tests. The parts were grinded prior to the testing with a 1000 grain size SiC paper. The measurements have been performed at a linear speed of 15 cm·s^{-1}, an acquisition rate of 10 Hz and a normal load of 10 N. The stop condition for the test was the completion of 50 000 laps.
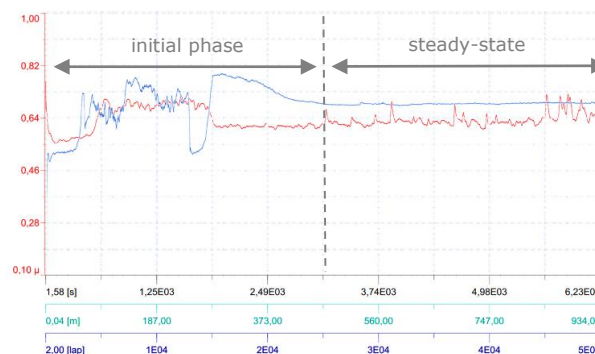

Figure 4.30 Coefficient of friction evolution of
NiCrBSi (blue) and NiCrBSi-TiB_2 (red) coatings against a 100Cr6 counterpart

Figure 4.30 and *Figure 4.31* represent the coefficient of friction of NiCrBSi and NiCrBSi-TiB$_2$ coating versus 100Cr6 and WC-Co as counterparts. All the curves present an initial region where the COF is rapidly increasing. This is happening due to the micro-convex bodies on the surface part. Once the contact area becomes smooth, the overall friction is balanced and the wear enters in a stable period. None of the parts failed during the test as shown by the stable COF value for all the coatings at the end of the measurement. In both graphs, a slightly higher value of the COF can be seen for the NiCrBSi coating. The lower value of the NiCrBSi-TiB$_2$ coating can be attributed to the reinforcement of the coating, causing oxidation on the surface and therefore declining the COF.
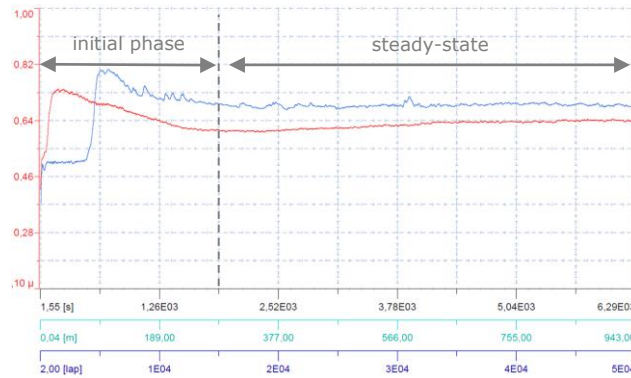

Figure 4.31 Coefficient of friction evolution of
NiCrBSi (blue) and NiCrBSi-TiB$_2$ (red) coatings against a WC-Co counterpart

The values from the *Table 4.14* correspond to the COF graphs from *Figure 4.30* and *Figure 4.31.* It can be seen that the maximal values reached are around 0.8 while the average value of the coatings are situated between 0.6 and 0.7. The values are comparable with the ones found in the peer reviewed literature [246,247].

Table 4.14 The minimal, average and maximal values of the COF for the NiCrBSi and NiCrBSi-TiB$_2$ coatings against 100Cr6 and WC-Co

Counterpart	Sample	Coefficient of friction value		
		Minimal	Average	Maximal
100Cr6	NiCrBSi	0.16	0.69	0.79
	NiCrBSi-TiB$_2$	0.55	0.65	0.77
WC-Co	NiCrBSi	0.19	0.67	0.80
	NiCrBSi-TiB$_2$	0.42	0.64	0.74

The energy formed due to the frictional contact between the two surfaces can be either kept in the tribosystem or dissipated in several ways. The mechanical energy produced by sliding can be converted to vibrations, heat, material deformations and generation of new surfaces. Consequently, a general correlation between the coefficient of friction and the wear rate cannot be established.
Following the COF analysis, the next natural step in order to assess the wear behaviour of the coating is to evaluate the track left by the test.

  Figure 4.32 displays the profile of the wear tracks of the NiCrBSi and NiCrBSi-TiB$_2$ coatings against the 100Cr6 and the WC-Co static partner.

  An analysis of a section of a wear track was performed by using 3D topographical maps acquired with the CSL microscope. By measuring the depth and width of the wear tracks in distinct spots it was possible to calculate the wear rate of the samples.

  Figure 4.32 shows a clear difference between the profiles of the four evaluated samples. The upper samples tested against a 100Cr6 ball exhibit a wider track than the ones evaluated against the WC-Co ball. The steel counterpart being a much softer material than the carbide, it will degrade faster during the test and the amount of dislocated material will be higher. The effect of the bigger dislocated material can be also seen in the diameter of the spherical caps evaluated in *Figure 4.34*. On the tests realized on the NiCrBSi-TiB2 samples but most notably in *Figure 4.32d*, small asperities can be seen on the wear track. This is realized by the pull-out effect due to the adhesion between the sample and the static partner.
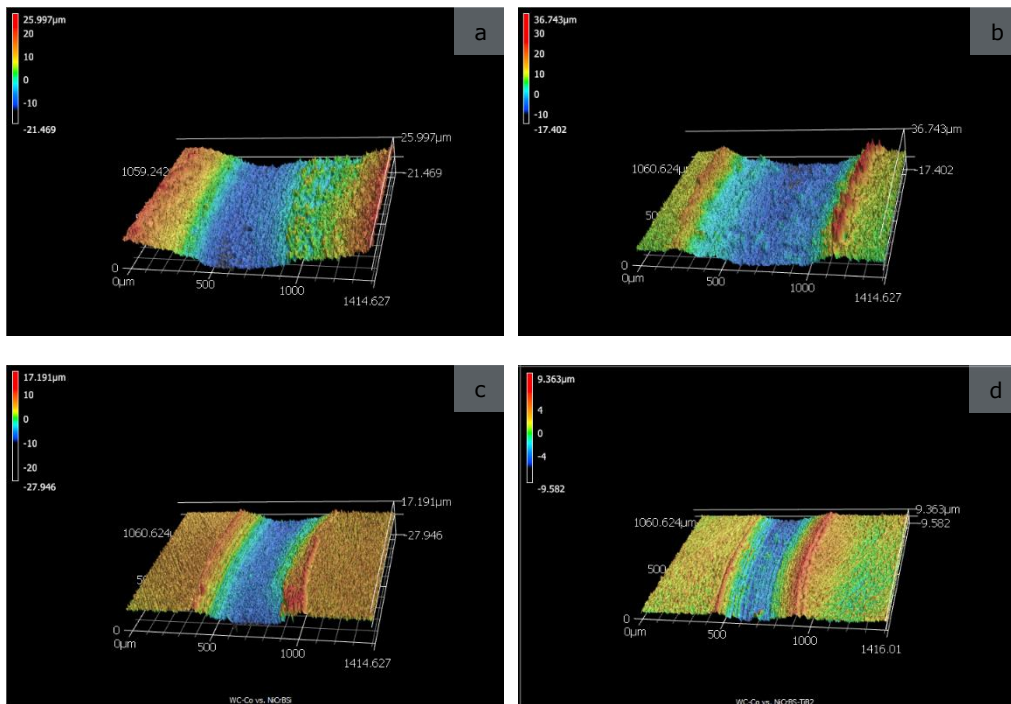
Figure 4.32 Wear track profile of (a) NiCrBSi and (b) NiCrBSi-TiB$_2$ vs. 100Cr6 and (c) NiCrBSi and (d) NiCrBSi-TiB$_2$ vs. WC-Co

  SEM micrographs and EDX spectra of the NiCrBSi-TiB$_2$ coating against the 100Cr6 and WC-Co ball can be seen in *Figure 4.33a* and *Figure 4.33b*. As expected, in the SE representations, different phenomena can be seen happening for the experiments with the two different static partners. The higher wear rate of the NiCrBSi-TiB$_2$ coating against the 100Cr6 ball can be attributed to layers transferred from the counterpart to the coating. As the EDX analysis confirms, parts of the steel ball smeared on the surface of the NiCrBSi coating, forming a transfer layer between the surfaces in contact. When the coating is exposed to a harder static partner,

regions of spalling can be observed. These areas are encountered just when tested against a very resistant WC-Co counterpart which shows that the coating exhibits a good inter-splat bonding. No microcrack can be seen on the surface, which shows that a good cohesion between the different phases has been realized through the post-treatment. As general remarks, no delamination or brittle fracture can be seen on the worn surfaces due to the low internal stresses found in the coating. The wear tracks of the NiCrBSi-TiB$_2$ coatings are fairly smooth after the test, which shows a good wear resistance against both steel and carbide counterparts.
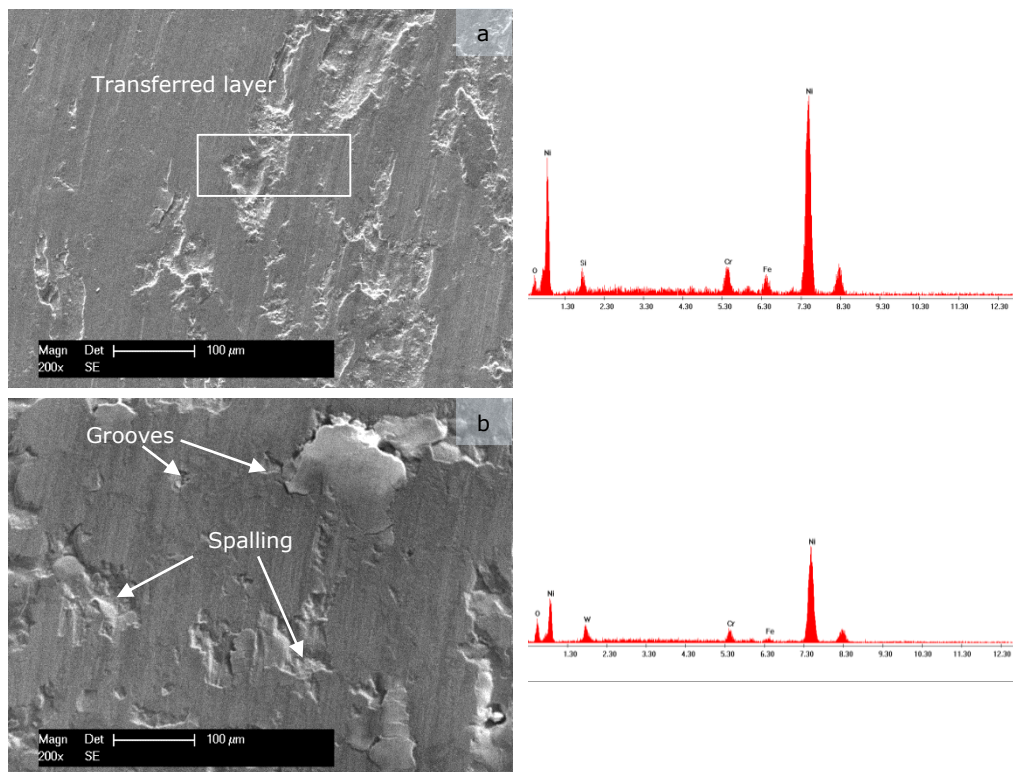
Figure 4.33 SE micrograph of the wear track of NiCrBSi-TiB$_2$ sample vs. a) 100Cr6 and b) WC-Co counterpart and their corresponding EDX spectra

Spherical balls represent typical solutions as static partners in pin-on-disc installations. The counterparts from the four combinations of tribological tests performed for the present can can be seen in *Figure 4.34*. The geometry of the counterpart eliminates in this way edge contacts and provides a fairly easy method of pin wear measurement as flat wear scars are produced during the test. The volume of the spherical cap [248] with a defined height *h* and a radius *R* can be calculated as:

$$W_c = \frac{1}{3}\pi h^2(3R - h) \tag{4.11.}$$

while the height *h* of the spherical cap be approximated as:

$$h \cong \frac{a^2}{2R}$$
(4.12.)

where *a* represents the radius of the spherical cap.

The mathematical calculations of the height of the spherical can be substituted in *Eq. 4.11.*. By approximation, the calculation of the wear volume of the spherical cap can be considered:

$$W_c \cong \frac{1}{3}\pi \left(\frac{a^2}{2R}\right)^2 \left(3R - \frac{a^2}{2R}\right) \cong \frac{\pi a^4}{4R}$$
(4.13.)

Finally, the volume of the spherical cap has been used to calculate the wear rate by using the Archard mathematical expression from *Eq. 2.13.*.
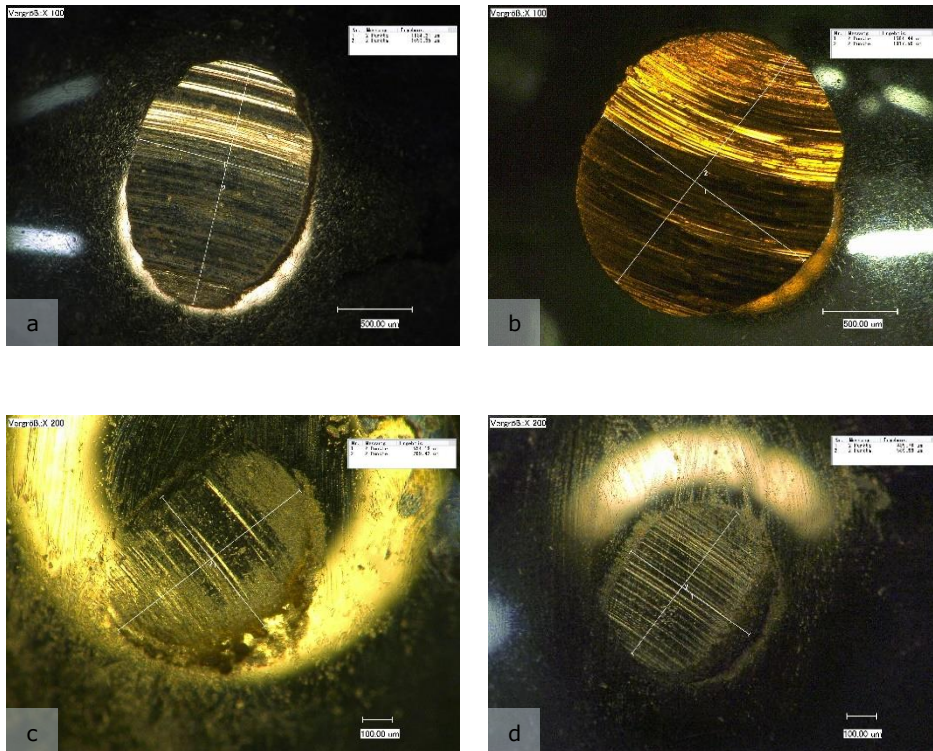
Figure 4.34 Micrographs of the 100Cr6 static partner against (a) NiCrBSi and (b) NiCrBSi-TiB$_2$ coatings and of WC-Co ball against (c) NiCrBSi and (d) NiCrBSi-TiB$_2$ coatings

A graphical representation of the wear rates of the coatings and of the counterparts can be seen in *Figure 4.35* and *Figure 4.36*.
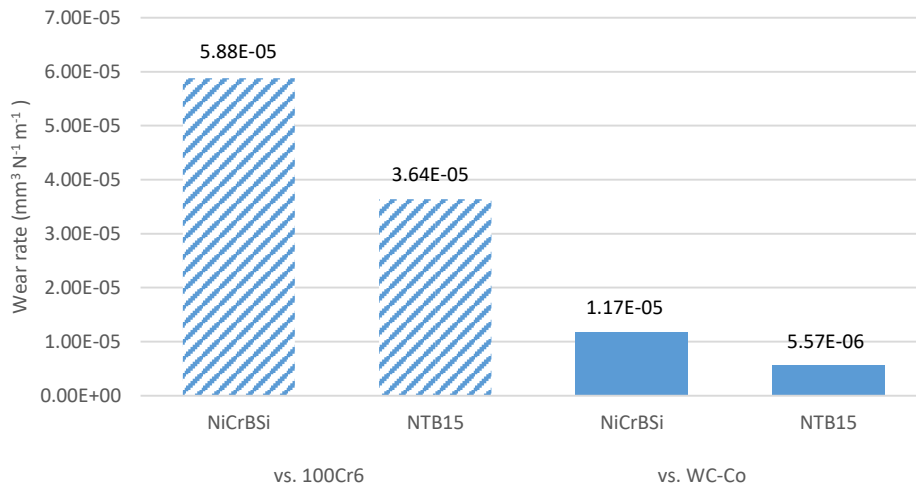
Figure 4.35 Wear rate of the NiCrBSi and NiCrBSi-TiB$_2$ coating
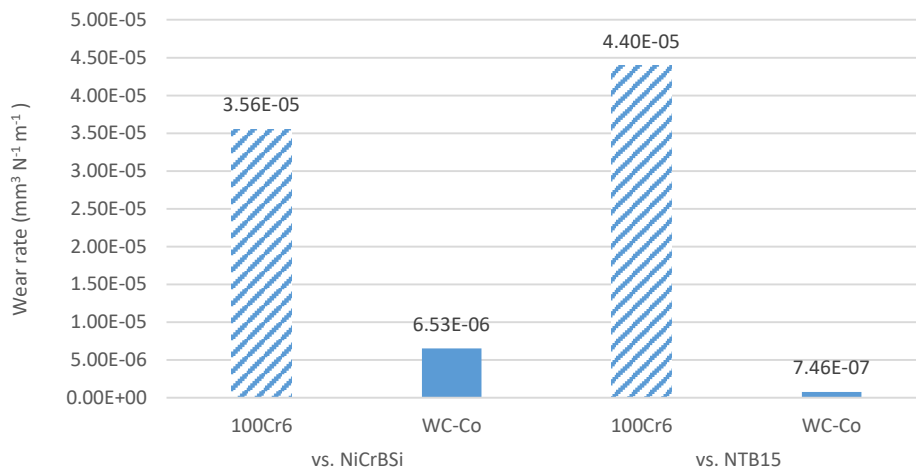
Figure 4.36 Wear rate of the 100Cr6 and WC-Co counterpart

When looking at the wear rates of the coatings, the NiCrBSi-TiB$_2$ showed both times a lower value than the NiCrBSi. The superiority of the coating is a result of the combination of factors such as the phase composition, a properly chosen furnace program and the used reinforcement, all of them leading to a resistance against the destructive test. Regarding the wear of the counterpart, the steel ball against the NiCrBSi-TiB$_2$ ended up with a bigger worn volume while in the case of the WC-Co ball a higher wear rate of the static partner could be observed when tested against the NiCrBSi coating.

4.6.4.   Corrosion behaviour

Corrosion is an inevitable process occurring at the vast majority of the thermally sprayed coatings. For corrosion to take place in thermally sprayed coatings, an electrolyte, a surface region with a positive charge, another one with a negative charge and an electrically conductive route must be present. This type of degradation is an electrochemical phenomenon in which atoms of a material surface create a reaction with an environment in which they are placed.

The protection against corrosion for applications like bridges, oil tanks, valves or pipelines are of a great importance and selecting the right material is not always simple. Showing good corrosive behaviour, the self-fluxing Ni-based coatings can represent a good solution when exposed to seawater. For the end user, having a high quality coating that effectively protects against degradation in the environment in which is placed in, leads to substantial cost saving and high performance. The presently investigated coating has the premise of a good corrosion resistance. The lower particle temperatures reached during the deposition compared to other spraying processes mean as well less particle oxidation. A low calculated porosity should also not let the electrolyte penetrate the coating and create a damage in the deposition. Moreover, the metallurgical bonding in the interface region should reduce the risk of degradation of the surface. Like for the wear behaviour analysis, the reference sample for the assimilation of the corrosion behaviour of the developed coatings has been a vacuum Ni-based deposition.

The corrosion behaviour of the NiCrBSi-based coatings was assessed in a 3.5% NaCl solution (pH~7), at room temperature, using a three electrode-cell configuration, applying quasi stationary conditions (scan rate 0.16 mV·s^{-1}). A SCE was defined as reference and a Pt disk as counter electrode. A Luggin capillary is used to measure the potential in the proximity of the working electrode. The capillary consists of a bent glass tube with a large enough opening on one side to fit the reference electrode and a smaller opening on the other side, still large enough to allow the diffusional activity of the electrolyte. The capillary minimizes any iR drop in the electrolyte associated with the passage of current through the electrochemical cell. The working electrode was represented by the vacuum remelted NiCrBSi and NiCrBSi-TiB$_2$ coatings.

Prior to the corrosion tests, in order to remove possible contaminants and to ensure the same testing conditions for all the samples, the working electrodes were grounded with 1000 grain size SiC paper until reaching a roughness of Ra ≈ 0.1. The samples were afterwards embedded in polymer resin leaving 1 cm^2 active surface to be tested.

Potentiodynamic polarization of the sample was performed using a VoltaLab PGP201 Potentiostat/Galvanostat. The specimens were scanned from -1000 mV vs. SCE to 1000 mV vs. SCE in order to determine the corresponding corrosion current density (i_{corr}) and corrosion potential (E_{corr}) and to detect any tendency of passivation in the scanning potential range for the given conditions. The experimental corrosion current densities and corrosion potentials extracted from the polarisation curves are listed in *Table 4.15*.

Typical potentiodynamic polarization curves for the investigated samples in 3.5 wt.% NaCl solution can be seen in *Figure 4.37* as *i-E* representation and in *Figure 4.38* as log *i-E* representation.
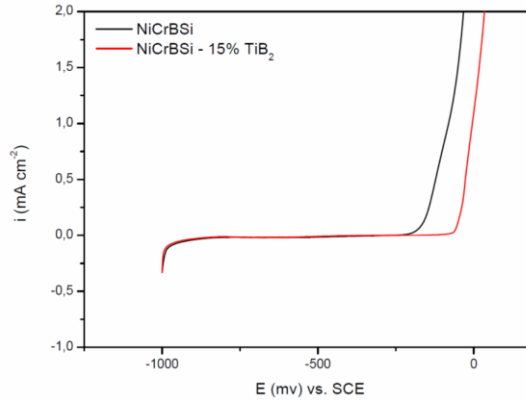
Figure 4.37 Linear plot of the polarization behaviour of NiCrBSi and NiCrBSi – 15% TiB$_2$ in 3.5% NaCl

The polarization curve can be divided into two distinct potential regions, the cathodic and the anodic one – that both contain three different domains: transition, passive, and transpassive. Usually, corrosion potential is found between the equilibrium potential of the anodic metal dissolution and the cathodic reduction of other present species. Consequently, the cathodic and the anodic regions are separated by the E_{corr} value, which can be easily determined from the log *i-E* representation of the polarisation curve.

Corrosion of thermally sprayed coatings generally occurs around the particles that are not melted during the deposition process and usually starts at defects such as pores, inclusions and microcracks. This phenomenon is followed by the propagation along the paths formed by pores, microcracks and lamellar structure, resulting in exfoliation or delamination.

The coating degradation during corrosion tests is a complex process where some constituents of the deposition go in the solution as ions, whether some ions combine further combine with each other to form corrosion products. Specifically, the NiCrBSi coatings experience corrosion in the testing conditions, according to the following proposed equations:

$$M - ze^- \rightarrow M^{z+} \qquad (metal\ anodic\ oxidation) \qquad (4.14.)$$
$$O_2 + 2H_2O + 4e^- \rightarrow 4OH^- \qquad (oxygen\ cathodic\ reduction) \qquad (4.15.)$$
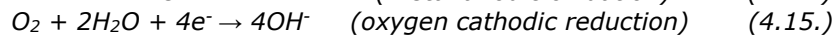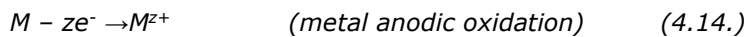
The resulted ions can move out from the corrosion pores and combine with OH$^-$.

$$M^{z+} + n\ OH^- \rightarrow M(OH)_n \qquad (4.16.)$$
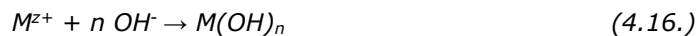
The semi-log plot of the polarization of the two coatings in 3.5% NaCl from *Figure 4.38* can deliver plenty of information regarding the behaviour of the samples in a seawater environment. Difference in both, corrosions current and potential, can be easily observed.

Figure 4.38 Semi-log plot of the polarization behaviour of
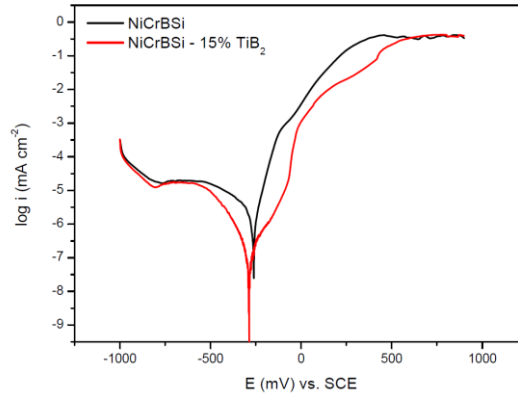NiCrBSi and NiCrBSi- 15% TiB$_2$ in 3.5% NaCl

The solid metals corrode only at the surface of the parts while for thermal sprayed coatings, the corrosion can easily happen in the inner part of the coating due to several reasons (*e.g.* porosity). The dense structure of the NiCrBSi-TiB$_2$ sample exhibits a lower corrosion current (i_{corr}=0.7·10^{-7} mA cm^{-2}) in comparison with the reference NiCrBSi coating (i_{corr}=10·10^{-7} mA cm^{-2}), resulting in a superior corrosion resistance of the coating containing TiB$_2$.

Table 4.15 Values of the electrochemical tests in 3.5% NaCl

Sample	E_{corr} (mV) vs. SCE	$E_{b.d.}$ (mV) vs. SCE	i_{corr} (mA cm^{-2})
NiCrBSi	-260	-240	10·10^{-7}
NiCrBSi – TiB$_2$	-290	-60	0.7·10^{-7}

Anodic metal passivation generally arises at a so-called passivation potential, in the anodic branch of the polarisation curve, and over this value, the anodic current for metal dissolution considerably decreases. This aspect indicates that the metallic passivity is produced by the generation of an oxide film on the metal surface, called usually passive film, which is extremely thin and protects the coating from a further oxidation. For most of the metal alloys, the passive film is less than several nanometres in thickness in the stable potential region. Depending on the Cr amount from the chemical composition, these alloys might exhibit a certain degree of passivation. The alloys which contain more than 12% Cr are able to form a stable passivation layer. The stability of the formed passive layer in a chlorine solution can be determined by means of such electrochemical polarisation tests.

For applications in which the present coating is employed, the corrosion E_{corr} and breakdown $E_{b.d}$ potential are important notions to follow. Corrosion experts consider that materials exhibiting higher values of $E_{b.d.}$ (defined as the potential at which the passive film is breaking) are more resistant to pitting corrosion. When comparing the two potentials, for the non-alloyed coating the values are very close, while for the TiB$_2$ a difference of about 200 mV can be noticed. Considering the above-mentioned aspects, on may declare that the TiB$_2$ containing coating exhibits a better pitting corrosion resistance in comparison with the reference NiCrBSi coating.

Looking at the top view and cross-sectioned view of the corroded sample in *Figure 4.39* and *Figure 4.40*, it can be seen that the TiB_2 remain skeletal on the surface and do not dissolve in comparison to the Ni-based matrix and possibly acts as an internal physical barrier to the corrosion1 propagation. The EDX spectra corresponding to the micrograph remains the presence of Si, Ti, Ni and O_2. Therefore, it can be supposed that the Ti_3O phase, also identified through the XRD analysis, can act in this way as passivation compound, hence the over 200 mV E_{corr}-$E_{b.d.}$ difference and better behaviour of the composite coating on the anodic region of the polarisation curves.

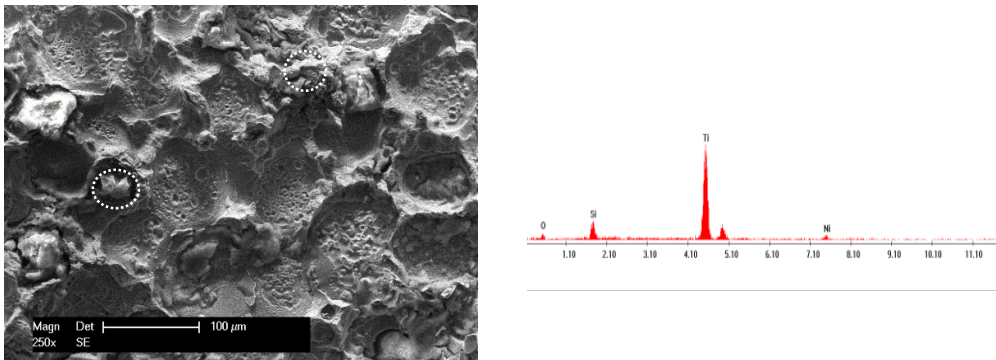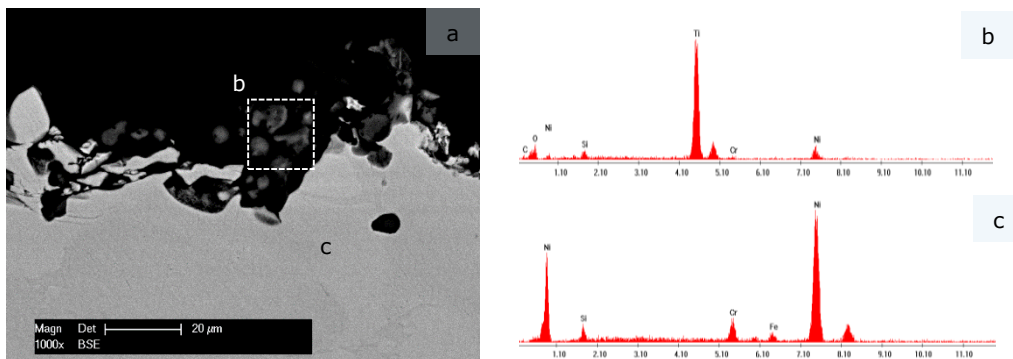Figure 4.39 Top-view SE micrograph of the 3.5% NaCl NiCrBSi-TiB_2 corroded sample

Figure 4.40 BSE cross-section micrograph and corresponding EDX spectra after electrochemical corrosion tests

In conclusion, the addition of corrosion resistance ceramic TiB_2 particles into the NiCrBSi matrix will reduce the degree of corrosion attack and consequently enhance the resistance of the coatings in environment containing chlorine.

5. Conclusions and future work

5.1. Conclusions

The present work consisted in obtaining high quality flame sprayed and vacuum furnace post-processed NiCrBSi-TiB$_2$ coatings. The research focused on the optimization of the chemical composition and vacuum parameters as well as on the characterisation of the obtained samples in comparison with reference coatings used in the industry.

With a rapid increase in the economy, the coating technology deposited through powder is a growing and extremely competitive industry with a continuous need for improvement. The thermal spraying technology distinguishes itself as a group of processes that is able to deposit a large number of materials in a wide spectrum of thicknesses. Although it is one of the first technologies that have been developed, flame spraying was successfully used to deposit high-qualitative coatings. The powder used has a Ni-based matrix in the chemical composition. The 1% boron and 4% silicon content conferred to the powder the so-called self-fluxing property, that helps pushing towards the surface the oxides trapped inside of the coating, purifying the material. The two chemical elements helped lowering the melting temperature of the powder of a few hundred degrees. As in many other situations, the wear and corrosion resistance of the alloy was considerably helped by chromium. The properties of the coating have been decisively influenced by the addition of the reinforcing material. The borides are among the most important and widely used refractory materials. The Me$_2$B to MeB$_{12}$ to MeB$_{66\cdot100}$ structures and especially the diborides present a series of properties worth to investigate. A TiB$_2$ powder was chosen as the reinforcing material. The powder is a compound with a high melting point and hardness, good thermal conductivity and chemical stability. Although its declared low fracture toughness had raised concern over crack propagation in the coating, this phenomenon did not occur. Having B as a common element with the matrix, the formation of new phases was likely to happen.

The methodology and experimental procedure used for the present research are specific to materials science and can be consulted in the third chapter of the thesis.

Looking at the experimental work of the research, the results can be split in several parts:

> ➢ Materials:
- A commercially available water-atomized and spheroidized NiCrBSi powder with a fraction size of -60 +100 µm and a hardness of 30 – 35 HRC was used as a matrix material
- A DTA curve of the matrix showed that its melting range varies between 1009°C and 1068°C
- Following a XRD scattering of the powder, the following compounds were identified: γ-Ni, Ni$_3$B, NiSi, Fe$_2$Si, and Cr$_5$B3
- A commercially available TiB$_2$ powder with a size range of -3.5 +7 µm was used as a reinforcement
- The TiB$_2$ was confirmed as a phase through a XRD investigation of the material

- SEM combined with EDX investigations confirmed the morphology and chemical composition of the materials
- Because of its wide usage, a S355JR structural steel was used as a substrate of the coatings

> Powder mixing and deposition
- The matrix and the reinforcement have been combined in four different volumetric mixes NiCrBSi:TiB$_2$ 95:5, 90:10, 85:15 and 80:20 by mechanical mixing for 600 s in a dedicated screw conveyor for powder mixing
- Following SEM investigation, it was concluded that the TiB$_2$ particles attach to the matrix as satellites. This phenomenon is favouring a better distribution of the reinforcement in the coating
- The structural steel substrate was grit blasted with chilled iron grit prior to the deposition and brought to a roughness of minimum Ra 75 μm helping the mechanical hooking of the mixed powder during the deposition process
- The four prepared batches were successfully deposited with combustion flame-spraying equipment in a wide range of thicknesses, from 200 μm to 2000 μm

> Vacuum furnace optimization
- The fusion of the coatings was performed in a cold wall vertical furnace at a pressure of $3.5 \cdot 10^{-2}$ Pa
- Considering the importance of the coating processing for the category of self-fluxing alloys, a design of experiments methodology (response surface methodology) was selected for the optimisation of the depositions
- The selected experimental factors to vary were the holding time and temperature while the followed response variables were the porosity, hardness and hardness standard deviation
- A central composite design $2^2 + *$ was selected as an experimental model
- Following a D-optimal screening, 9 recommended programs were run
- After the correlation of the regression analysis with the results of the tests, it was concluded that sample NiCrBSi-TiB$_2$ reached the highest desirability of 0.82 at a time of 90 min and a temperature of 1110°C

> Characteristics of the coating
- It could be observed that following the vacuum furnace fusion of the samples, the coating thickness decreased between 20% and 30% because of evacuation of the gas that was trapped inside the deposition and the porosity decreased from approximately 25% down to about 1-2%
- Because of the mechanical mixing of the powders, a heterogeneous distribution of the reinforcement in the coating could be observed
- Following a correlation of the SEM/EDX, mapping analysis with the XRD spectra in different metallographic planes, four distinct areas consisting of nine phases could be identified
- The matrix consists of BNi$_2$ and γ-Ni, and σ-Cr$_3$Ni$_5$Si$_2$. While the first two compounds are well-known phases of Ni-based self-fluxing coatings, the formation of the latter is being favoured by the low Si content and is a sign of the right temperature of the post-processing as the element is not diluting in the matrix and aids for the coating ductility
- Small dark regions in the coating correspond to the hard TiB$_2$. The formation of SiO$_2$ and Ti$_3$O compounds was inevitable as the oxygen partial pressure was not low enough to avoid the forming of such phases

- For the present research work interface toughness measurements and surface and cross-section hardness testing were performed
- A succession of several indentations with increasing loads was performed at the interface. Although large indentations were generated, no visible cracks were observed. The maximum applied load was 50 kgf on the HV scale and 62.5 kgf on the HBW one. The good fracture toughness is a result of the diffusion in the coating between the different phases on one hand and between the coating and the substrate on the other hand. The coating-substrate diffusion was confirmed through a line-scan in the region of interest
- The matrix powder respects its delivery specification maintaining a hardness of approximately 350 ± 20 HV. Although losing from its hardness, the reinforcing of the coatings still presents satisfactory values ranging between 450 HV and 600 HV
- A flame sprayed NiCrBSi coating was chosen as a reference comparison sample for tribological and corrosion tests. The comparison with a material that is already established in the industry is crucial in order to test the industrial implementation
- Non-conformal pin-on-disc tests were performed on the NiCrBSi and the NiCrBSi-TiB$_2$ coatings against 6 mm radius 100Cr6 and WC-Co balls. Several tests were performed in order to assure the reproducibility of the results. Although in the tests against 100Cr6 balls the coefficient of friction stabilized much later (after approximately 450 m) compared to the ones against WC-Co (after approximately 250 m) no other major difference could be established between the samples. All the tested coatings reached a maximum COF around 0.75 and 0.80 while the average COF was situated between 0.64 and 0.69
- The SE/EDX analysis of the samples after the pin-on-disc tests revealed transferred layer, grooves and spalling phenomena on the wear tracks
- The wear rates of the coatings and counterparts were calculated using the *Archard* mathematical equation by dividing the worn volume by the applied load and the distance
- Regarding the coatings, it can be highlighted that the NiCrBSi-TiB$_2$ sample performed better during wear tests than the NiCrBSi sample against both 100Cr6 and WC-Co balls. When tested against the steel counterpart, the reinforced coating showed an approximately 40% smaller wear rate than the reference sample. In the tests against the WC-Co static partner, the NiCrBSi-TiB$_2$ coating performed about 50% better than the NiCrBSi sample. The difference can be attributed to the good resistance of the reinforcement against sliding wear and the optimized post-processing parameters
- In the case of the counterparts, the 100Cr6 ball showed a 40% higher wear when tested against the reinforced sample than against the reference sample. The relatively soft steel ball generated a larger spherical cap when encountering the reinforced sample, hence the wear rate difference. In the case of the WC-Co counterpart, it can be pointed out that the test against the NiCrBSi-TiB$_2$ sample showed an approximately 10 times smaller sliding wear than in the case of the reference sample
- The corrosion behaviour of the coatings was assessed in a 3.5% NaCl solution (pH~7) at room temperature, using a three electrode-cell configuration, applying quasi stationary conditions (scan rate 0.16 mV·s^{-1}). The specimens were scanned from -1000 mV to 1000 mV vs. SCE
- The lNiCrBSi-TiB$_2$ sample concludes a lower corrosion current density (i_{corr}=0.7·10^{-7} mA cm^{-2}) in comparison with the NiCrBSi coating

(i_{corr} $10 \cdot 10^{-7}$ mA cm^{-2}), resulting in a superior corrosion resistance of the coating containing TiB$_2$ due to the reduced number of defects on the investigated surface.

• The breakdown potential of the NiCrBSi-TiB$_2$ (-60 mV vs. SCE), happens much later than in the case of the NiCrBSi sample (-240 mV vs. SCE) indicating for the newly developed coating a longer stable region and consequently a better corrosion resistance in chlorine environment

The personal contributions of the present study may be regarded as following:

• Reinforced NiCrBSi-TiB$_2$ mechanically mixed powder in different volumetric proportions were successfully thermally sprayed on a structural steel substrate in order to investigate the behaviour of the coating against various mechanical and degradation tests

• Acknowledging the importance of post-processing of self-fluxing coatings, a statistical approach was used to optimize the holding time and temperature during the vacuum furnace heat treatment and to select the best proportions among the samples with different matrix-reinforcement volumetric concentrations, in a close correlation with thermogravimetrical measurements

• A comprehensive characterisation using different methods was used to investigate the porosity, chemical composition, phase distribution and interface region of the optimized NiCrBSi-TiB$_2$ coating

• The tribological and corrosion behaviour of the reinforced coating was analysed in comparison with a conventional NiCrBSi alloy.

Even though the goals of the study have been reached, due to practical and technical difficulties, certain limitations have been encountered. Regarding the materials, because of the high melting point of the reinforcement, no comprehensive study of the melting range of the mixed powder could be performed. The mechanical mixing of the powders led to a heterogeneous distribution of the reinforcement in the coating and locally influenced the behaviour of the coating during the performed sliding wear and corrosion tests.

The thermally sprayed coatings are commonly found as solutions in applications that require combined wear and corrosion resistance. The developed NiCrBSi-TiB$_2$ is an ideal solution for machine components that need a long lifespan in hardly challenging environments. The TiB$_2$ reinforced coatings, because of their excellent tribological behaviour can be a real alternative for the more common NiCrBSi in applications like valve seats, pump sleeves or shafts.

All in all, thermally sprayed NiCrBSi-TiB$_2$ coatings have been successfully post-treated, optimized and thoroughly characterized. A coating resulting from the combination of the selected matrix and reinforcement could replace well-established industrial materials and might be considered for new applications concerning protection and restoration.

5.2. Future directions

The thesis has been mainly focused on the development, optimization, characterisation and to some extent testing of the developed deposition. New approaches could be focused on trying different deposition methods, on the analysis of particular mechanisms or performing other type of investigations on the developed materials.

Further research could be also built on the present one based on some of the following ideas:

• The present study already confirmed the deposition possibility of the developed material through combustion flame-spraying, but other techniques could be as well experimented. Processes like laser cladding, atmospheric plasma spraying or laser cladding would certainly deliver coatings with different microstructures and properties

• Considering the importance of the interface region, further research can be performed in this direction. As an interface toughness measurement through the fracture mechanics approach could not be performed, tensile adhesion or bending tests are recommended. Shearing tests could be also used to test the adhesive-cohesive strength of the deposition

• The mechanical mixing of the powders created partial attachment of the reinforcing particles to the matrix. Nevertheless, a significant amount did not immediately combine with the Ni-based powder and a heterogeneous coating was obtained through deposition. By using techniques like ball milling, mechanical alloying, fusing, sintering or crushing, a superior blending of the reinforcement-matrix mix could be obtained leading to potentially more homogeneous coating

• The optimization of the present coatings was performed using the response surface methodology. It could be also applied to the optimization of other parts of the vacuum furnace post-processing program, like the heating or cooling rates. Trying types of designs other than central composite, like Box-Behnken or factorial, or simply including into analysis data like effect plots, F-ratio or P-value could also change the perception of the results.

In a nutshell, the conducted research work did meet its objectives and can as well provide a good starting point for further studies and discussions.

References

1. Goldschmidt A, Streitberger H-J. Basics of Coating technology. 2nd ed. Münster, Germany: BASF; 2007.
2. von Helmershausen R. Schedula Diversarium Artium. Wien, Austria: Hirzel; 1874.
3. Dohnke K. Die Lack Story: 100 Jahre Farbigkeit zwischen Schutz, Schönheit und Umwelt. 1st ed. Hamburg: Dölling und Galitz; 2000.
4. Agricola G. De Re Metallica. London, UK: The Mining Magazine, Salbury House; 1912.
5. Siegmann S, Abert C. 100 years of thermal spray: About the inventor Max Ulrich Schoop. Surf Coat Technol. 2013 Apr 15;220:3–13.
6. Davis JR. Handbook of Thermal Spray Technology. 1st ed. US: ASM International; 2004.
7. Mellor BG. Surface coatings for protection against wear. 1st ed. Cambridge, UK: Woodhead Publishing Limited; 2006. 448 p.
8. Nasr GG, Connor NE. Natural gas engineering and safety changes: downstream process, analysis, utilization and safety. 1st ed. Switzerland: Springer; 2014. 402 p.
9. Sagar A. A review on thermal spray coating processes. Int J Curr Trends Eng Res. 2016 Apr;2(4):556–63.
10. Hermanek FJ. Thermal spraying: what it was and what it has become. Int J Powder Metall. 2002;38(7):35–44.
11. World Paint & Coatings [Internet]. The Freedonia Industry Research Group; 2016 [cited 2018 Oct 9]. Available from: https://www.freedoniagroup.com/industry-study/world-paint-coatings-3418.htm?referrerid=fl-focus
12. Paints & Coatings Market by Resin (Acrylic, Alkyd, Epoxy, Polyurethane, Polyester), Technology (Water-Based, Solvent-Based, High Solids, Powder), Application (Architectural & Industrial), and Region - Global Forecasts to 2022 [Internet]. Markets and Markets; 2017. Available from: https://www.marketsandmarkets.com/Market-Reports/paint-coating-market-156661838.html
13. Statista. Coating World [Internet]. [cited 2018 Oct 2]. Available from: https://www.statista.com/statistics/751323/global-distribution-of-coatings-market-value-by-region/.
14. GDP estimates for the third and fourth quarter of 2018. Bruxelles: Eurostat; 2018 Nov p. 3. Report No.: 174/2018.
15. Kusumar, Nerlfi & Growney. Third Global Paint & Coatings Report, 2016-2021 [Internet]. [cited 2018 Oct 1]. Available from: https://www.coatingsworld.com/issues/2017-09-01/view_market-research/kusumgar-nerlfi-amp-growney-publish-third-global-p/
16. Vardelle A, Moreau C, Akedo J, Ashrafizadeh H, Berndt CC, Berghaus JO, et al. The 2016 Thermal Spray Roadmap. J Therm Spray Technol. 2016 Dec 1;25(8):1376–440.
17. Soeiro Junior JC, da Luz MA, Brandi SD. Comparison of deposition rate and deposition efficiency between ER70S-6 and E71T-1C consumables. Weld Int. 2017 Feb 1;31(2):79–89.

18. Koch GH, Michiel PH, Thompson Neil. G., Virmani YP, Payer JH. Corrosion Costs and Preventive Strategies in the United States. Houston, US: NACE International; p. 12. Report No.: FHWA-RD-01-156.

19. Knight R, Smith RW. Powder Metal Technologies and Applications. 1st ed. US; 1998. (ASM Handbook; vol. 7).

20. Walser B. The importance of thermal spray for current and future applications in key industries. Spraytime. 2004;10(4):1–7.

21. Ohring M. Materials Sciece of Thin Films - Deposition and Structure. 2nd ed. US: Academic Press; 2012. 831 p.

22. Schneider KE, Belascchenko V, Dratwinski M, Seigmann S, Zagorski A. Thermal spraying for power generation components. 1st ed. Germany: Wiley; 2006. 286 p.

23. Weman K. Welding processes handbook. 1st ed. US: Woodhead Publishing Limited; 2003. 196 p.

24. Arendt SA, Bailey SJ, Baldini NC, McElrone EK. ASTM Dictionary of engineering science & technology. In: 10th ed. US: ASTM; 2005.

25. DIN EN ISO 14917: Thermal spraying - terminology , classification. Deutsches Institut für Normung; 2005.

26. Pawlowski L. The science and engineering of thermal spray coatings. 2nd ed. UK: John Wiley & Sons, Ltd; 2008. 647 p.

27. Witherspoon FD, Massey DW, Kincaid RW, Whichard GC, Mozhi TA. High velocity pulsed plasma thermal spray. J Therm Spray Technol. 2002 Mar 1;11(1):119–28.

28. Bouyer E, Henne R, Müller-Steinhagen H, Schäfer D, Asano H. Improved heat transfer by RF plasma produced structured surfaces. In: Thermal Spray: Advancing the Science and Applying the Technology. Orlando, US: ASM International; 2003. p. 559–66.

29. An introduction to thermal spray. Oerlikon Metco; 2016.

30. Kasparova M, Zahalka F, Houdovka S. Evaluation of the bond strength of thermally sprayed coatings. In Brno, Czech Republic: Tanger; 2014.

31. Korenev VN, Barabash VV, Semenov AV. The bonding strength of powder coatings in gas-flame spraying with the hydrogen–oxygen flame. Weld Int. 2017 Apr 3;31(4):333–6.

32. Allcock B, Gu S, Kamnis S. Nozzle for a thermal spray gun and method of thermal spraying. 9,834,844 BS, 2017. p. 18.

33. Wang X, Song Q, Yu Z. Numerical Investigation of Combustion and Flow Dynamics in a High Velocity Oxygen-Fuel Thermal Spray Gun. J Therm Spray Technol. 2016 Feb 1;25(3):441–50.

34. Tian J-J, Yao S-W, Luo X-T, Li C-X, Li C-J. An effective approach for creating metallurgical self-bonding in plasma-spraying of NiCr-Mo coating by designing shell-core-structured powders. Acta Mater. 2016 May 15;110:19–30.

35. Olakanmi EO, Doyoyo M. Laser-Assisted Cold-Sprayed Corrosion- and Wear-Resistant Coatings: A Review. J Therm Spray Technol. 2014 Jun 1;23(5):765–85.

36. Zheng YZ, Li Q, Zheng ZH, Zhu JF, Cao PL. Modeling the impact, flattening and solidification of a molten droplet on a solid substrate during plasma spraying. Appl Surf Sci. 2014 Oct 30;317:526–33.

37. Tucker RCJr. Thermal Spray Technology. US: ASM International; 2013. 412 p. (ASM Handbook; vol. 5A).

38. Chandra S, Fauchais P. Formation of Solid Splats During Thermal Spray Deposition. J Therm Spray Technol. 2009 Jun 1;18(2):148–80.

39. Salimijazi HR, Coyle TW, Mostaghimi J, Leblanc L. Microstructure and failure mechanism in As-deposited, vacuum plasma-sprayed Ti-6Al-4V alloy. J Therm Spray Technol. 2005 Jun 1;14(2):215–23.

40. Danouni S, Abdellah El-hadj A, Zirari M, Belharizi M. A thermo-mechanical analysis of a particle impact during thermal spraying. Appl Surf Sci. 2016 May 15;371:213–23.

41. Dosta S, Bolelli G, Candeli A, Lusvarghi L, Cano IG, Guilemany JM. Plastic deformation phenomena during cold spray impact of WC-Co particles onto metal substrates. Acta Mater. 2017 Feb 1;124:173–81.

42. Morks MF, Tsunekawa Y, Okumiya M, Shoeib M. Microstructure of Plasma-Sprayed Cast Iron Splats with Different Particle Sizes. Mater Trans. 2003;44(4):743–8.

43. Chraska T, King AH. Effect of different substrate conditions upon interface with plasma sprayed zirconia—a TEM study. Surf Coat Technol. 2002 Aug 22;157(2):238–46.

44. Morks MF, Tsunekawa Y, Okumiva M, Shoeib MA. Splat morphology and microstructure of plasma sprayed cast iron with different preheat substrate temperatures. J Therm Spray Technol. 2002 Jun 1;11(2):226–32.

45. Kromer R, Costil S, Cormier J, Courapied D, Berthe L, Peyre P, et al. Laser surface patterning to enhance adhesion of plasma sprayed coatings. Surf Coat Technol. 2015 Sep 25;278:171–82.

46. Kromer R, Cormier J, Costil S. Role of Powder Granulometry and Substrate Topography in Adhesion Strength of Thermal Spray Coatings. J Therm Spray Technol. 2016 Jun 1;25(5):933–45.

47. ISO 17836: Thermal spraying - Determination of the deposition efficiency for thermal spraying. International Organization for Standardization; 2017.

48. Toma F-L, Potthoff A, Berger L-M, Leyens C. Demands, Potentials, and Economic Aspects of Thermal Spraying with Suspensions: A Critical Review. J Therm Spray Technol. 2015 Oct 1;24(7):1143–52.

49. Liquid masking compounds for thermal spray processing - Material product data sheet. Oerlikon Metco; 2017.

50. EN ISO 8501: Preparation of steel substrates before application of paints and related products - Visual assessment of surface cleanliness - Part 1: Rust grades and preparation of uncoated steel substrated and of streel substreates after overall removal of previous coatings. International Organization for Standardization; 2008.

51. Warnes BM, Schilbe JE. Molten metal hydroxide removal of thermal barrier coatings. Proc 28th Int Conf Metall Coat Thin Films. 2001 Sep 1;146–147:147–51.

52. Takeda K, Takeuchi S. Removal of Oxide Layer on Metal Surface by Vacuum Arc. Mater Trans JIM. 1997;38(7):636–42.

53. Taylor TA. Surface roughening of metallic substrates by high pressure pure waterjet. Surf Coat Technol. 1995 Nov 1;76–77:95–100.

54. Knapp JK, Taylor TA. Waterjet roughened surface analysis and bond strength. Surf Coat Technol. 1996 Dec 1;86–87:22–7.

55. Coddet C, Montavon G, Ayrault-Costil S, Freneaux O, Rigolet F, Barbezat G, et al. Surface preparation and thermal spray in a single step: The PROTAL process—Example of application for an aluminum-base substrate. J Therm Spray Technol. 1999 Jun 1;8(2):235–42.

56. DIN EN ISO 13507: Thermal spraying - Pre-treatment of surfaces of metallic parts and components for thermal spraying. Deutsches Institut für Normung; 2010.

57. DIN EN ISO 12679: Thermal spraying - Recomendations for thermal spraying. Deutsches Institut für Normung; 2015.

58. MS 2138-A: Metal sprayed coatings for corrosion protection aboard naval ships (Metric). American Navy Military Standard; 1992.

59. Varacalle DJ, Rhodaverger W, Post Guillen D, Deason D, Sampson E. Surface preparation of steel substrates using grit-blasting. In US; 2005.

60. Bobzin K, Öte M, Linke TF, Sommer J, Liao X. Influence of Process Parameter on Grit Blasting as a Pretreatment Process for Thermal Spraying. J Therm Spray Technol. 2016 Jan 1;25(1):3–11.

61. Begg H, Riley M, de Villiers Lovelock H. Mechanization of the Grit Blasting Process for Thermal Spray Coating Applications: A Parameter Study. J Therm Spray Technol. 2016 Jan 1;25(1):12–20.

62. Dong S, Song B, Liao H, Coddet C. Effect of dry-ice blasting on the deposition behavior of molybdenum particles onto aluminum and stainless steel substrates using plasma spraying: From single splat to coating. 6th Rencontres Int Proj Therm. 2015 Apr 25;268:46–51.

63. Pawlowski L. Quality improvement of coating by a prespray and postspray process. J Therm Spray Technol. 1998 Mar 1;7(1):3–6.

64. DIN EN ISO 14924: Thermal spraying - post-treatment and finishing of thermally sprayed coatings. Deutsches Institut für Normung; 2005.

65. Verdian MM. 3.13 Finishing and Post-Treatment of Thermal Spray Coatings. In: Hashmi M, editor. Comprehensive Materials Finishing [Internet]. Oxford: Elsevier; 2017. p. 191–206. Available from: http://www.sciencedirect.com/science/article/pii/B9780128035818092006

66. Thorpe MerleL. Thermal spraying: practice, theory and application. 1st ed. US: American Welding Society; 1985. 188 p.

67. Knuuttila J, Sorsa P, Mäntylä T, Knuuttila J, Sorsa P. Sealing of thermal spray coatings by impregnation. J Therm Spray Technol. 1999 Jun 1;8(2):249–57.

68. Skarvelis P, Papadimitriou GD. Plasma transferred arc composite coatings with self-lubricating properties, based on Fe and Ti sulfides: Microstructure and tribological behavior. Surf Coat Technol. 2009 Feb 25;203(10):1384–94.

69. Proskurovsky DI, Rotshtein VP, Ozur GE, Markov AB, Nazarov DS, Shulov VA, et al. Pulsed electron-beam technology for surface modification of metallic materials. J Vac Sci Technol A. 1998 Jul 1;16(4):2480–8.

70. von Allmen M, Blatter A. Laser-Beam Interactions with Materials: Physical Principles and Applications. 2nd ed. Switzerland: Springer; 1995. 205240 p.

71. Serres N, Hlawka F, Costil S, Langlade C, Machi F. Microstructures and environmental assessment of metallic NiCrBSi coatings manufactured via hybrid plasma spray process. Proc Fourth Workshop RIPT Rencontres Int Sur Proj Therm Third Workshop Suspens Solut Therm Spray S2TS. 2010 Nov 15;205(4):1039–46.

72. Feldshtein E, Kardapolava M, Dyachenko O. Structure, phases and tribological behaviour of Fe-based self-fluxing alloy coatings formed by plasma spraying and follow-up flame and laser remelting. Int J Surf Sci Eng. 2015;9(1):395–407.

73. Yuan Q, Feng X, Ji G. Comparative Analysis on the Microstructure and Property of Ni-Based Coatings Remelted by Laser and Flame. J Comput Theor Nanosci. 2012 Sep 1;9(9):1347–51.

74. Loh NL, Sia KY. An overview of hot isostatic pressing. J Mater Process Technol. 1992 Feb 1;30(1):45–65.

75. Herø H, Wie H, Jørgensen RB, Ruyter IE. Hydroxyapatite coatings on Ti produced by hot isostatic pressing. J Biomed Mater Res. 1994 Mar;28(3):343–8.

76. Khor KA, Yip CS, Cheang P. Post-spray hot isostatic pressing of plasma sprayed Ti6Al4V/hydroxyapatite composite coatings. J Mater Process Technol. 1997 Nov 15;71(2):280–7.

77. Chen HC, Pfender E, Heberlein J. Structural changes in plasma-sprayed ZrO2 coatings after hot isostatic pressing. Thin Solid Films. 1997 Jan 30;293(1):227–35.

78. AlMangour B, Grzesiak D, Yang J-M. Selective laser melting of TiB2/316L stainless steel composites: The roles of powder preparation and hot isostatic pressing post-treatment. Powder Technol. 2017 Mar 1;309:37–48.

79. DIN EN ISO 12944-5: Paints and varnishes - Corrosion protection of steel structures by protective paint systems - Part 5: Protective paint systems. Deutsches Institut für Normung; 2008.

80. Morisada Y, Fujii H, Mizuno T, Abe G, Nagaoka T, Fukusumi M. Modification of thermally sprayed cemented carbide layer by friction stir processing. Surf Coat Technol. 2010 Apr 25;204(15):2459–64.

81. Pawlowski L. Technology of thermally sprayed anilox rolls: State of art, problems, and perspectives. J Therm Spray Technol. 1996 Sep 1;5(3):317–34.

82. Marple BR, Voyer J, Béchard P. Sol infiltration and heat treatment of alumina–chromia plasma-sprayed coatings. J Eur Ceram Soc. 2001 Jul 1;21(7):861–8.

83. Totten GE. Steel Heat Treatment Handbook: Equipment and Process Design. 2nd ed. Taylor & Francis; 2007. 709 p.

84. Boyer HE. Practical Heat Treating. 3rd ed. US: ASM International; 1987. 247 p.

85. ASM Handbook - Heat Treating. 1st ed. Vol. 4. ASM International; 1991. 2173 p.

86. Nemenyi R. Controlled atmosphere for heat treatment. UK: Pergamon Press; 1984. 245 p.

87. Kubota K. Vacuum carburizing method and device, and carburized products. 5,702,540, 1997. p. 11.

88. Beadle JE. Product Treatment & Finishing - Production Engineering Series. UK: The Maacmillan Press Limited; 1972. 156 p.

89. Hoffman DM, Singh B, Thomas JHI. Handbook of Vacuum Science and Technology. 1st ed. US: Academic Press; 1998. 861 p.

90. Fabian R. Vacuum Technology - Practical Heat Treating and Brazing. 3rd ed. US: ASM International; 1998. 263 p.

91. Umrath U. Fundamentals of Vacuum Technology. Germany: Leybold Heraeus; 1998. 200 p.

92. DIN 28400: Vacuum technology; designations and definitions. Deutsches Institut für Normung; 1990.

93. DIN ISO 10012: Measurement manangement systems - Requirements for measurement processes and measuring equipment. Deutsches Institut für Normung; 2003.

94. Pascal D-T, Kazamer N, Muntean R, Valean P-C, Serban V-A. Electrochemical Corrosion Behavior of High Temperature Vacuum Brazed WC-Co-NiP Functional Composite Coatings. IOP Conf Ser Mater Sci Eng. 2018;416(1):012003.

95.   Pascal D-T, Muntean R, Kazamer N, Marginean G, Brandl W, Serban V-A. Characteristics of High Temperature Vacuum Brazed WC-Co-NiCrBSi Functional Composite Coatings. In Brno, Czech Republic: Tanger; 2016. p. 775–80.

96.   Global Vacuum Heat Treatment Market 2016-2020. US: Technavio; 2016 p. 56. Report No.: SKU: IRTNTR8310.

97.   Liang Z. Nozzle for cooling vacuum heat treatment furnace. Shanghai;

98.   X. Haohua, X. Tao, T. Jian, F. Lulu, X. Tianshuang, Y. Tatsuo. Research on the Temperature Uniformity of Vacuum Furnace and Size Optimization of Working Zone. In: 2015 8th International Conference on Intelligent Computation Technology and Automation (ICICTA). 2015. p. 789–92.

99.   Totten G. Heat treating in 2020: What are the most critical issues and - What will the future look like? In Society for Advancement of Heat Treatment & Surface Engineering; 2004.

100. Sonawane GD, Gunjal SU. Review on recent trends & optimisation in heat treatment. IOSR J Mech Civ Eng. 2014;11(3 (VI)):52–8.

101. Fisher RA. The design of experiments. Oxford, England: Oliver & Boyd; 1935. xi, 251. (The design of experiments.).

102. Montgomery DC. Design and Analysis of Experiments. 9th ed. US: Wiley; 2017. 640 p.

103. Taguchi G, Chowdhury S. Robust Engineering: Learn How to Bosst Quality While Reducing Costs & Quality to Market. US: McGrar Hill Book Co; 1999. 241 p.

104. Myers RH, Montgomery DC, Anderson-Cook CM. Response Surface Methodology: Process and Product Optimization Using Designed Experiments. 3rd ed. US: John Wiley & Sons, Ltd; 2009. 1247 p.

105. Box GE., Hunter JS, Hunter WG. Statistics for Experimenters: Design, Innovation and Discovery. 2nd ed. US: John Wiley & Sons, Ltd; 2005. 655 p.

106. Barrentine LB. An Introduction to Design of Experiments. US: ASQ Quality Press; 1999. 116 p.

107. Dyshlovenko S, Pawlowski L, Roussel P, Murano D, Le Maguer A. Relationship between plasma spray operational parameters and microstructure of hydroxyapatite coatings and powder particles sprayed into water. Surf Coat Technol. 2006 Mar 31;200(12):3845–55.

108. Cannillo V, Lusvarghi L, Sola A. Design of Experiments (DOE) for the Optimization of Titania–hydroxyapatite Functionally Graded Coatings. Int J Appl Ceram Technol. 2009 Jun 24;6(4):537–50.

109. Guessasma S, Montavon G, Coddet C. On the neural network concept to describe the thermal spray deposition process: an introduction. In Ohio, US: ASM International; p. 57–61.

110. Oksa M, Turunen E, Suhonen T, Varis T, Hannula S-P. Optimization and Characterization of High Velocity Oxy-fuel Sprayed Coatings: Techniques, Materials, and Applications. Coatings. 2011 Sep;1(1):17–52.

111. Pierlot C, Pawlowski L, Bigan M, Chagnon P. Design of experiments in thermal spraying: A review. 3 Rencontres Int Proj Therm. 2008 Jun 15;202(18):4483–90.

112. NIST U.S. Department of Commerce. NIST/SEMATECH e-Handbook of Statistical Methods [Internet]. [cited 2018 Nov 15]. Available from: https://www.itl.nist.gov/div898/handbook/pri/section3/pri33.htm

113. Ramkumar T, Narayansamy P, Selvakumar M, Balasundar P. Effect of B4C Reinforcement on the Dry Sliding Wear Behaviour of Ti-6Al-4V/B4C Sintered

Composite Using Response Surface Methodology. Arch Metall Mater. 2018;3:1179–200.

114. Thirumalaikumarasamy D, Balasubramanian V, Sree Sabari S. Prediction and optimization of process variables to maximize the Young's modulus of plasma sprayed alumina coatings on AZ31B magnesium alloy. J Magnes Alloys. 2017 Mar 1;5(1):133–45.

115. Liu K, Bai Y, Kang YX, Zhang L, Tang JJ, Wang Y, et al. Investigation of particle characteristics, composition and microstructure of LaxCe1−xO2−x/2 thermal barrier coatings during supersonic atmospheric plasma spray using Box–Behnken design. Surf Coat Technol. 2016 Jan 25;286:9–15.

116. Rico A, Salazar A, Escobar ME, Rodriguez J, Poza P. Optimization of atmospheric low-power plasma spraying process parameters of Al2O3-50wt%Cr2O3 coatings. Surf Coat Technol. 2018 Nov 25;354:281–96.

117. Salavati S, Coyle TW, Mostaghimi J. Twin wire arc spray process modification for production of porous metallic coatings. Surf Coat Technol. 2016 Jan 25;286:16–24.

118. Candidato RT, Sokołowski P, Pawłowski L, Lecomte-Nana G, Constantinescu C, Denoirjean A. Development of hydroxyapatite coatings by solution precursor plasma spray process and their microstructural characterization. 7th Rencontres Int Proj Therm. 2017 May 25;318:39–49.

119. Pascal D-T. Development of high temperature vacuum brazed WC-Co-NiP functional composite coatings [PhD]. [Timisoara]: University Politehnica Timisoara; 2017.

120. Kovářík O, Haušild P, Siegl J, Chráska T, Matějíček J, Pala Z, et al. The influence of substrate temperature on properties of APS and VPS W coatings. 6th Rencontres Int Proj Therm. 2015 Apr 25;268:7–14.

121. ISO 14232-1: Thermal spraying - Powders- Part 1: Characterization and technical supply conditions. International Organization for Standardization; 2017.

122. DIN ISO 1274: Thermal spraying - powders - composition, technical supply conditions. Deutsches Institut für Normung; 1996.

123. DSMW-0002.6 - Nickel-Based Supperalloy Powders for Laser Clading. Oerlikon Metco; 2017.

124. Certilas. Gas atomized self fluxing nickel powder alloy against heavy wear [Internet]. [cited 2018 Nov 23]. Available from: http://www.certilas.nl/nl/product/nicrbsi-62

125. GTV GmbH. GTV Spray powder catalogue [Internet]. [cited 2018 Nov 23]. Available from: https://www.gtv-mbh.com/_old/gtv-mbh-englisch/www.gtv-mbh.de/cms/upload/downloads/GTV_Spray_Powder_Catalogue_08-2012.pdf

126. LSN Diffusion. Nickel Based Alloys [Internet]. [cited 2018 Nov 23]. Available from: http://lsndiffusion.com/products/nickel-based-alloys/

127. Pettersson T. Characterization of metal powders produced by two gas atomizing methods for thermal spraying application. [Stockholm]: KTH Royal Institute of Technology; 2015.

128. Terence A. Particle size measurement: Powder sampling and particle size measurement. 5th ed. Vol. 1. US: Chapman & Hall; 1997. 512 p.

129. Terence A. Particle size measurement: Surface area and pore size determination. 5th ed. Vol. 2. US: Chapman & Hall; 1997. 255 p.

130. ASTM-E2651-13: Standard Guide for Powder Particle Size Analysis. American Society for Testing and Materials; 2013.

131. ASTM-B214-07: Standard Test method for Sieve Analysis of Metal Powders. American Society for Testing and Materials; 2016.
132. Viana M, Fonseca AS, Querol X, López-Lilao A, Carpio P, Salmatonidis A, et al. Workplace exposure and release of ultrafine particles during atmospheric plasma spraying in the ceramic industry. Sci Total Environ. 2017 Dec 1;599–600:2065–73.
133. Galey L, Audignon S, Witschger O, Lacourt A, Garrigou A. Toward a Better Assessment of Occupational Exposure to Nanoparticles Taking into Account Work Activities. In: Bagnara S, Tartaglia R, Albolino S, Alexander T, Fujita Y, editors. Proceedings of the 20th Congress of the International Ergonomics Association (IEA 2018). Springer International Publishing; 2019. p. 465–78.
134. Krolczyk GM, Nieslony P, Krolczyk JB, Samardzic I, Legutko S, Hloch S, et al. Influence of argon pollution on the weld surface morphology. Measurement. 2015 Jun 1;70:203–13.
135. Devojno OG, Feldshtein E, Kardapolava MA, Lutsko NI. On the formation features, microstructure and microhardness of single laser tracks formed by laser cladding of a NiCrBSi self-fluxing alloy. Opt Lasers Eng. 2018 Jul 1;106:32–8.
136. Fauchais P, Heberlein J. J, Boulos M. Thermal Spray Fundaments: From Powder to Part. 1st ed. US: Springer; 2014. 1587 p.
137. Sbrizher AG. Structure and properties of coatings made of self-fluxing alloys. Met Sci Heat Treat. 1988 Apr 1;30(4):296–9.
138. Mrdak MR. Microstructure and mechanical properties of nickel-chrome-bor-silicon layers produced by the atmospheric plasma spray process. Vojnoteh Glas. 2012;183–200.
139. Sakata K, Nakano K, Miyahara H, Matsubara Y, Ogi K. Microstructure Control of Thermally Sprayed Co-Based Self-Fluxing Alloy Coatings by Diffusion Treatment. J Therm Spray Technol. 2007 Dec 1;16(5):991–7.
140. Harada Y, Shin H. Method of production of self-fusing alloy spray containing member. Japan; US 6,326,063 B1. p. 10.
141. Chun E-J, Park C, Nishikawa H, Kim M-S. Microstructural characterization of Ni-based self-fluxing alloy after selective surface-engineering using diode laser. Appl Surf Sci. 2018 Jun 1;442:726–35.
142. Chun E-J, Kim M-S, Nishikawa H, Park C, Suh J. Laser-assisted selective fusing of thermal sprayed Ni-based self-fluxing alloys by using high-power diode lasers. Opt Laser Technol. 2018 Mar 1;100:317–24.
143. Lukas HL, Fries SG, Sundman B. Computational thermodynamics: The CALPHAD method. 1st ed. UK: Cambridge University Press; 2007. 323 p.
144. Materials Science International Team MSIT. Non-Ferrous Metal Systems. Part 3 (B-Cr-Ni Ternary Systems: Phase diagrams, Crystallographic Structure and Thermodynamic Data). Germany: Springer; 2007. (Landolt-Börnstein - Group IV Physical Chemistry).
145. Scientific Group Thermadata Europe (SGTE). Thermodynamic Properties of Inorganic Materials (Part 1: Ternary Steel Systems: Phase Diagrams and Phase Transition Data). 1st ed. Germany: Springer; 2012. 429 p. (Landolt-Börnstein - Group IV Physical Chemistry; vol. 19 Subvolume C).
146. Lee B-J. Upgrade of Steel Database: Bibliographic data for the Ni-Si system [Internet]. Korea; 1999. Available from: http://steel.ndsl.kr/htm/Ni-Si.htm
147. Guo C, Zhou J, Chen J, Zhao J, Yu Y, Zhou H. High temperature wear resistance of laser cladding NiCrBSi and NiCrBSi/WC-Ni composite coatings. Wear. 2011 Mar 10;270(7):492–8.

148. Chaliampalias D, Vourlias G, Skolianos S, Polychroniadis EK, Stergioudis F. Surface Microstructure of NiCrBSi Coatings Deposited by Flame Spray and Evaluation of the Oxidation Resistance. Solid State Phenom. 2010;163:51–4.

149. Smith RW, Knight R. Thermal spraying I: Powder consolidation—From coating to forming. JOM. 1995 Aug 1;47(8):32–9.

150. Liu X, Wang K, Hu P, Chen Q, Volinsky AA. Spheroidization of molybdenum powder by radio frequency thermal plasma. Int J Miner Metall Mater. 2015 Nov 1;22(11):1212–8.

151. Tong. JB, Lu X, Liu CC, Wang LN, Qu XH. Fabrication of micro-fine spherical high Nb containing TiAl alloy powder based on reaction synthesis and RF plasma spheroidization. Powder Technol. 2012 Oct;283:9–15.

152. Hogekamp S, Pohl M. Porosity measurement of fragile agglomerates. Powder Technol. 2003 Feb;130(1–3):385–92.

153. Korosteleva NE, Korzhova VV, Krinitcyn GM. Sintering Behavior and Microstructure of TiC-Me Composite Powder Prepared by SHS. Metals. 2017;7(8).

154. Bartuli C, Smith RW, Shtessel E. SHS powders for thermal spray applications. Ceram Int. 1997 Jan 1;23(1):61–8.

155. Talako T, Ilyuschenko A, Letsko A. SHS Powders for Thermal Spray Coating. KONA Powder Part J. 2009;27:55–72.

156. Serebryakova T. Classification of borides. J Common Met. 1979 Oct 1;67(2):499–503.

157. Basu B, Raju GB, Suri AK. Processing and properties of monolithic TiB2 based materials. Int Mater Rev. 2006 Dec 1;51(6):352–74.

158. Murray JL, Liao PK, Spear KE. The B−Ti (Boron-Titanium) system. Bull Alloy Phase Diagr. 1986 Dec 1;7(6):550–5.

159. Munro RG. Material Properties of Titanium Diboride. J Res Natl Inst Stand Technol. 2000 Oct 1;105(5):709–20.

160. Jones AH, Trueman C, Dobedoe RS, Huddleston J, Lewis MH. Production and EDM of Si3 N4–TiB2 ceramic composites. Br Ceram Trans. 2001 Feb 1;100(2):49–54.

161. Liu H, Lavernia EJ, Rangel RH. Numerical simulation of impingement of molten Ti, Ni, and W droplets on a flat substrate. J Therm Spray Technol. 1993 Dec 1;2(4):369–78.

162. Șerban V-A, Răduța A. Știința și Ingineria Materialelor. 2nd ed. Timișoara: Editura Politehnica; 2010. 525 p.

163. Havrlisan S, Simunovic K, Vukelic D. Modelling of abrasive wear of Ni-based self-fluxing alloy coatings by the application of experimental design. Tech Gaz. 2006;23(6).

164. Natarajan S, Edward Anand E, Akhilesh KS, Rajagopal A, Nambiar PP. Effect of graphite addition on the microstructure, hardness and abrasive wear behavior of plasma sprayed NiCrBSi coatings. Mater Chem Phys. 2016 Jun 1;175:100–6.

165. Chen T, Wu F, Wang H, Liu D. Laser Cladding In-Situ Ti(C,N) Particles Reinforced Ni-Based Composite Coatings Modified with CeO2 Nanoparticles. Metals. 2018;8(8).

166. Vallauri D, Atías Adrián IC, Chrysanthou A. TiC–TiB2 composites: A review of phase relationships, processing and properties. J Eur Ceram Soc. 2008 Jan 1;28(8):1697–713.

167. I. Sulima. Tribological Properties of Steel/Tib2 Composites Prepared by Spark Plasma Sintering/ Własności Tribologiczne Kompozytów Stal/Tib2 Otrzymywanych Metodą Sps. Arch Metall Mater. 2014;59(4):1263–8.

168. Momentive. Titanium Dibordie Powder HCT-30 and HCT-F [Internet]. 2018 [cited 2018 Dec 9]. Available from: https://www.momentive.com/en-us/products/literature/titanium-diboride-powder-grades-hct-30--26amp-3b-hct-f/

169. Wojnar L. Image analysis: applications in materials engineering. Crc Press; 1998.

170. Laksmana FL, Van Vliet LJ, Hartman Kok PJA, Vromans H, Frijlink HW, Van der Voort Maarschalk K. Quantitative Image Analysis for Evaluating the Coating Thickness and Pore Distribution in Coated Small Particles. Pharm Res. 2009 Apr 1;26(4):965–76.

171. Deshpande S, Kulkarni A, Sampath S, Herman H. Application of image analysis for characterization of porosity in thermal spray coatings and correlation with small angle neutron scattering. Surf Coat Technol. 2004 Oct 1;187(1):6–16.

172. Kossman S, Iost A, Chicot D, Mercier D, Serrano-Muñoz I, Roudet F, et al. Mechanical characterization by multiscale instrumented indentation of highly heterogeneous materials for braking applications. J Mater Sci. 2018 Nov 30;

173. Sciortino L, Giannici F, Martorana A, Ruggirello AM, Liveri VT, Portale G, et al. Structural Characterization of Surfactant-Coated Bimetallic Cobalt/Nickel Nanoclusters by XPS, EXAFS, WAXS, and SAXS. J Phys Chem C. 2011 Apr 14;115(14):6360–6.

174. Chicot D, Ageorges H, Voda M, Louis G, Ben Dhia MA, Palacio CC, et al. Hardness of thermal sprayed coatings: Relevance of the scale of measurement. Surf Coat Technol. 2015 Apr 25;268:173–9.

175. Straffelini G. Friction and Wear: Methodologies for Design and Control. 2015th ed. Switzerland: Springer; 2015. 292 p. (Springer Tracts in Mechanical Engineering).

176. Popov ValentinL. Contact Mechanics and Friction: Physical Principles and Application. Berlin: Springer; 2010. 367 p.

177. Straffelini G. A simplified approach to the adhesive theory of friction. Wear. 2001 Apr 1;249(1):78–84.

178. DIN 50320: Wear; Terms, Systematic Analysis of Wear Processes, Classification of Wear Phenomena. Deutsches Institut für Normung; 1979.

179. Dorfman MR. Chapter 22 - Thermal Spray Coatings. In: Kutz M, editor. Handbook of Environmental Degradation of Materials (Third Edition) [Internet]. William Andrew Publishing; 2018. p. 469–88. Available from: http://www.sciencedirect.com/science/article/pii/B978032352472800023X

180. Edrisy A, Alpas AT, Nserc, Perry T. Wear mechanism maps for thermal-spray steel coatings. Metall Mater Trans A. 2005 Oct 1;36(10):2737–50.

181. Kato K. Classification of wear mechanisms/models. Proc Inst Mech Eng Part J J Eng Tribol. 2002 Jun 1;216(6):349–55.

182. Guilemany JM, Miguel JM, Armada S, Vizcaino S, Climent F. Use of scanning white light interferometry in the characterization of wear mechanisms in thermal-sprayed coatings. Mater Charact. 2001 Sep 1;47(3):307–14.

183. Holmberg K, Ronkainen H, Laukkanen A, Wallin K. Friction and wear of coated surfaces — scales, modelling and simulation of tribomechanisms. ICMCTF 2007. 2007 Dec 15;202(4):1034–49.

184. Lawn BR, Swain MV. Microfracture beneath point indentations in brittle solids. J Mater Sci. 1975 Jan 1;10(1):113–22.

185. Friction, Lubrication, and Wear Technology. 4th ed. US: ASM International; 1992. 1879 p. (ASM Handbook; vol. 18).

186. Campbel FC. Fatigue and Fracture: Understand the Basics. 1st ed. US: ASM International; 2012. 699 p.

187. Moridi A, Hassani-Gangaraj SM, Vezzú S, Trško L, Guagliano M. Fatigue behavior of cold spray coatings: The effect of conventional and severe shot peening as pre-/post-treatment. Surf Coat Technol. 2015 Dec 15;283:247–54.

188. DIN EN ISO 8044: Corrosion of metals and alloys - Basic terms and definitions. International Organization for Standardization; 2015.

189. Sandvik. Uniform corrosion (general corrosion). https://www.materials.sandvik/en/materials-center/corrosion/wet-corrosion/general-corrosion/. 2018.

190. Turnbull A. Stress Corrosion Cracking in Metals – Mechanisms. In: Reference Module in Materials Science and Materials Engineering [Internet]. Elsevier; 2016. Available from: http://www.sciencedirect.com/science/article/pii/B9780128035818030642

191. Espallargs N. Future Development of Thermal Spray Coatings: Types, Designs, Manufacture and Applications. Woodhead Publishing Series; 2015. 301 p. (Metals and Surface Engineering).

192. A Beginner`s Guide to Thermogravimetric Analysis. PerkinElmer; 2016.

193. del Castillo E. Process Optimization: A Statistical Approach. US: Springer; 2007. 480 p. (International Series in Operations Reseach and Management Science).

194. Instructions: Leica DMR - Das Mikroskop, 2nd Edition. Leica Mikrokopie und Systeme GmbH;

195. Zou Y, Malzbender J. Development and optimization of porosity measurement techniques. Ceram Int. 2016 Feb 1;42(2, Part A):2861–70.

196. Schneider CA, Rasband WS, Eliceiri KW. NIH Image to ImageJ: 25 years of image analysis. Nat Methods. 2012 Jun 28;9:671.

197. Goldstein JI, Newbury DE, Michael JR, Ritchie NWM, Scott JHJ, Joy DC. Scanning Electron Microscopy and X-Ray Microanalysis. 4th ed. US: Springer; 2017. 554 p.

198. MyScope Training [Internet]. 2019 [cited 2019 Jan 9]. Available from: https://myscope.training/

199. Technical Manual: XL 30 ESEM TMP - Scanning Electron Microscope. FEI Company; 1999.

200. Muntean R. Development of catalyst materials based on carbon nanofirbers for electrochemical cell aplications [PhD]. [Timișoara]: University Politehnica Timisoara; 2016.

201. Prince RL, Jerome WG (Jay). Basic Confocal Microscopy. 1st ed. US: Springer; 2011. 3015 p.

202. User's Manual - 3D Laser Scanning Microscope VK-X100K/X105/X110, VK-X200K/X210. Keyence;

203. Wased Y, Matsubara E, Kozo S. X-ray Diffraction Crystallography: Introduction, Examples and Solved Problems. Springer; 2011. 322 p.

204. X`Pert - MPD Service Manual 940601. Philips Analytical; 1994.

205. ZwickRoell - ZHVµ- M Micro Vickers Hardness Tester - from manual to fully automatic. ZwickRoell;

206. DIN EN ISO 4545-1: Metallic Materials - Knoop Hardness test - Part 1: Test method. Deutsches Institut für Normung; 2018.

207. DIN EN ISO 6507-1: Metallic materials - Vickers Hardness test - Part 1: Test method. Deutsches Institut für Normung; 2018.
208. ASTM E384-17: Standard Test Method for Microindentation Hardness of Materials. American Society for Testing and Materials; 2017.
209. ASTM G99-17: Standard Test Method for Wear Testing with a Pin-on-Disk Apparatus. American Society for Testing and Materials; 2017.
210. Tribometer, Pin-on-disc machine S/N: 18-301. CSM Instruments;
211. Davis JR. Surface Engineering for Corrosion and Wear Resistance. 1st ed. US: American Society for Testing and Materials & IOM Communications; 2001. 328 p.
212. Kusoglu IM, Alpinar I, Bulbul B. Gas atomization of NiCrBSi powders. In Florence: Taylor & Francis;
213. Salimijazi HR, Golozar MA, M.R. K. Effects of remelting processes on porosity of NiCrBSi flame sprayed coatings. Surf Eng. 2016 Mar 3;32(3):238–43.
214. González R, García MA, Peñuelas I, Cadenas M, Fernández Ma del R, Battez AH, et al. Microstructural study of NiCrBSi coatings obtained by different processes. 16th Int Conf Wear Mater. 2007 Sep 10;263(1):619–24.
215. Greenwood NN, Earnshaw A. The Chemistry of Elements. 2nd ed. UK: Elsevier; 1997. 1600 p.
216. Lih W-C, Yang SH, Su CY, Huang SC, Hsu IC, Leu MS. Effects of process parameters on molten particle speed and surface temperature and the properties of HVOF CrC/NiCr coatings. Surf Coat Technol. 2000 Nov 1;133–134:54–60.
217. Bertrand G, Bertrand P, Roy P, Rio C, Mevrel R. Low conductivity plasma sprayed thermal barrier coating using hollow psz spheres: Correlation between thermophysical properties and microstructure. Surf Coat Technol. 2008 Feb 15;202(10):1994–2001.
218. Jaworski R, Pawlowski L, Roudet F, Kozerski S, Petit F. Characterization of mechanical properties of suspension plasma sprayed TiO2 coatings using scratch test. Surf Coat Technol. 2008 Mar 15;202(12):2644–53.
219. Molnar A, Buza G, Balogh A. Hardness test and microstructure analysis of NiCrBSi sprayed, laser remelted coatings. Prod Process Syst. 2013;6:35–46.
220. Izdinska Z, Nasher A, Izdinsky K. The structure and mechanical properties of NiCrBSi coatings prepared by laser beam cladding. Mater Eng. 2010;17(1):11–6.
221. Kazamer N, Kossman S, Baranyi I, Chicot D, Serban V-A, Rajnai Z, et al. Effet de l'addition de TiB2 sur les propriétés mécaniques et tribologiques de revêtements NiCrBSi déposés par projection thermique. Matér Tech [Internet]. 2018;106(2). Available from: https://doi.org/10.1051/mattech/2018026
222. Stoica V, Ahmed R, Itsukaichi T. Influence of heat-treatment on the sliding wear of thermal spray cermet coatings. Surf Coat Technol. 2005 Sep 1;199(1):7–21.
223. Mahmud TB, Farrokhzad MA, Khan TI. Effect of Heat Treatment on Wear Performance of Nanostructured WC-Ni/Cr HVOF Sprayed Coatings. Tribol Online. 2017;12(1):18–28.
224. Makarov AV, Soboleva NN, Gibzun MS, Malygina IYu, Korobov YuS. Increasing the resistance of a NiCrBSi coating to heat wear by means of combined laser heat treatment. AIP Conf Proc. 2018 Dec 19;2053(1):030037.
225. University of Cambridge. Ellingham Diagrams [Internet]. [cited 2018 Nov 4]. Available from: https://www.doitpoms.ac.uk/tlplib/ellingham_diagrams/index.php

226. Korpiola K. High temperature oxidation of metal, alloy and cermet powder in HVOF spraying process. [Espoo]: Helsinki University of Technology; 2004.

227. Meng G-H, Zhang B-Y, Liu H, Yang G-J, Xu T, Li C-X, et al. Vacuum heat treatment mechanisms promoting the adhesion strength of thermally sprayed metallic coatings. Surf Coat Technol. 2018 Jun 25;344:102–10.

228. Ivanov VV, Balakai VI, Ivanov AV, Arzumanova AV. Synergism in composite electrolytic nickel-boron-fluoroplastic coatings. Russ J Appl Chem. 2006 Apr 1;79(4):610–3.

229. Balakai VI, Balakai IV. Wear resistance of electrolytic nickel-boron alloy deposited from a chloride electrolyte. Russ J Appl Chem. 2009 Sep 1;82(9):1547–50.

230. Wu YS, Qiu WQ, Yu HY, Zhong XC, Liu ZW, Zeng DC, et al. Cycle oxidation behavior of nanostructured Ni60TiB2 composite coating sprayed by HVOF technique. Appl Surf Sci. 2011 Sep 15;257(23):10224–32.

231. Zhu HB, Li H, Li ZX. Plasma sprayed TiB2–Ni cermet coatings: Effect of feedstock characteristics on the microstructure and tribological performance. Surf Coat Technol. 2013 Nov 25;235:620–7.

232. Singh S, Kaur M. Solid particle erosion behaviour of NiCrFeSiBC/Cr3C2 composite coatings – Part II. Surf Eng. 2016 Jul 2;32(7):475–89.

233. Karagoz M, Islak S, Buytoz S, Kurt B. Microstructural Characteristics of High Velocity Oxygen Fuel (HVOF) Sprayed NiCrBSi-SiC Composite Coating on a Low Alloy Steel. In Elazig, Turkey; 2011. p. 13–21.

234. Schuster JC, Du Y. Experimental investigation and thermodynamic modeling of the Cr-Ni-Si system. Metall Mater Trans A. 2000 Jul 1;31(7):1795–803.

235. Sampath S, Neiser RA, Herman H, Kirkland JP, Elam WT. A structural investigation of a plasma sprayed Ni-Cr based alloy coating. J Mater Res. 1993;8(1):78–86.

236. Barsoum MW, El-Raghy T, Rawn CJ, Porter WD, Wang H, Payzant EA, et al. Thermal properties of Ti3SiC2. J Phys Chem Solids. 1999 Apr 1;60(4):429–39.

237. Duarte LI, Klotz UE, Leinenbach C, Palm M, Stein F, Löffler JF. Experimental study of the Fe–Ni–Ti system. Intermetallics. 2010 Mar 1;18(3):374–84.

238. Atkins P, de Paula J. Physical Chemistry: Thermodynamics, Structure, and Change. 10th ed. W.H. Freeman and Company; 2014.

239. Wang Y, Stella J, Darut G, Poirier T, Liao H, Planche M-P. APS prepared NiCrBSi-YSZ composite coatings for protection against cavitation erosion. J Alloys Compd. 2017 Mar 30;699:1095–103.

240. Xiao J-K, Wu Y-Q, Zhang W, Chen J, Wei X-L, Zhang C. Microstructure, wear and corrosion behaviors of plasma sprayed NiCrBSi-Zr coating. Surf Coat Technol. 2019 Feb 25;360:172–80.

241. Valean P-C, Muntean R, Pascal D-T, Kilic Y, Marginean G, Serban V-A. Investigations on the Characteristics of Thermally Sprayed NiCrBSi Coatings Fused by Flame and Inductive Processing. IOP Conf Ser Mater Sci Eng. 2018;416(1):012002.

242. Lesage J, Staia MH, Chicot D, Godoy C, De Miranda PEV. Effect of thermal treatments on adhesive properties of a NiCr thermal sprayed coating. Int Conf Metall Coat Thin Films. 2000 Dec 1;377–378:681–6.

243. Toma D, Brandl W, Marginean G. Wear and corrosion behaviour of thermally sprayed cermet coatings. Surf Coat Technol. 2001 Apr 16;138(2):149–58.

244. Leivo EM, Vippola MS, Sorsa PPA, Vuoristo PMJ, Mäntylä TA. Wear and corrosion properties of plasma sprayed AI2O3 and Cr2O3 coatings sealed by aluminum phosphates. J Therm Spray Technol. 1997 Jun 1;6(2):205–10.

245. Lanzutti A, Lekka M, Fedrizzi L. Tribological Behavior of Thermal Spray Coatings, Deposited by HVOF and APS Techniques, and Composite Electrodeposits Ni/SiC at Both Room Temperature and 300° C. Tribol Ind. 2013;35(2):113–22.

246. Devoino OG, Feldshtein EÉ, Kardapolova MA, Lutsko NI. Structure-Phase Condition and Tribological Properties of Coatings Based on Self-Fluxing Nickel Alloy PG-12N-01 After Laser Surfacing. Met Sci Heat Treat. 2017 Mar 1;58(11):748–52.

247. García A, Fernández MR, Cuetos JM, González R, Ortiz A, Cadenas M. Study of the Sliding Wear and Friction Behavior of WC + NiCrBSi Laser Cladding Coatings as a Function of Actual Concentration of WC Reinforcement Particles in Ball-on-Disk Test. Tribol Lett. 2016 Aug 8;63(3):41.

248. Burris DL, Sawyer WG. Measurement Uncertainties in Wear Rates. Tribol Lett. 2009 Oct 1;36(1):81–7.

Appendix

		NiCrBSi-TiB$_2$				
n	t	T	P	H	σ	D [a]
	[min]	[°C]	[%]	[HV0.3]		
1	30	1020	5.94	313.7	24	0.53
2	90	1020	4.15	311	43	0.60
3	30	1110	2.34	288	24	0.69
4	90	1110	0.55	277	43	0.72
5	28	1065	3.71	304	49	0.63
6	92	1065	1.79	352	69	0.65
7	60	1016	8.80	301	47	0.27
8	60	1114	4.89	315	47	0.52
9	60	1065	6.84	319	80	0.37

[a] *Desirability*

Predicted results of the experimental design program for the NTB samples
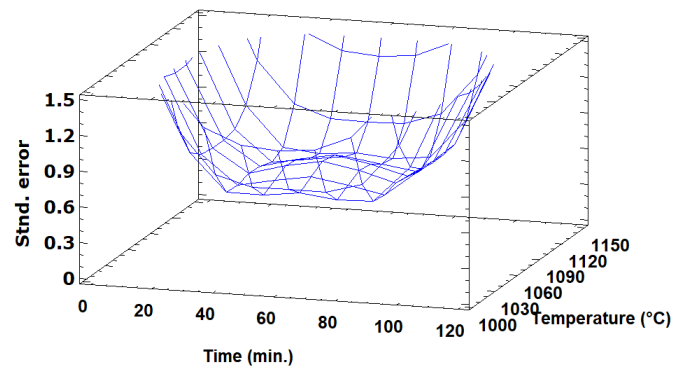
Prediction variance plots of the (a) NTB5, (b) NTB10, (c) NTB15 and (d) NTB20 samples

Scientific activity

Articles published in journals

Valean P-C, **Kazamer N**, Pascal D-T, Muntean R, Baranyi I, Marginean G, Serban V-A. Characteristics of Thermally Sprayed NiCrBSi Coatings before and after Electromagnetic Induction Remelting Process. Acta Polytechnica Hungarica 2019;16:7–18 doi: 10.12700/APH.16.3.2019.3.1

Kazamer N, Kossman S, Baranyi I, Chicot D, Serban V-A, Rajnai Z, Voda M. Effet de l'addition de TiB_2 sur les propriétés mécaniques et tribologiques de revêtements NiCrBSi déposés par projection thermique. Matériaux & Techniques 2018;106. doi:10.1051/mattech/2018026

Kazamer N, Pascal D-T, Uţu ID. Short Review Regarding the HVOF Thermal Spraying Technology, Material Usage and Future Developments. Scientific Bulletin of the Politehnica University of Timișoara (Transaction on Mechanics) 2015;58.

Articles and presentations at conferences

Kazamer N, Valean P-C, Pascal D-T, Muntean R, Marginean G, Serban V-A. Microstructure and Phase Composition of NiCrBSi-TiB_2 Vacuum Furnace Fused Flame-Sprayed Coatings. IOP Conference Series: Materials Science and Engineering 2018;416:012001. doi: 10.1088/1757-899X/416/1/012001

Valean P-C, **Kazamer N**, Muntean R, Pascal D-T, Kilic Y, Marginean G, Serban V-A. Investigations on the Characteristics of Thermally Sprayed NiCrBSi Coatings Fused by Flame and Inductive Processing. IOP Conference Series: Materials Science and Engineering 2018;416:012002. doi: 10.1088/1757-99X/416/1/012002.

Pascal D-T, **Kazamer N**, Muntean R, Valean P-C, Marginean G., Serban V-A. Electrochemical Corrosion Behavior of High Temperature Vacuum Brazed WC-Co-NiP Functional Composite Coatings. IOP Conference Series: Materials Science and Engineering 2018;416:012003. doi: 10.1088/1757-899X/416/1/012003.

Nedeloni L, Korka Z, Pascal D-T, **Kazamer N**, Nedeloni MD. Comparative Study on Dry Sliding Wear Resistance of Carbon Steel, Alloyed Steel and Cast Iron. IOP Conference Series: Materials Science and Engineering 2018;416:012026. doi: 10.1088/1757-899X/416/1/012026.

Paduraru L, Nedeloni L, **Kazamer N**, Muntean R, Pascal D-T, Valean P-C,, Nedeloni M-D. Investigations on Dry Sliding Wear and Corrosion Resistane of Thermal Sprayed Molybdenum Coatings IOP Conference Series: Materials Science and Engineering 2018;416:012027. doi: 10.1088/1757-899X/416/1/012027

Kazamer N, Pascal D-T, Marginean G, Serban V-A, Brandl W, Valean P-C. Aspects concerning the wear and corrosion behaviour of WC-CoCr coatings and respectively DLC/WC-CoCr systems. 8th International Conference on Nanomaterials - Research and Application, Brno, Czech Republic: Tanger; 2017, p. 383–8. WOS:000410656100067

Kazamer N, Pascal DT, Marginean G, Şerban VA, Codrean C, Uţu ID. A Comparison between Hardness, Corrosion and Wear Performance of APS Sprayed WC-CoMo and WC-Co Coatings. Solid State Phenomena 2016;254:71–6. doi: 10.4028/www.scientific.net/SSP.254.71.

Pascal D-T, Muntean R, **Kazamer N**, Marginean G, Brandl W, Serban V-A. Characteristics of High Temperature Vacuum Brazed WC-Co-NiCrBSi Functional Composite Coatings, Brno, Nanocon, Czech Republic: Tanger; 2016, p. 775–80. WOS:000410656100134

Kazamer N, Valean P-C, Pascal D-T, Marginean G, Serban V-A. The Influence of the Phase Composition on the Characteristics of APS sprayed WC-Co and WC-CoMo coatings, Junior Euromat, Lausanne, Switzerland: 2016.

Valean, Petru-Cristian, **Kazamer N**, Muntean R, Marginean G, Serban V-A. Characteristics of NiCrBSI Thermal Sprayed Coatings Remelted by an Electromagnetic Induction Process, Junior Euromat, Lausanne, Switzerland: 2016.

Participation to other scientific events

Kazamer N, Valean P-C, Pascal D-T, Marginean G, Serban V-A. Optimierung des Umschmelzverfahrens Flammgespritzter NiCrBSi-TiB$_2$-Beschichtungen und Untersuchung der tribologischen Eigenschaften. Koopkaffee, Gelsenkirchen, Germany: 2019.

Kazamer N, Valean P-C, Pascal D-T, Muntean R, Koziolek J, Kiryc M, Marginean G., Serban V-A. Mikrostruktur und Phasenzusammensetzung von in Vakuumofen umgeschmolzen NiCrBSi-TiB$_2$ glammgespritzten Beschichtungen, Koopkaffee, Gelsenkirchen, Germany: 2018.

Kazamer N, Koziolek J, Pascal D-T, Marginean G, Serban V-A. Charakterisierung eines 3D-gedrucktes Werkzeugsstahl, Koopkaffee, Gelsenkirchen, Germany: 2017.

Kazamer N, Kiryc M, Marginean G, Serban V-A. APS-gespritzte WC-Co- und WC-CoMo-Schichten als Alternative zu Cr-haltingen Beschichtungen. KoopKaffee, Gelsenkirchen, Germany: 2016.

Participation in grants and projects

Personal information

Norbert Kazamer

Nationality: Romanian, Hungarian
Date of birth: 26th of June 1990
E-mail: norbert.kazamer@student.upt.ro | norbert.kazamer@w-hs.de

Education

Doctoral studies

Politehnica University of Timișoara, Romania – Faculty of Mechanical Engineering, Department of Materials Engineering and Manufacturing
2015 - Present

Westpahlian University of Applied Sciences, Germany – Faculty of Mechanical Engineering, Department of Materials Science and Testing
2015 – Present

Master's degree

Politehnica University of Timișoara, Romania – Faculty of Mechanical Engineering
2013 - 2015
Study program: Integrated Engineering

> *Erasmus Scholarships:*
> Westpahlian University of Applied Sciences, Germany – Faculty of Mechanical Engineering (Department of Materials Science and Testing) – 2015
> Çukurova University, Turkey – Faculty of Mechanical Engineering – 2014

Bachelor's degree

Politehnica University of Timișoara, Romania – Faculty of Mechanical Engineering
2009 - 2013
Study program: Mechanical Engineering

> *Erasmus Intensive Programme:*
> Universidad de Valladolid, Spain: Integrating Sustainable Techniques into Applied Science - 2013

Languages

English (professional proficiency), German (working proficiency) and French (elementary)